Session 2

FUEL REPROCESSING

TUESDAY: August 3, 1982
Co-CHAIRMEN: J.L. Kovach, NCS
J. Jacox, NCS

BALANCE AND BEHAVIOR OF GASEOUS RADIONUCLIDES RELEASED DURING INITIAL PWR FUEL REPROCESSING OPERATIONS
A. Leudet, P. Miquel, J.P. Goumondy, G. Charrier

TIME-DEPENDENT ANALYSES OF DISSOLVER OFF-GAS CLEANING INSTALLATIONS IN A REPROCESSING PLANT
k. Nagel, J. Furrer, G. Becker, W. Obrowski, Y.P. Seghal, J. Weyman

A MODEL OF IODINE-129 PROCESS DISTRIBUTIONS IN A NUCLEAR FUEL REPROCESSING PLANT
G.J. McManus, F.A. Duce, S.J. Fernandex, L.P. Murphy

CARBON DIOXIDE-KRYPTON SEPARATION AND RADON REMOVAL FROM NUCLEAR REPROCESSING OFF-GAS STREAMS
P.M. Hirsch, K.Y. Higuchi, J. Abraham

ADSORPTION OF GASEOUS RuO_4 BY VARIOUS SORBENTS II
Lj. Vujisic, R. Nikolic

TEST RESULTS IN THE TREATMENT OF HTR REPROCESSING OFF-GAS
H. Barnert-Wiemer, B. Bendick, B. Juergens, A. Nafissi, H. Vygen, W. Krill

SOURCE TERM AND MATERIAL TRANSPORT

SURFACE DEPOSITION OF RADON DECAY PRODUCTS WITH AND WITHOUT ENHANCED AIR MOTION
S.N. Rudnick, E.F. Maher, W.C. Hinds, M.W. First

FORMATION AND CHARACTERIZATION OF FISSION-PRODUCT AEROSOLS UNDER POSTULATED HTGR ACCIDENT CONDITIONS
I.N. Tang, H.R. Munkelwitz

BALANCE AND BEHAVIOR OF GASEOUS RADIONUCLIDES RELEASED DURING INITIAL PWR FUEL REPROCESSING OPERATIONS*

A.Leudet, P.Miquel, P.J.Goumondy, G.Charrier+

Commissariat à l'Energie Atomique
Division d'Etudes de Retraitement et des Déchets
et de Chimie Appliquée

+ Direction des Essais
France

Abstract

Five fuel pins, taken from a PWR fuel assembly with 32 000 MWD/t burn-up were chopped and dissolved in leak-proof equipment designed for accurate determination of the composition and quantity of gaseous elements released in these operations.

Analytical methods were specially developped to determine directly the noble gases, tritium and gaseous carbon compounds in the gas phase. Volatile iodine was kept as close as possible to the source by cold traps, then transferred to a caustic solution for quantitative analysis.

The quantities and activities of gaseous fission products thus determined were compared with predicted values obtained through computation. Very good agreement was generally observed.

I. Introduction

For a number of years the Commissariat a l'Energie Atomique has devoted a significant part of its R & D activities to the development of gaseous radioactive waste containment and trapping methods / 1 /, with a view to achieve minimal release and in any case, compliance with prevailing regulations.

The design of safe, efficient processes for dissolver off-gas purification in fuel reprocessing plants requires the accurate determination of the quantities of gaseous fission products involved, and their physical and chemical properties. It is important to establish the release process of such products during mechanical and chemical processing, as well as their distribution among the various liquid and gaseous flows.

The information is of special importance because it directly affects the design of equipment and ventilation systems.

It is also important to compare measured quantities and activities with computed data, in order to validate or adjust some of the basic input data used in computations.

For accurate analysis, it is essential to use whole fuel rods with clearly defined characteristics. Hence, the five rods treated were taken from a spent fuel assembly from the Dutch Borssele reactor, which was selected for the following reasons :

*Supported in part by the Commission of the European Communities.

. the Borssele reactor is a typical pressurized water power reactor

. the assembly had undergone three irradiation cycles ; burnup was approximately 32 000 MWD/t.

. initial fuel enrichment was 3.1 %.

Assembly characteristics are therefore very close to those on which reprocessing and safety investigations are based. The results of this work can thus be transposed easily.

II. Gas sampling techniques

The experimental system designed for these investigations essentially consists of a leaktight chopper and dissolver connected to a sampling glove box.

However, since PWR fuel rod lenght exceeded shear capacity, the rods were first cut in two following recovery of internal gas.

Chopping (Figure 1)

Each half-rod was chopped into 15 mm lenghts which were collected in a container used subsequently for dissolving.

After chopping, the released gas was pumped by a cryogenic system into a tubular trap cooled by liquid helium. Three flushing cycles eliminated the last traces of fission gases.

The trap was isolated, heated to 200°C to homogenize its contents, and a gas sample taken for analysis. Since the trap volume was accurately known, the amount of gas was calculated from accurate pressure and temperature readings.

Two - 50°C cold traps were placed between the chopper and the cryogenic pump to retain any iodine present.

Dissolution (Figure 2)

After chopping, the dissolver was connected to a reflux condenser. The gases released during dissolution passed through a - 50°C iodine trap, and to the sampling glove box, where they were homogenized and continuously recycled to the dissolver.

Dissolution occured without recombination of nitrogen oxides, and only the dioxide was partly crystallized in the cold traps. To prevent any gas leakage, the system pressure was kept slightly below atmospheric by draining excess gas to a collection vessel under vacuum.

On termination of dissolution and gas release the collection vessel was isolated. Boiling is maintained for four hours for maximum iodine desorption from the dissolver liquor. Recycled nitrogen oxide was bubbled through the solution to prevents oxidation of iodine by nitric acid, with the formation of non-volatile compounds.

The quantity of gas released during dissolution was determined on the basis of :

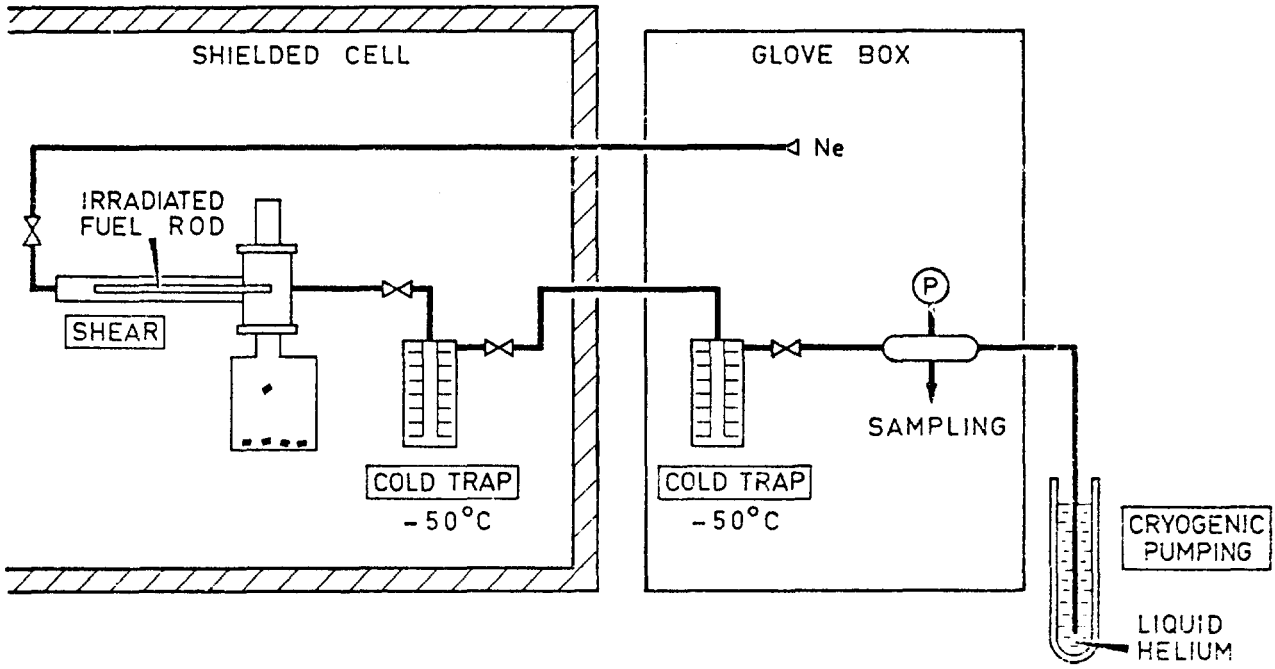

FIG. 1._ SHEARING

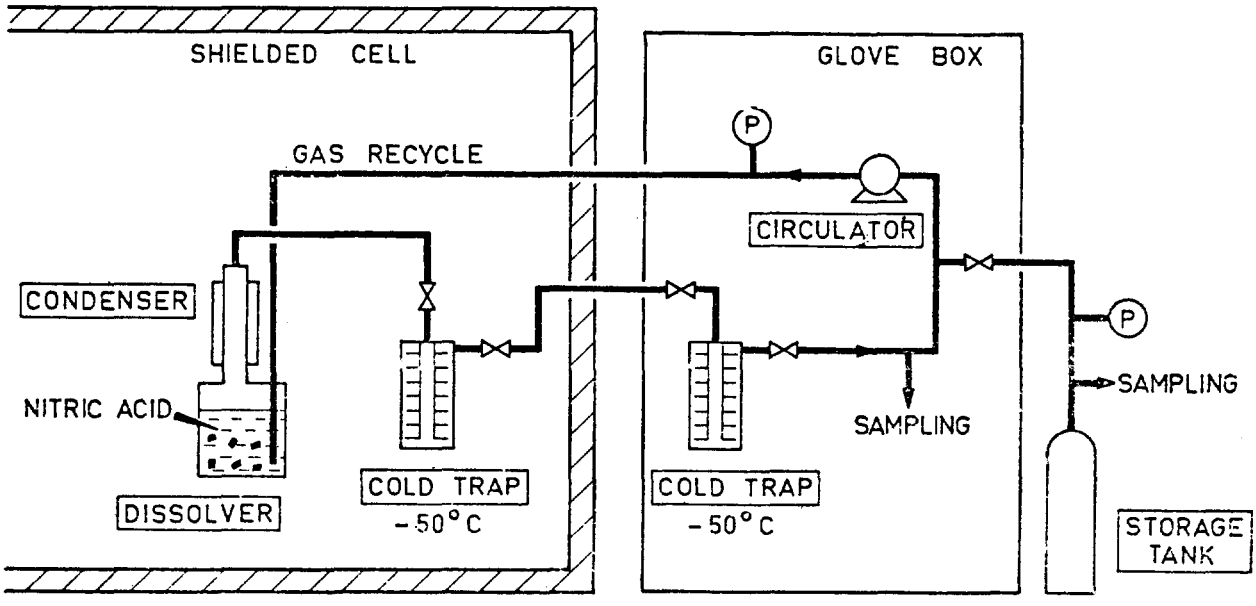

FIG. 2._ DISSOLUTION

. analysis of gas in the collection vessel

. analysis of gas remaining in the dissolver system.

In this respect, the presence of a boiling liquid phase and the fact that system temperatures were not accurately known prevented accurate determination of the real gas volume. To overcome this difficulty, an accurately known quantity of carbon-13 and natural isotopes of krypton and xenon was introduced into the dissolver system. The quantities of carbon-14 and noble gases released from the fuel were then readily computed by isotopic analysis.

Finally, the two cold traps were isolated and gradually heated. Nitrogen flushing entrained the iodine to a caustic solution in two absorbers placed in series. A third absorber, filled with methanol, was provided to trap any methyl iodide present.

III. Gas analysis methods

Much work has been devoted to the development of highly sophisticated gas sample analysis methods.

The gas concentration and specific activity of tritium and carbon-14 were measured in a single chromatographic analysis, although the activity of Krypton 85 was higher by a factor of 10^4 to 10^6 (figure 3).

A HP 5880 chromatograph featuring a liquid nitrogen cryogenic system was used. Stable gases were detected by a catharometer and active gases by a Panax type, low background noise circulation counter.

A porapak-Q column was used to separate H_2, N_2, Ar, CO and NO at a constant temperature of - 65°C, and then Kr, CO_2, N_2O and Xe at programmed temperatures up to 60°C.

Tritium and ^{14}CO measurements were easy because these gases are eluted before Krypton 85. As for $^{14}CO_2$, thorough krypton decontamination was necessary.

As soon as CO_2 elution began, the gas flow was diverted to a Porapak - N column for good separation of residual krypton 85 and $^{14}CO_2$ which was then easily measured.

During CO_2 analysis, N_2O and Xe were retained in the Porapak - Q configuration. The column was reconnected to the system on completion of CO_2 elution.

Krypton 85 activity was measured directly by gamma spectrometry, using a Ge-Li detector.

Chromatography was also used for hydrocarbon detection with a flame ionization detector, and also for methyl iodide detection with an electron-capture detector.

The isotopic composition of noble gases was measured by mass spectrometry, a method also frequently used for quantitative analysis of krypton and xenon by isotopic dilution, using a mixture of ^{80}Kr and ^{124}Xe as a tracer.

Complete analysis involved the following steps :

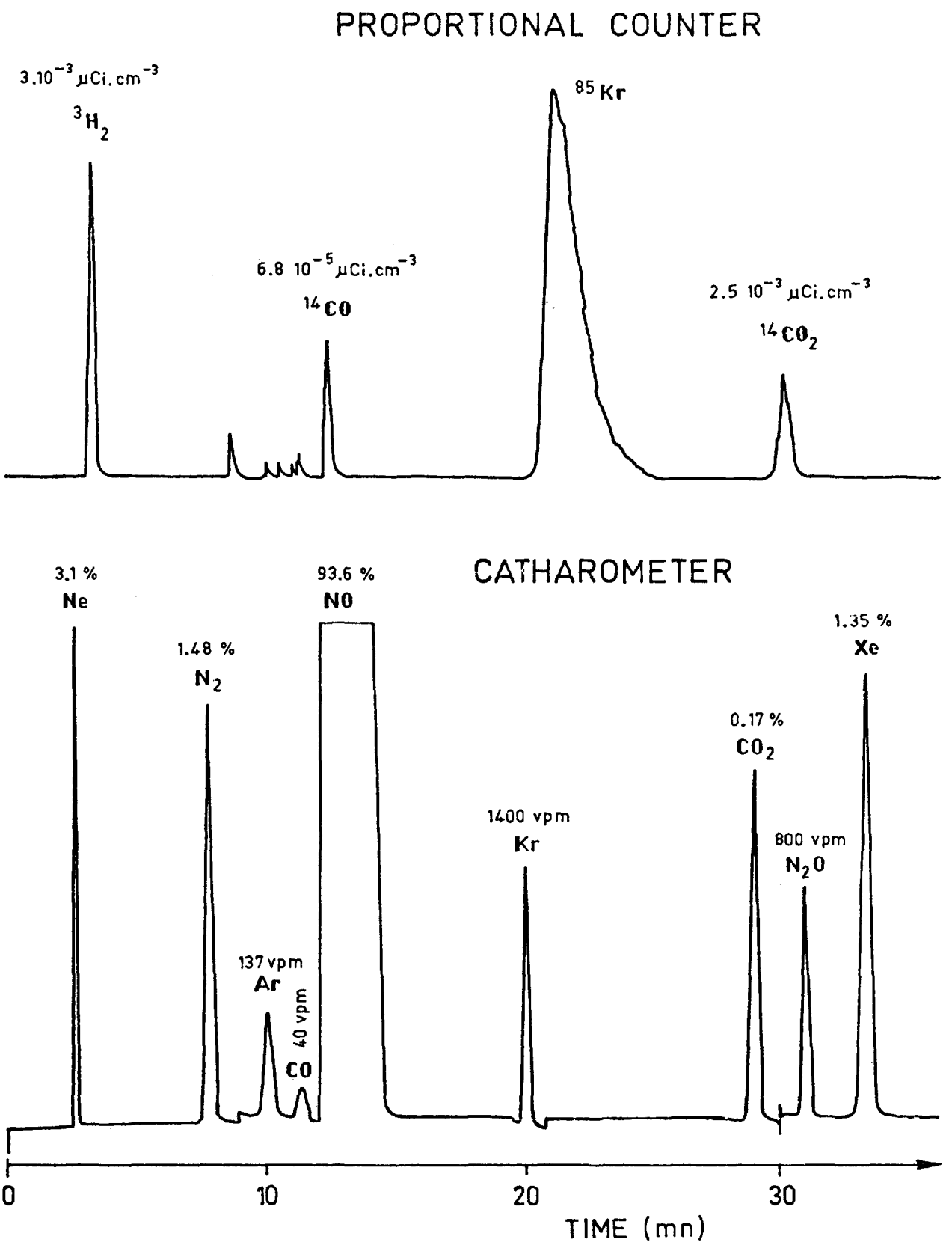

Figure 3 : Typical chromatogram

. preparation and analysis of tracer mixture by reverse dilution, using a mixture of natural krypton and xenon.

. isotopic measurement of the test gas

. isotopic measurement of the test gas/tracer mixture

Although the procedure may seem complex, the number of manipulations is reduced by using a single tracer mixture. The quantities of krypton and xenon can be readily calculated from measured values of $^{80}Kr/^{86}Kr$ and $^{124}Xe/^{136}Xe$ isotopic ratios.

This method only requires a few ml of gas, which is an overwhelming advantage in active gas analysis. Mixtures are prepared by a purely barometric method, and all transfers performed using liquid helium. Utilization of a highly accurate pressure sensor (0.1 m bar) yields results with less than 1 % error in a concentration range of a few hundred vpm.

IV. Behavior of gaseous fission products

All the results are given for 1 - year cooling time.

Noble gases

The quantities of gas collected at the various stages of fuel pin processing are given in table I.Krypton and xenon released during chopping respectively account for 4.4. % and 3.8 % of the total quantity collected. A fraction of the gas was measured during the first cut of the clad, and corresponded to the fraction of noble gases present in the gas plenum ; the balance, i.e., 1 % to 2 % of the total, was released during chopping. This operation is relatively ineffective in opening the micropores in which gas remains trapped.

PIN		1	2	3	4	5	MEAN
Kr	SHEARING %	2.6	3.3	5.3	5.8	5.0	4.4
	DISSOLUTION %	97.4	97.6	94.7	94.2	95.0	95.6
Xe	SHEARING %	2.2	2.8	4.6	5.1	4.3	3.8
	DISSOLUTION %	97.8	97.2	95.2	94.9	95.7	96.2

TABLE I.- NOBLE GAS DISTRIBUTION

BURN-UP GWd/t_u	KRYPTON		KRYPTON – 85		XENON	
	g/t_u	Adjusted to 33 GWd/t	Ci/t_u	Adjusted to 33 GWd/t	g/t_u	Adjusted to 33 GWd/t
31.0	342	364	8930	9510	5250	5590
31.8	340	353	9030	9370	5240	5440
31.6	333	348	8660	9040	5110	5340
31.5	322	337	8750	9170	4930	5160
31.0	346	368	9250	9850	5300	5640
MEASUREMENTS (MEAN)		354		9390		5430
CALCULATED		370		9150		5430
$\frac{M-C}{C}$ %		- 4.3		+2.6		0

TABLE II – NOBLE GAS CONTENT

The experimentally determined krypton and xenon masses and krypton 85 activities are shown in Table II. Average values show good agreement with computed values, and the maximum discrepancy, found for the mass of krypton was only 4.3 %. The next table gives the average isotopic composition of noble gases.

Kr		Xe	
82	0.2 %	130	0.1 %
83	11.5 %	131	8.2 %
84	30.8 %	132	20.7 %
85	6.3 %	134	28.4 %
86	51.2 %	136	42.6 %

Table III : isotopic composition of noble gases

Iodine

Our procedure permits the detection of volatile iodine from 10^{-4}g, i.e., less than 0.1 % of the mass contained in each half-rod.

Iodine release during chopping was less than this detection limit.

It is well known that fission-generated iodine in oxide fuel combines with the more electro-positive elements, especially cesium, of which a large amount is present. / 2 /.

Since cesium iodide is not volatile, at least at standard reprocessing temperatures, it seems normal that no iodine is released during shearing.

It is only when the fuel is dissolved that practically all the iodine is released by oxidation of iodides under the combined actions of nitric and nitrous acids in the dissolver solution.

More than 99 % of the iodine can be readily eliminated from the dissolution liquor and carried into the off-gas. Insufficient desorption may be caused by :

- insufficient oxidation of the iodides due to the lack of nitrous acid. This acid, resulting from NO_2 absorption, shows little stability in a boiling solution.
- lack of carrier gas, so that molecular iodine cannot be carried into the off-gas.
- formation of non-volatile compounds such as HIO_3, due to the oxidizing action of boiling concentrated nitric acid. However, these compounds are probably reduced to the elementary form by nitrous acid.

In our experiment, operating conditions were such that the above difficulties were avoided. The analysis of Iodine 129 in the fuel solution confirmed that the residual amount was under 1 %.

Initially an attempt was made to evaluate the amount of methyl iodide present through analysis of Iodine 129 in the ethanol solutions through which the gas stream flowed. Although this compound was not detected, the trapping efficiency remains highly questionable.

An analytical method is currently being developed for the direct determination of organic iodine compounds in the gas. Early results appear to show that only traces of these compounds are present. This, however, is subject to confirmation by further tests.

Nevertheless, the formation of organic iodides seems to be related to the presence of organic impurities in liquid or gaseous reagents. The products used in our experiments were of high purity, which suggests that organic iodides are only formed in very small quantities.

The table IV shows the total quantity of iodine as well as iodine 129 activity. Disregarding one incorrect value due to experimental error, very good agreement is observed with predicted quantities computed using a CEA code.

These results also allow the estimate of the respective proportions of isotopes 127 and 129. Calculations show that Iodine 129 accounts for an average 82 % of total iodine.

Carbon 14

Volatile carbon compounds consist almost entirely of CO_2. Carbon monoxide CO is only 1 % to 2 % of the amount of dioxide. No traces of light hydrocarbons (to C6) were detected in the off-gas.

Measured carbon-14 activity was 0.24 $Ci.t_u^{-1}$

BURN-UP GWd/t	TOTAL IODINE		IODINE-129	
	g / t_u	Adjusted to 33 GWd/t	mCi / t_u	Adjusted to 33 GWd/t
31.0	201	214	28.2	30.0
31.8	215	223	30.6	31.8
31.6	122*	-	17.9*	-
31.5	204	214	29.5	30.9
31.0	202	215	30.0	31.9
MEASUREMENTS (MEAN)		216		31.2
CALCULATED		223		31.4
$\frac{M-C}{C}$ %		- 3.1		-0.6

* Erroneous measurement (loss of iodine during experiment)

TABLE IV.- IODINE CONTENT

Carbon-14 only accounts for 0.1 % of the total carbon measured, in monoxide as well as dioxide form.

The amount of CO_2 collected was approximately 80 l STP.t_u^{-1} . The gas released during chopping contained less than 1 % of the total CO_2.

BURN-UP GWd/t	CARBON-14		TRITIUM	
	mCi/t_u	Adjusted to 33 GWd/t	Ci/t_u	Adjusted to 33 GWd/t
31.0	223	237	147	156
31.8	229	238	418	434
31.6	230	240	81	85
31.5	246	258	66	69
31.0	228	243	173	184
MEAN		243		186

TABLE V .- CARBON-14 AND TRITIUM CONTENTS

Tritium

Tritium quantities measured and shown in table V only relate to the fraction contained in the fuel, not including tritium in the zirconium clad.

The fraction of tritium gas released during chopping was very small and variable, representing 10^{-6} to 10^{-4} of the total tritium measured.

During dissolution, more than 99.5 % of the tritium was measured in the dissolution liquor, and 0.2 to 0.4 % was determined in the form of tritiated hydrogen in the gas phase.

Total tritium activity varied widely, from 66 to 420 $Ci.t_u^{-1}$ (180 $Ci.t_u^{-1}$ on the average). This spread of results is highly surprising ; it is generally estimated that in LWR fuel, 40 % of the tritium formed remains in the oxide / 3 /. It is also unlikely that such differences in tritium behavior could be accounted for by dissimilarities in thermal conditions affecting different rods in a single fuel assembly.

Experimental error is ruled out by the fact that results are consistent from one half-rod to the other. Furthermore , the tritium in the gas, determined by entirely different methods, shows fluctuations of the same magnitude.

A complete tritium balance will also require determination of tritium trapped in the clad. Attempts are currently being made to achieve tritium desorption by heating the hulls in a sealed oven.

REFERENCES

/ 1 / A.CHESNE, J.P.GOUMONDY, P.MIQUEL, A.LESEUR
Etat de la Recherche - Développement française dans le domaine du traitement des gaz produits par les usines de retraitement.
CEE Seminar on Radioactive Effluents from Nuclear Fuel Reprocessing Plants, Karlsruhe, 22-25 nov.1977

/ 2 / ANAV, CHESNE, LESEUR, MIQUEL, PASCARD
Brevet français n° 7.730.371 (1977)

/ 3 / E.HENRICH, H.SCHMIEDER, K.H.NEEB
The concentration of tritium in the aqueous and solid waste of LWR fuel reprocessing plants.
International Symposium on the Management of Gaseous Wastes from Nuclear Facilities, Vienna, 18-22 Feb.1980.

DISCUSSION

FURRER: In simulation tests we found that about 99.8 - 99.9% of the iodine was released in the DOG during dissolution. Have you added UI, NO_2, or O_3 to get the whole amount of iodine in the DOG?

LEUDET: No, we didn't require such a complete iodine desorption. Boiling and continuous bubbling of recycled NO_x in the dissolution liquor allowed us to carry out more than 99% of the total iodine into the DOG.

MOELLER: To what degree might the data you have developed be applicable in estimating airborne releases from an accident in a nuclear power plant?

LEUDET: I think that accident conditions in a nuclear power plant would be quite different than our operating conditions and make it impossible to transpose the results of this work.

FERNANDEZ: Could you tell me if the chromatographic conditions for the measurement of methyl iodide were the same as for the noble gases, and if any evidence was found for organic iodides heavier than methyl iodide?

LEUDET: Chromatographic conditions were different for methyl iodide and for noble gas measurements. Concerning the detector, we used an electron-capture detector instead of a catharometer. The material filling the separation column was also different. Up to now, no real evidence has been found for heavier organic iodides.

TIME-DEPENDENT ANALYSES OF DISSOLVER OFF-GAS CLEANING INSTALLATIONS IN A REPROCESSING PLANT.

K. Nagel, J. Furrer

Kernforschungszentrum Karlsruhe GmbH
Postfach 3640, D-7500 Karlsruhe

G. Becker, W. Obrowski, Y.P. Seghal, J. Weymann

Technische Universität Berlin
Institut für Kerntechnik
D-1000 Berlin 10

Abstract

The iodine- and aerosol-filtering test facility PASSAT of the Nuclear Research Centre in Karlsruhe has been investigated using a method which allows time dependent analyses under accident conditions. This method which is closely related to fault tree analysis needs subdivision in barriers of the system, and their logical combination in a tree. The barriers have binary states: 'defect' and 'intact'. The 'defect' state will be described by a fault tree, whereas the 'intact' state includes dependences of a barrier operation on physical parameters. The 'intact' state enables time dependent calculations.

Calculations have been done for iodine filtering, because the best known entrance data are given. Results demonstrate clearly that the amount of iodine released increases only if both heaters failed, which heat the off-gas from 30° C to 80° C and then to 130° C. Additionally the integrated amount of iodine released depends on time period between the failures of the heaters.

1. Introduction

The dissolver off-gas of a reprocessing plant contains I-129, Kr-85, C-14, and H-3 as gaseous radioactive fission products as well as droplet and solid aerosols. These aerosols may carry along with them toxic fission products such as Ce-144, Cs-134, Cs-137, Sr-90, Ru-106, Sb-124, and the transuranic-elements Np, Pu, Am, Cm. Because of the radiotoxicity of these elements the dissolver off-gas has to be cleaned. At our research centre several independent parts of a planned dissolver off-gas cleaning system have been built in order to accumulate experimental results and experience. The two major parts are called PASSAT and KRETA. PASSAT is to remove aerosols and iodine, KRETA is to retain Kr-85. This paper is focused on PASSAT as a prototype of a filtering facility.

The aim of this work is to analyze the possibilities of failure, to define probabilities and to calculate amounts of radioactivity released under accident conditions. First investigations dealt with the definition of top events and, subsequently, with the construction of fault trees for the independent parts. It means a restriction if one describes the failure behavior of such technical systems by fault

trees. In cooperation with the Technical University of Berlin it was possible to apply an existing software program, which allows performing time-dependent calculations of the amount of toxic fission products released. In the following this work deals with:

2. Operation of PASSAT,
3. The basic method modelling technical facilities,
4. Models of the barriers,
5. Assumptions and results simulating the PASSAT off-gas sytem.

2. Operation of PASSAT

PASSAT is a prototype of a aerosol and iodine filtering facility. This facility was built to investigate the behavior of filter components in a compound system, to get experience in optimal operation conditions and to develop filter vessels which are easy to handle. Based on these different scopes of duties it will be difficult to give a satisfactory description of the system, which met not only the test facility but also the filtering facility of a reprocessing plant. Figure 1 shows the scheme of PASSAT, which is the basis of all investigations in this work. The source at the beginning of the scheme represents essentially dissolver, condensor, NO/NO_2 separation and coarse droplet separator. Source data which have been used in subsequent calculations are given in Table 1.

Tabelle 1 : Source data of PASSAT, which have been used in the calculations.

Aerosol Spectra

liquid		solid	
size (µm)	mg/std.m^3	size (µm)	mg/std.m^3
5	0.02	0.5	1.2
10	0.2	7.5	0.6
15	0.6	12.5	0.2
20	0.6	15.0	0

Concentration of Aerosols:	
liquid:	2mg/std.m^3
solid:	2mg/std.m^3
Off-gas Temperature:	30°C
Relative Humidity:	100%
Concentration of Iodine:	1g/std.m^3

The following fiber packed mist eliminator with flushing capability (Brink filter) retains solid and liquid aerosols. Afterwards the off-gas is heated up to 80°C reducing relative humidity and vaporizing larger aerosol droplets. The heated off-gas flows through a HEPA-filter which separates mainly solid aerosols. Sorption is more effective at higher off-gas temperature. Therefore the heater in front of the first iodine-sorption-filter increases the temperature to 130°C,

which additionally improves the retention factor of the filter by decreasing relative humidity of the off-gas. All filters and heaters are protected against pressure increase by safety valves. The valves carry the off-gas over a safety iodine-sorption-filter to exhaust air. The flow rate of PASSAT is a constant of 150 std.m^3/h.

3. Basic Method Modelling Technical Facilities

The fundamental method, which allows time-dependent analyses of failures of technical systems, was elaborated from the Technical University of Berlin /1/. It takes into consideration the dynamic behavior of these systems under accidental conditions, i.e. the functional dependence of components will be covered with respect to time. For this purpose, the determination of the amount of pollutants released which is required for risk analysis was carried out by simulation. On the other hand the probability of events was determined analytically resting largely on conventional methods like evaluation of fault trees.

The mathematical model of the investigated system devides itself into three parts which must be provided by the analyst. These parts are:

- 'release-tree' of the system,
- fault tree of the barriers in defect state,
- 'simulation-models for the behavior of barriers in 'intact' and 'defect' state, further referenced as 'transport cells'.

Firstly, the analysis requires a facility description by means of a so-called 'release-tree'. A 'release-tree' is closely related to a fault tree its top event being the release of toxic fission products. Basic events of a 'release-tree' are barriers of the system taking either 'intact' or 'defect' state. Fig. 2 shows the beginning of the 'release-tree' for PASSAT with essential details. The construction of a 'release-tree' needs simple considerations. The amount of toxic products released depends upon the amount of these arriving in front of the last barrier and on its penetration. The amount of toxic products arriving in front of the last barrier is dependent on the amount of material reaching the next but last barrier and on the amount penetrating it, and so on.

In the second step, fault trees are drawn up by means of conventional methods. They describe conditions under which barriers shift from 'intact state' to 'defect state'. Thirdly, the models of the barriers have to be developed. The models include the time dependent physical behavior of the system components.

Based on the complete 'release-tree' of PASSAT, the software program finds out all possible 'release-paths' of this tree. A 'release-path' corresponds exactly to an accidental state of the system. It contains all barriers which the toxic products have to penetrate in order to reach the atmosphere. The amount released will then be calculated for every 'release-path' by means of simulation. First of all a realisation of all the random events will be carried out using a random-digitgenerator. That means, the time at which barriers go into 'defect state', the duration of this state, actual loading etc. will be chosen randomly. Obviously, those random numbers are not independent of one another, but have to be chosen in such a way, that the combination of

accidents required for a special path occurs with overlapping intervals. This severely reduces the number of Monte-Carlo-trials required but on the other hand makes it necessary to calculate frequencies for all 'release-paths' analytically before simulation take place. Once the random events are fixed the amounts released can be calculated. The simulation-models then are coupled with one another in the order as described by the 'release-path'. The accident sequence of the coupled system is calculated in small discrete time increments from beginning to end. The amount of toxic substances released from the whole system considered can be calculated under accidental conditions. The simulation trials are repeated as often as necessary to determine the expected value of the amount released with sufficient accuracy.

Frequency of the occurrence of accidents is derived from the fault trees. For this purpose cut-sets are determined and evaluated using the known Vesely-relation.

Total risk of the whole system is calculated in the following manner:

$$R_{system} = \sum_{I=1}^{NP} (\overline{AM}_I \cdot H_I)$$

NP = Total numbers of 'release-paths'

$\overline{AM}_I$ = Expected value of the amount released by every 'release-path'

H_I = Analytically determined expected value of the frequency of a 'release-path'.

calculations of the amount of products released are based on two assumptions:

a) the 'release-paths' are independent of one another,
b) moment and duration of change of a barrier state are independent of the special cut-set causing change of state.

4. Models of the Barriers

The description of the models of the barries will be followed individually. First of all, in order to have a better understanding of the different criterion for the modelling, the simulation of the barriers will be explained in general. The simulation of the off-gas cleaning installations under normal and accidental conditions has to be carried out with these models. All the process variables which influence the barriers or are being influenced by these must be covered and treated accordingly to these models. Since the process variables are being transfered from one barrier-model to another one, it is urgently needed that each model is in a position to deal with all the present variables even if it does not influence any particular varible and is also not being influenced by it. A list of variables which have been taken into consideration for simulation of the PASSAT off-gas system is shown in Fig. 3. A barrier-model should fit not only in some particular off-gas system but should be as general as possible. As a consequence to this, it should be flexible and easily adaptable with regard to the sets of parameters. With sensible and skilful structuring of the models care is taken of that these can be switched over even to other larger or smaller sets of parameters. At the Institute

for Nuclear-techniques of the Technical University in Berlin (West Germany), a structure for the models has been developed which matches these requirements closely. The models developed here are in principle not confined to the number and combinations of the process variables. Their application is however restricted because of the fact that the mathematical description of the behavior of the models is valid within certain range. Generally, with a little effort, these can be adapted even to the other ranges of validity by inserting correlations which describe the behavior of these barriers within these ranges. After these initial remarks we shall be describing the modelling of each barrier in detail. The essential barriers of the off-gas system are:

- packed fiber mist eliminator
- HEPA-filter
- iodine-sorption-filter
- heater

A modelling of the behavior of these components under normal and accidental conditions is required in order to assess the behavior of the off-gas system.

4.1 Packed Fiber Mist Eliminator

It removes droplet and solid aerosols from the off-gas. It consists of not vitrified glass fibres with a packing thickness of 5 cm and a packing density of 300 kg/m³. The interesting operating parameters of the separator are the decontamination factor for droplet as well as solid aerosols and the pressure drop over the separator. Experiments have been carried out at Nuclear Research Centre in Karlsruhe (West Germany) to determine these values.

4.1.1 Droplet Aerosols

The separation of the larger drops ($d>1\mu m$) takes place mainly due to hindering and the effects of inertia. The drops strike the fibres and are pressed through the fibre network by the gas. Very small particles are held back mainly by diffusional effects. The liquid which has been held back flows down on the clean gas side of the network and is withdrawn off.

The measurement of the decontamination factors for the droplet aerosols dependent on the diameter of the drops has yielded values as shown in Fig. 4 /2/.

The correlation used for this dependency is as follows:

$$\log DF = 7.4 \log d + 1.11$$

with d = diameter of the aerosols in µm.

As evident from Fig. 5, this correlation describes the real behavior satisfactorily within the range of $1.5<d<5\mu m$.

The measurements of the decontamination factors were carried out at different volumetric flow rates and temperatures. However there was no evidence that the decontamination factor depends on both parameters within the realistic operational range of the PASSAT off-gas system.

4.1.2 Solid Aersols

The experiments were also carried out to determine the decontamination factor for solid aerosols. The model particles consist of Uranin. The distribution of the particle diameter has been shown in Fig. 6, the most frequent diameter of the particles occuring at 0.12 µm /2/. It was not possible to relate the decontamination factor with the size of the particles, however a total decontamination factor was determined for the given spectrum of the particles in dependence on the volumetric flow rate. The following correlation was used for this purpose.

$$DF = \frac{1289 \cdot 10^{10}}{V^{5.1}} + 1062$$

with V = flow rate in Nm^3/h.

The correlation matches well with the experimental values for the whole range as shown in Fig. 7 /2/.

4.1.3 Determination of the Pressure Drop

Although the pressure drop does not have any influence on the separation efficiency, still it is interesting to know about its value. Complete information is not available for the pressure drop over the separator in the off-gas system. Both the main parameters which influence the pressure drop are flow rate and loading. The pressure drop in dependence on the flow rate is known only for the unloaded filter and is determined with the following correlation:

$$p(v) \text{ mbar} = 0.08\ v + 1.6$$

where v = volumetric flow rate in Nm^3/h.

The dependence of the pressure drop on loading is known only at a constant flow of 75 Nm^3/h and is determined by the correlation:

$$p(m) \text{ mbar} = 0.09\ m + 8$$

with m = loading in gm.

The pressure drop in dependence on loading and flow rate is determined for the model of this barrier by the following correlation:

$$p(m,v) = (0,09\ m + 8)\ \frac{0.08 \cdot V_{akt} + 1.6}{0.08 \cdot 75 + 1.6}$$

with V_{akt} = actual flow rate in Nm^3/h.

i.e. the pressure drop will be calculated as a function of loading and is corrected with a factor which is given on the basis of deviation from a flow rate of 75 Nm^3/h.

The modelling of the mist eliminator is an example for the description of the behavior of a well known equipment on the basis of the measured quantities. The adjustment to other operational ranges is possible by means of changing the correlations.

4.2 HEPA-Filter

The HEPA-filter cleans the off-gas from aerosols. It consists of folded filter paper with a thickness of 0.4 mm.

The quantities necessary for modelling this filter are mainly the decontamination factor and the pressure drop over the filter.

4.2.1 Pressure Drop

Since the mechanical stability of the thin filter mat is very small, the pressure drop over the filter plays a decisive role in the operation of this component. If the pressure drop over the filter exceeds a certain maximum value the filter mat cannot withstand the force and tears off. This leads not only to a distinct decrease in the decontamination factor but also the filter cake which has already formed on the crude gas side is at least partially washed away and gets on to the clean gas side. Thus, if the filter breaks through, it looses not only its decontamination effect but also acts as a source of aerosols.

The pressure drop in dependence on the loading is shown by Fig. 8. The pressure drop over the filter is given by the Darcy equation:

$$p = K_D \cdot \eta_G \cdot V_a \cdot h_f$$

K_D = filter drag coefficient

η_G = dynamic viscosity of the gas

V_a = flow velocity

h_f = thickness of the filter mat.

The filter drag coefficient for the model is split as:

$$K_D = K_O + K_{Bel}$$

K_O = filter constant of the unloaded filter

K_{Bel} = additive corrective term for the loaded filter

The values of K_D and K_{Bel} are determined with the help of the Darcy equation from Fig. 8.

While K_O is a real constant, K_{Bel} will be determined in each time interval during the simulation.

4.2.2 Decontamination Factor

The values of the decontamination factor depending upon the size of the aerosols are not known for this filter. Therefore a half empirical formula of Friedlander was used which will be explained as follows. There are three main mechanisms which influence the separation of the aerosols on a filter mat. These mechanisms are:

- influence due to the forces of inertia (the aerosols cannot follow the path of the gas flow between fibres because of inertia)
- diffusion (contact with the particles because of the Brownian movement)
- electrical effects.

For every single effect of separation there are a number of theoretical and half empirical solutions. The total separation efficiency, however, cannot be calculated as a sum of each effect individually and a solution which takes into account all the main three effects is not available. The superposition of the effects due to forces of inertia and diffusion is described by Friedlander as follows /3/:

$$\varepsilon_{M_D} = \frac{6\left[\frac{KT}{3\pi\eta_G}\right]^{2/3}}{\nu_G^{1/6} \cdot d_f^{1/2} \cdot d_p^{2/3} \cdot v^{1/2}} + 3\,\frac{d_p^2 \cdot v^{1/2}}{\nu_G^{1/2} \cdot d_f^{3/2}}$$

ε_{M_D} = separation efficiency of a single fibre due to forces of inertia and diffusion

K = Boltzmann - constant

T = temperature in K

η_G = dynamic viscosity of the gas

ν_G = kinematic viscosity of the gas

d_f = diameter of a fibre

d_p = diameter of the particle

v = flow velocity

(all units in cgs-system)

The first term of the equation describes the diffusional effects while the second term takes into account the effects due to the forces of inertia.

The total separation efficiency of the filter network is calculated as follows:

$$\varepsilon_g = 1 - e^{-\alpha}$$

with

$$\alpha = \frac{4}{\pi}\,\varepsilon_{M_D}\,\frac{1-\beta}{\beta} \cdot \frac{h_f}{d_f}$$

β = porosity of the filter network

h_f = thickness of the filter network

This results in a decontamination factor

$$D_f = \frac{1}{1-\varepsilon_g} = e^{\alpha}$$

The decontamination factors determined in this way dependent on particle diameter have been illustrated in Fig. 9.

While simulating aerosol filter, the droplet and solid particles have been treated equally and the swelling of the filter due to dampness thereby resulting in the increase of the pressure drop has not been considered.

If the filter breaks through (p= 20 mbar), then it is assumed, that the whole filter cake will be washed away within an hour and gets on to the clean gas side.

4.3 Iodine-Sorption-Filter

A considerable amount of iodine is released during the dissolution of the spent fuel. The off-gas system, therefore, has been provided with an iodine filter. It is a chemisorption filter and consists of silver impregnated silicagel. The decontamination factor for this filter is largely dependent upon the retention time of the gas in the filter and the relative humidity of the gas. The maeasured decontamination factors dependent on these quantities are illustrated in Fig. 10.

The retention time determined not only by the geometric dimensions of the filter but also by the loading which has already accumulated over the filter. The filter has approximately a capacity of 12 kg of iodine and is exchanged after a loading of nearly 80 %. In order to keep the relative humidity as low as possible, the filter is operated at a temperature of about 130° C.

A distinct decrease in temperature can result in a deterioration of the decontamination factor because the relative humidity of the gas increases with decreasing temperature. Apart from the excessive loading of the filter, this is the single factor affecting the decontamination factor which has been modeled. The resorption processes by which iodine is released from the filter have been neglected. For example, high contents of nitric oxides in the off-gas system may cause resorption.

4.3.1 Modelling of the Separation Efficiency

An eventual break down of the iodine filter has not been provided in the modelling of this filter i.e. its decontamination factor will be calculated in any case from the Fig. 10. However, it is quite possible to obtain a decontamination factor near 1. Such a decontamination factor is never reached because of a sudden failure of this component but always due to relative gradual change of the state of the gas or the loading.

The curves of Fig. 10 have been provided with a raster (10 % relative humidity). The actual values of the decontamination factor are determined by interpolating between the points of the raster in the direction of humidity as well as in the direction of retention time. It was found, that each of the two centre-curves (Fig. 10) could be described as a linear interpolation of the two neighbouring curves with poor results only. The half logarithmic scale of Fig. 10 led to the conclusion, that the logarithm of the decontamination factor should be interpolated rather than the decofactor itself. This method was tested with good success against the measured curves and then was used to interpolate for the current values of the remaining retention time and the relative humidity within the raster mentioned above.

Another quantity modeled is the pressure drop over the filter. The values are known for this pressure drop in dependence on flow rate and it can be calculated with the following correlation:

$$p = 0.73 \cdot V^{1.28}$$

with V = flow rate in Nm^3/h.

The dependence of pressure drop on loading is not known.

4.4 Heaters

Two heaters are installed in teh PASSAT off-gas system, one in front of the HEPA-filter and the other one in front of the iodine-filter. They heat the off-gas to a temperature of 80° C and 130° C, respectively which is the operating temperature under normal conditions. This helps in keeping the relative humidity to an optimal level for both filters which is a crucial factor in determining the behavior of these components with respect to their decontamination factors. Both heaters have been modeled identically. Although the model has been developed for the PASSAT off-gas system, yet it can be adapted to any other system because of its general nature keeping in mind all the necessary points described already in the previous section of barrier models.

It was observed that once the heater is switched on or off, it attains the new stationary temperature after a transition stage which lasts for an hour. Due to this fact, a model was developed which takes into account the instationary behavior of this component. The following assumptions have been made in the model:

1. The pressure drop over the heater is negligible.
2. The evaporation of water in the liquid phase, for example, when the gas is over saturated, has been neglected.
3. The reduction of dropled aerosols to solid aerosols which can take place due to evaporation of water has not been considered. It will be necessary to account for this effect if the behavior of the system is modeled for droplet aerosols.
4. No attention has been given to the geometric configuration of the heater.

The time dependent electrical power P_{el} has two effects. Firstly, it heats up the heat capacity of the heater which can also include the capacities of other adjoining components. Secondly, it heats up the gas by convective heat transmission. This is described by a heat conductance αA.

The following balances have been used:

1. Heat output of the heater = heat taken by the gas

$$\alpha A\ (\delta_h - \delta_M) = c\ \dot{m}\ (\delta_2 - \delta_1) \qquad \text{(I)}$$

2. One part of the electrical energy goes in the heat capacity of the heater while the other part is transmitted to the gas by convection.

$$P_{el} \cdot dt = C_h\ d\delta_h + \alpha A\ (\delta_h - \delta_M)\ dt \qquad \text{(II)}$$

3. Mean temperature of the gas

$$\delta_M = \frac{\delta_1 + \delta_2}{2} \qquad \text{(III)}$$

From the above balances one can derive the following equation for the exit temperature δ_2 by eliminating δ_M and δ_h

$$\left(\frac{L_{tr}}{\alpha A} + \frac{1}{2}\right)\frac{d\delta_2}{dt} - \left(\frac{L_{tr}}{C_h} + \frac{1}{\alpha A} \cdot \frac{dL_{tr}}{dt}\right)\delta_2 = \frac{P_{el}}{C_h} + \left(\frac{L_{tr}}{\alpha A} - \frac{1}{2}\right)\frac{d\delta_1}{dt} +$$

$$+ \left(\frac{L_{tr}}{C_h} + \frac{1}{\alpha A}\ \frac{dL_{tr}}{dt}\right)\delta_1 \qquad \text{(IV)}$$

with $L_{tr} = c\ \dot{m}$

The quantity L_{tr} has the unit of a heat conductance and is described as transport conductance. It will be taken as time dependent because a flow control might effect the mass flow rate and heat capacity c depends on the composition of gas which also can vary with time.

Equation (IV) is a linear inhomogenous system with time dependent coefficients. If one neglects the time dependence of the coefficients, the homogenous solution of this equation is as follows:

$$\delta_2 = k\ e^{-t/T} \qquad k \in \mathbb{R} \qquad \text{(V)}$$

with the time constant as

$$T = C_h\left(\frac{1}{\alpha A} + \frac{1}{2\ L_{tr}}\right) \qquad \text{(VI)}$$

Equation (V) was programmed in discrete form.
The time dependent electrical power P_{el} is treated as follows:

In defect state P_{el} is zero.

In intact state, it will be adjusted during each time interval in such a way that the stationary output temperature becomes equal to the required value, provided P_{el} does not exceed a maximum value or becomes less than zero.

Symbols used:

A	:	effectiv heat transfer area	$[m^2]$
C_h	:	heat capacity of the heater	$[J/K]$
c	:	specific heat capacity of the gas	$[J/K \cdot kg]$
$\dot{m}$	:	mass flow rate	$[kg/s]$
α	:	heat transfer coefficient	$[W/K \cdot m^2]$
δ_1	:	inlet gas temperature	$[°C]$
δ_2	:	exit gas temperature	$[°C]$
δ_h	:	mean temperature of the heat capacity of the heater	$[°C]$

5. Assumptions and Results Simulating the PASSAT Off-gas System

5.1 Feasible States of the Barriers and their Functions

Using the models described earlier the simulation of the off-gas system has been carried out for normal and accidental conditions. The off-gas source parameters have been listed in the chapter 'Operation of PASSAT'. These parameters are kept constant in the evaluation of the simulations, the source of the off-gas system has not been considered so far under accidental conditions. Likewise, the droplet aerosols in the off-gas have been neglected, till now.

The mist eliminator does not go into defect state, it is always to be at disposal. It has a decontamination effect for solid aerosols but not for iodine.

The heaters have no decontamination effect at all. They compensate for the deviations of the required temperature within their range of regulation (range of regulation 0-3 kw, stationary output under operational conditions nearly 2.7 kw). Both the heaters have been modeled identically, they differ only in the range of temperature in which they operate. The heaters can take 'intact' or 'defect' state.

The aerosol filter does not have any decontamination effect for iodine, it retains only aerosols. It can take 'intact' or 'defect' state; it can fail either by chance or if the pressure drop exceeds 20 mbar, then it fails deterministically. The filter cake is washed away completely within an hour.

The iodine filter does not have any stochastic defect state. It can lose its effectiveness only due to excessive loading or because of too high humidity of the off-gas. Irrespective of all the other influences, its decontamination factor is always 2 for aerosols.

Nothing can be said about risk resulting from accidents, because no calculations of failure probabilities have been performed. Those calculations are planned for the future. Till today, only consequences

have been considered.

5.2 Results

With the boundary conditions described earlier, a large number of accidents are possible since each arbitrary combination of different states of the barriers represents an accident. From these numerous combinations, however, only two have significant effects. These are:

- the brakage of the HEPA-filter
- the simultaneous failure of both heaters.

Therefore, these two accidents will be dealt with in the following section.

5.2 Breakage of HEPA-Filter

This accident results in increase of the amount of aerosols released. It does not have decontamination effect any more and beyond that it releases the stock which has already accumulated on it. The releases the stock which has already accumulated on it. The release of the stock in this case is more dominant than the loss of decontamination effect. This result can be explained because of the fact that the content of the aerosols in the gas is very low and besides HEPA-filter, the mist eliminator is present which removes aerosols very effectively.

The deterministic breakage of HEPA-filter has in no case taken place while simulating the PASSAT off-gas system i.e. the permissible pressure drop of 20 mbar has never been exceeded. It can be exceeded due to increase in flow rate under accidental conditions. A time dependent model of the source is necessary for the investigation of the real dynamic behavior of the accident 'filter-breakage'. Such a model has been planned in the course of the further work. A flow controller will then also be considered which can take 'intact' or 'defect' state. It will then be possible to take into account the effects of other components on the behavior of the filter.

5.4 Failure of Heaters

The failure of heaters result mainly in the release of iodine. In contrast to filter breakage, this accident is a good example to demonstrate, that the consequences can be highly dependent on the course of accident. The failure of only one heater has no effect on the decontamination factor for iodine.

Fig. 11 shows the progress of the accident when both heaters go out of order almost simultaneously, About 0.7 hr after failure of heater 2, heater 1 goes out of order and the temperature falls down to the entrance temperature of 30° C. About two hours after beginning of the accident, the release-fraction of iodine increases because of the increase in relative humidity of the off-gas and finally reaches nearly 80 %. A similar type of accident is shown in Fig. 12, here heater 1 goes out of order firstly and after about 4.5 hrs the heater 2 fails. When the gas temperature behind heater 2 drops to 40° C, the release-fraction of iodine increases clearly. The time taken to repair the heaters is assumed to be 8 hrs. After repairing heater 1, the release fraction is nearly at once very low again and therefore

the simulation stops after 8 hrs. The effect of filter-loading has not been shown in both Figures as the iodine filters were almost empty in both simulation-trials. In the third example (Fig. 13) there is a gap of 7 hours between the failures of the two heaters. Thus, after 8 hours, when the repair of the first defect heater is finished, the temperature of the gas has not fallen down to such a level which could have resulted in a severe increase in the release-fraction. After 8 hrs, at the time of the lowest temperature, the release-fraction is still below 10^{-2} % and then becomes less temporarily. By this time, however, the iodine loading of the iodine filter has become excessive and once more the release-fraction increases. That is caused by the strategy decided for the simulation of the behavior of the personnel of the off-gas section. It was assumed that while repairing defect components no maintenance work, for example, change of filter, will be undertaken. The release of iodine varying with the timely sequence of the accident has been shown as follows:

A total number of 37 random trials 'both heaters defect' were carried out. On average 120 gms of iodine were released. The release of iodine in each case is as:

- in 11 trials less than 1 gm
- in 4 trials between 1 and 1o gm
- in 6 trials between 10 and 100 gm
- in 16 trials between 100 and 425 gm.

This finally leads to the conclusion, that the interaction of the components of a multibarrier system can be described adequately by the method of dynamic accident analysis. The insight in the behavior of technical systems under accidental conditions is significantly better than that gained with former (static) methods.

6. REFERENCES

/1/ R. Storck: "Eine Methode zur probabilistischen Risikoanalyse unter Verwendung dynamischer Freisetzungsmodelle". Ph. D. thesis, TU Berlin (1979)

/2/ J. Furrer, R. Kaempffer, A. Linek, A. Maerz: "Results of Cleaning Dissolver Off-gas in the PASSAT Prototype Dissolver Off-gas Filter System". CONF - 801038, p. 566 (1980)

/3/ S. K. Friedlander: "Theory of Aerosol Filtration". Ind. and eng. Chem. 50 (1958)

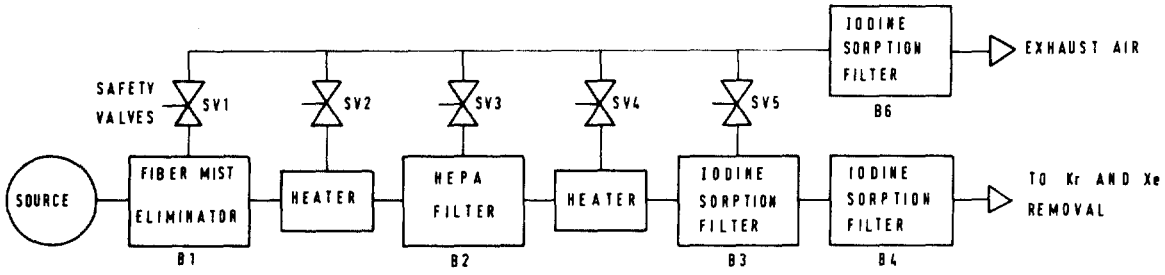

FIG. 1: BLOCKDIAGRAM OF THE AEROSOL- AND IODINE-FILTRATION FACILITY (PASSAT)

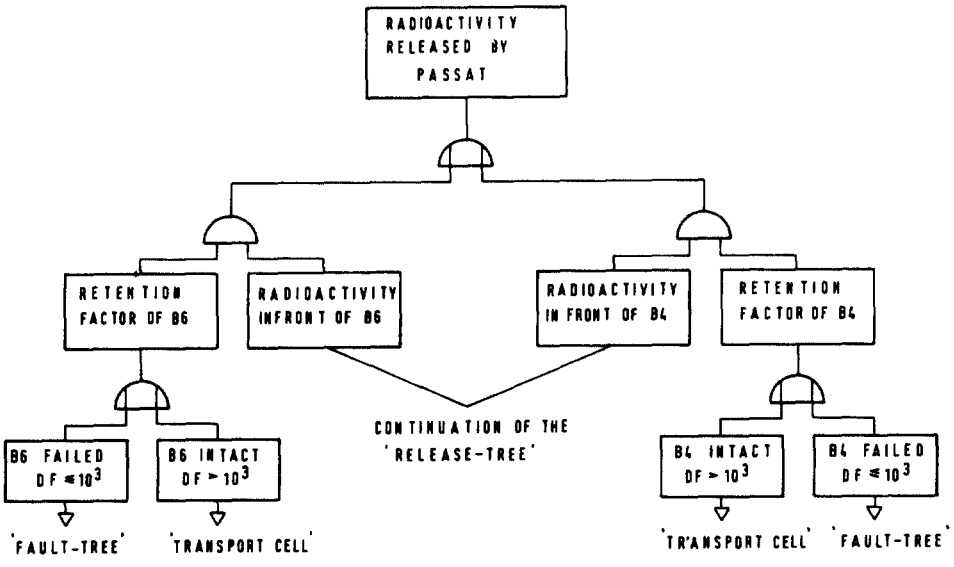

FIG. 2: DETAILS OF THE 'RELEASE-TREE' FOR PASSAT

1: VOLUME FLOW RATE (Nm^3/h)

2: AEROSOL-CONCENTRATION (g/Nm^3)

3: IODINE-CONCENTRATION (g/Nm^3)

4: AEROSOL-DIAMETER DISTRIBUTION
(4 CHARACTERISTIC GROUPS)

5: GAS TEMPERATURE (^oC)

6: REL. HUMIDITY (%)

7: PRESSURE (MBAR)

8: PRESSURE DROP (MBAR)

FIG. 3: LIST OF VARIABLES CONSIDERED

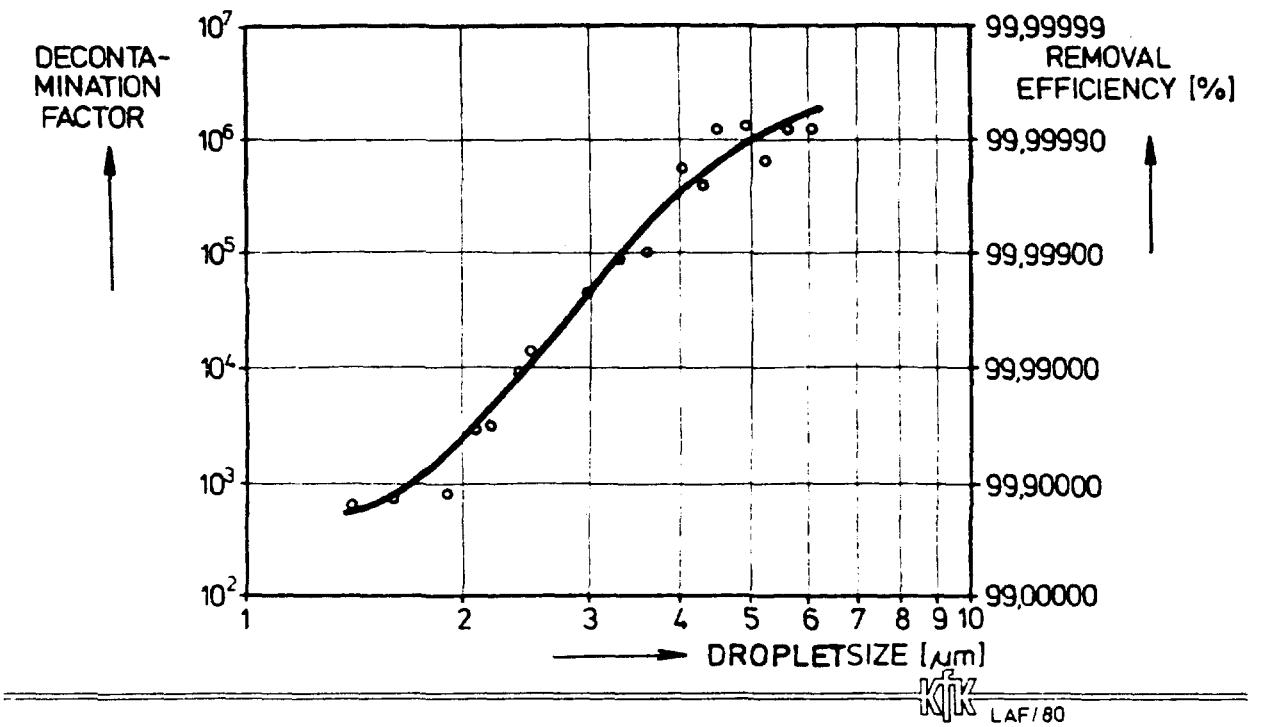

FIG. 4: DECONTAMINATION FACTOR AS A FUNCTION OF DROPLET SIZE (PFME/ 5 cm)

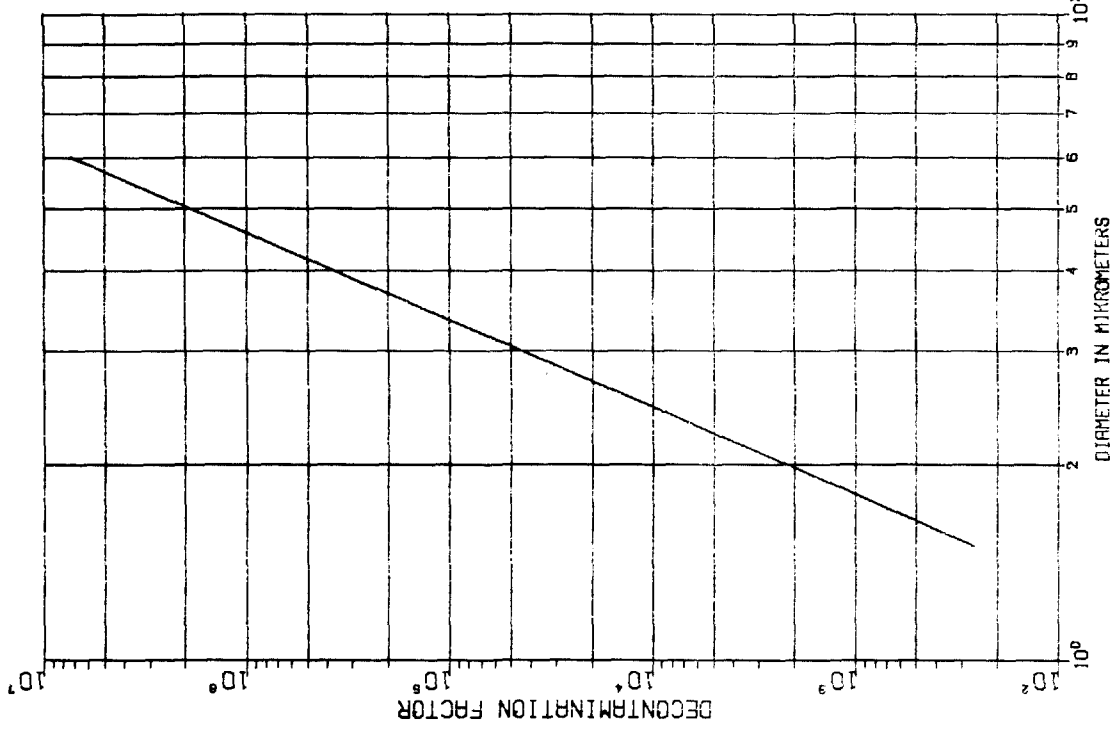

FIG. 5: DECONTAMINATION FACTOR AS A FUNCTION OF PARTICLE DIAMETER

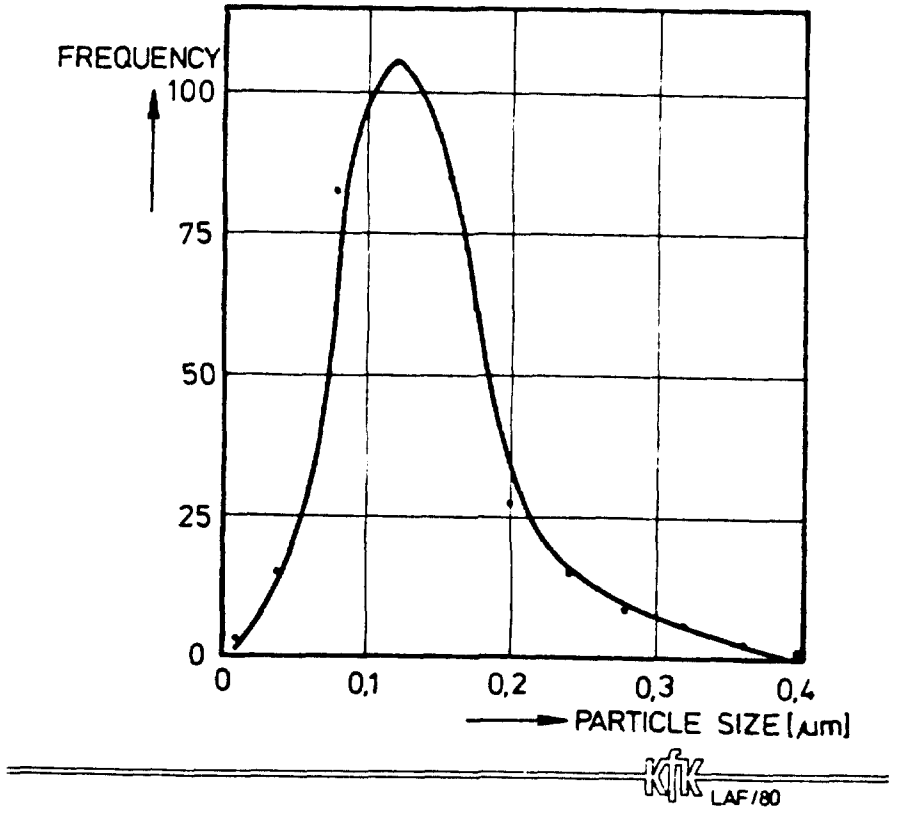

FIG. 6: URANIN PARTICLE SIZE DISTRIBUTION

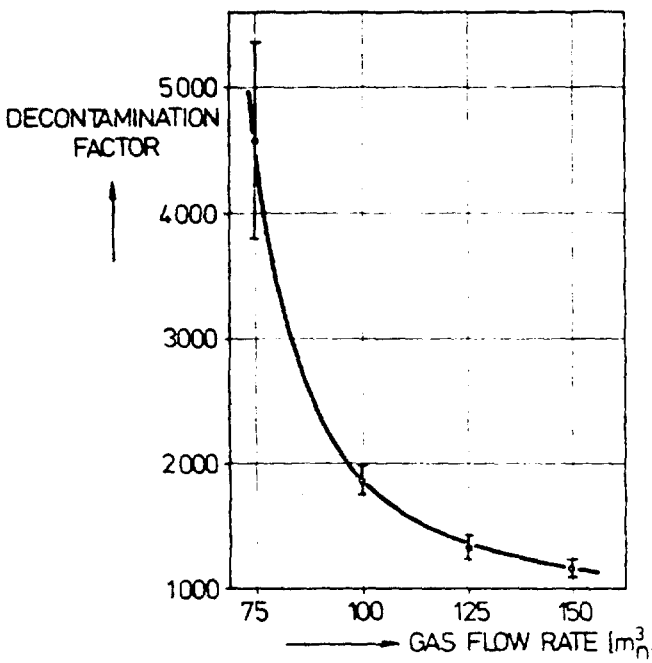

FIG. 7: DECONTAMINATION FACTOR AS A FUNCTION OF FLOWRATE AT PFME (5 cm)

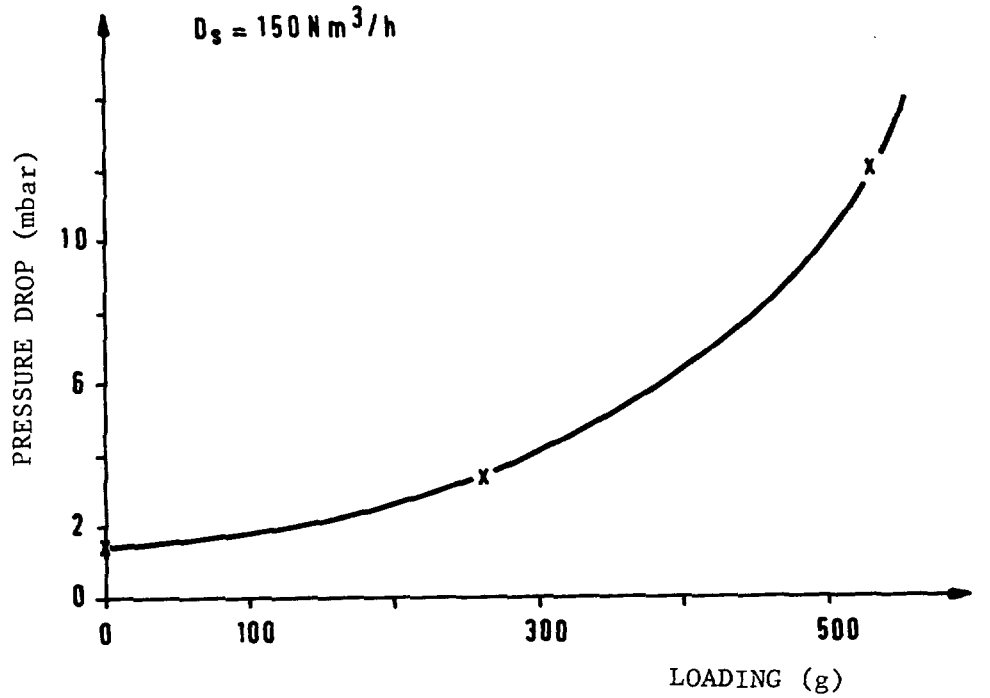

Fig. 8: PRESSURE DROP OF THE HEPA-FILTER AS A FUNCTION OF LOADING

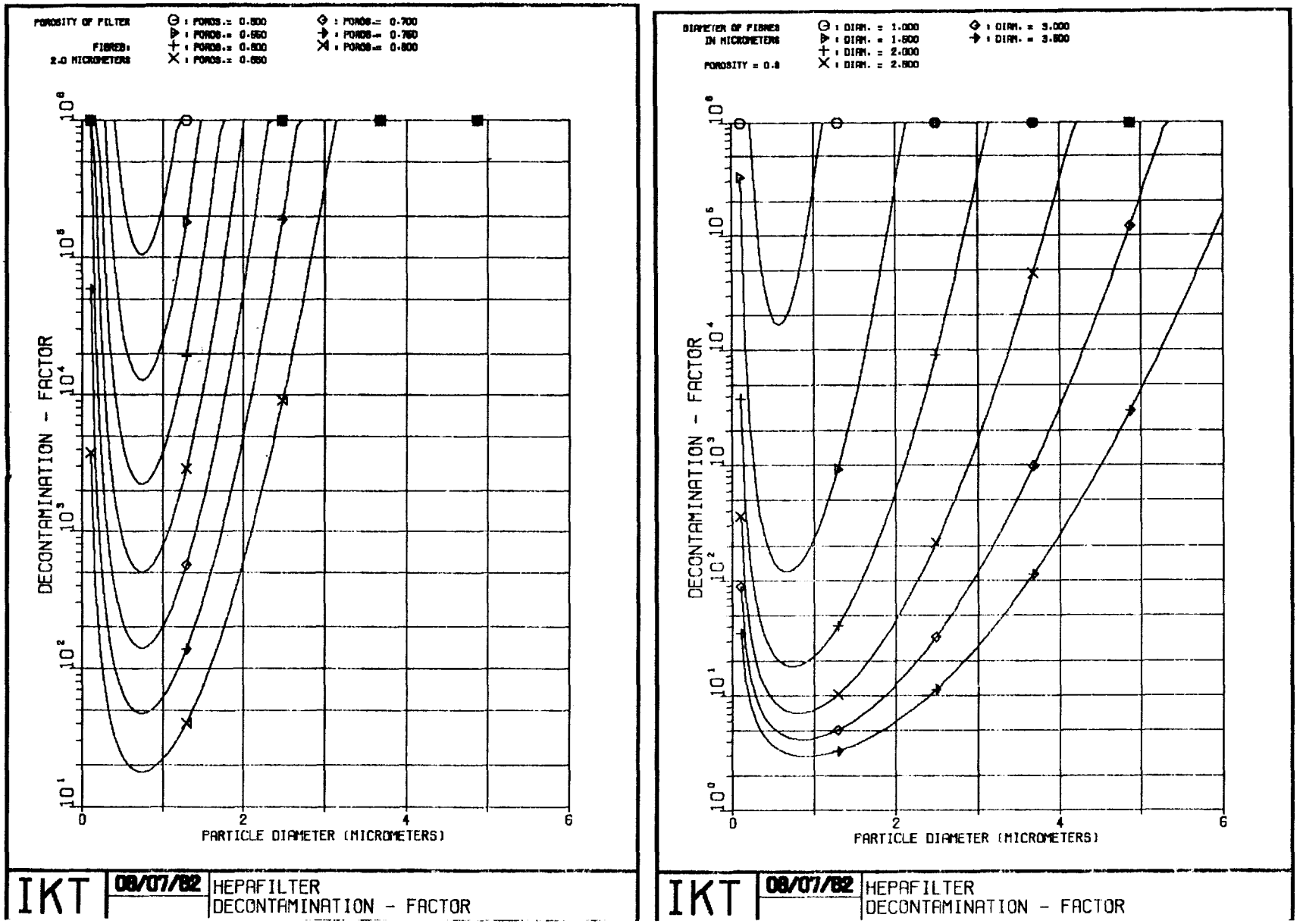

FIG. 9: DECONTAMINATION FACTOR OF THE HEPA-FILTER AS A FUNCTION OF PARTICLE DIAMETER

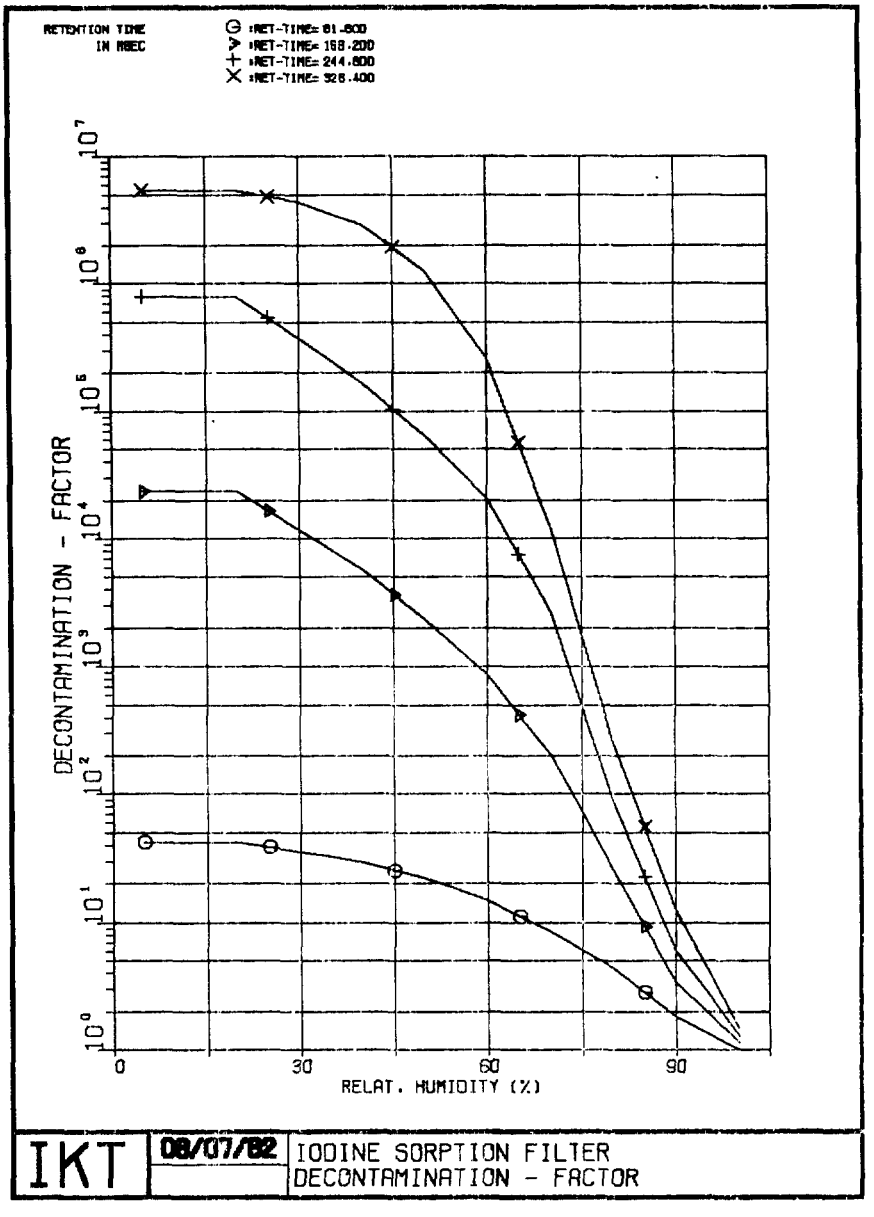

FIG. 10: DECONTAMINATION FACTOR OF THE HEPA-FILTER AS A FUNCTION OF RELATIVE HUMIDITY

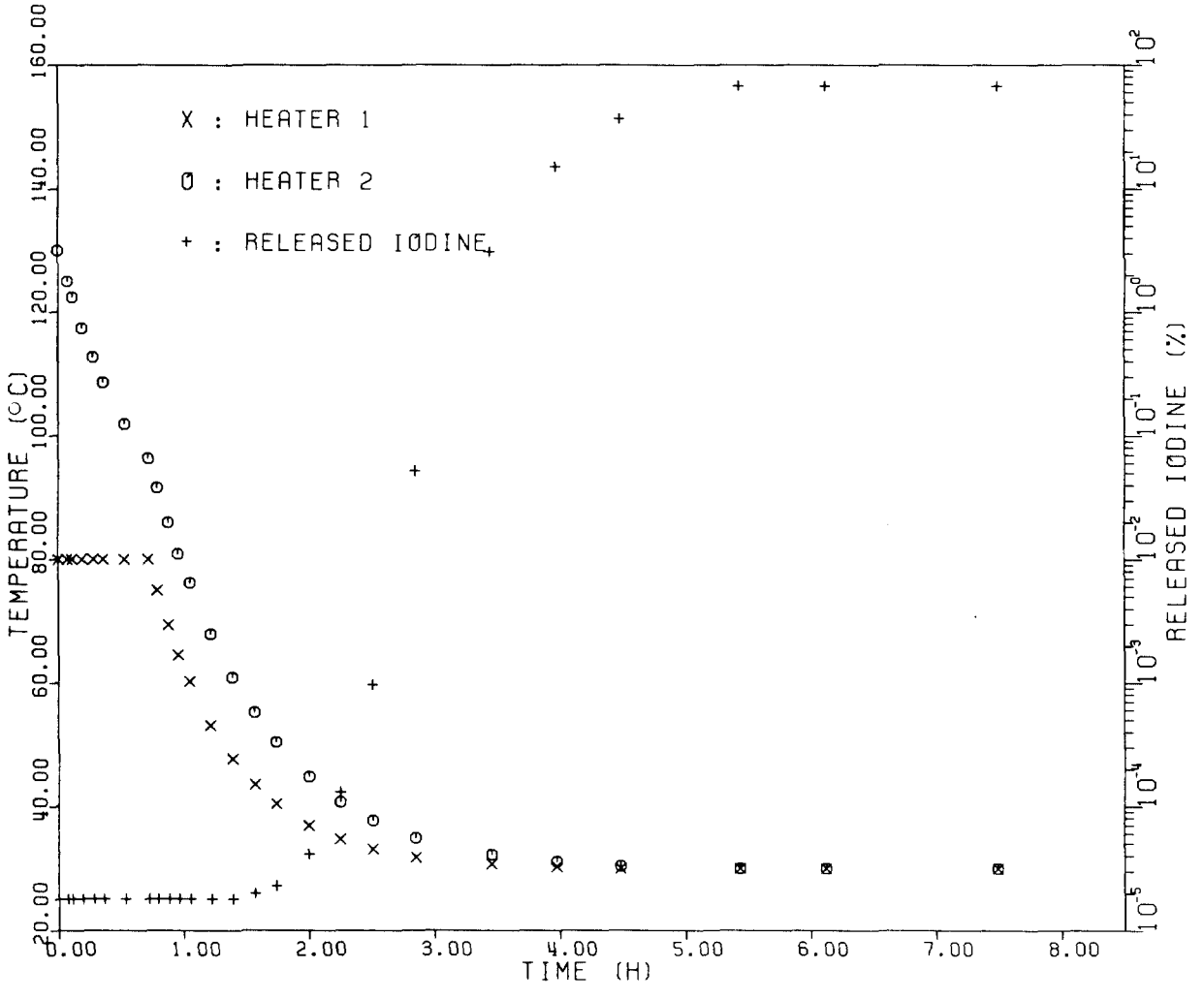

FIG. 11: TIME DEPENDENCE OF THE FAILURE OF BOTH HEATERS WITHIN 8 HOURS AND ACCORDING THE CHANGE OF IODINE RELEASED:

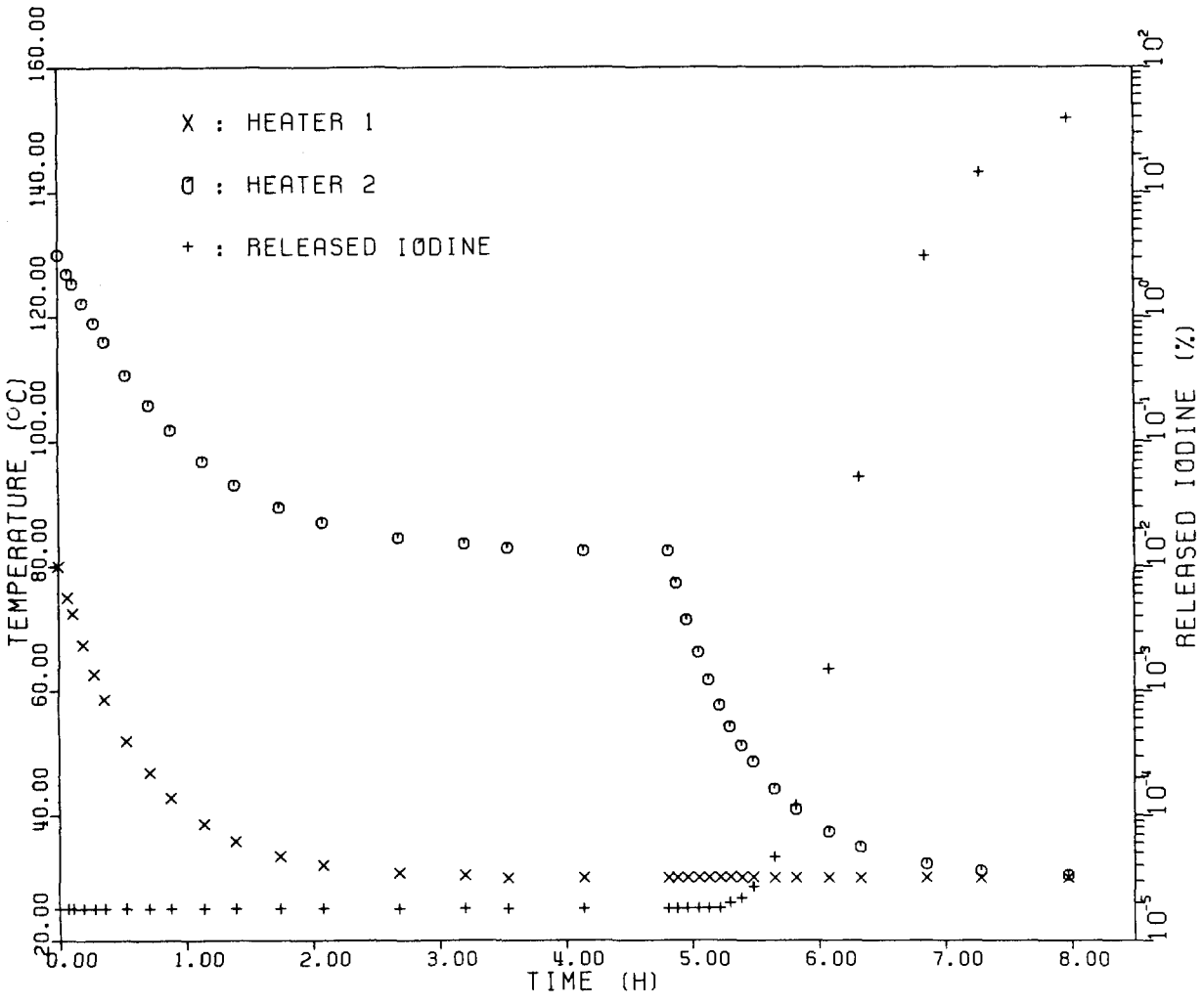

FIG. 12: TIME DEPENDENCE OF THE FAILURE OF BOTH HEATERS WITHIN 8 HOURS AND ACCORDING THE CHANGE OF IODINE RELEASED

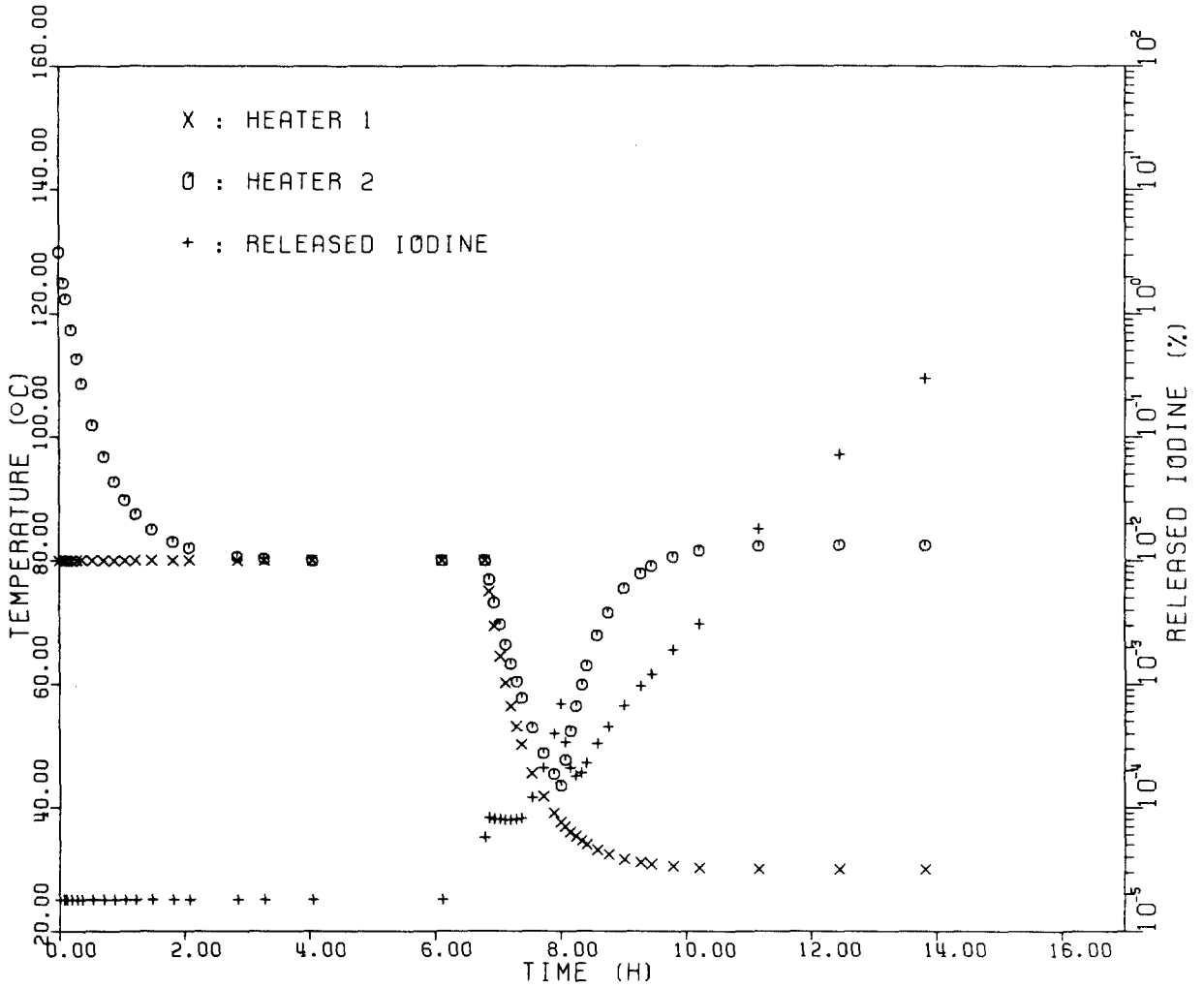

FIG. 13: TIME DEPENDENCE OF THE FAILURE OF BOTH HEATERS WITHIN 8 HOURS AND ACCORDING THE CHANGE OF IODINE RELEASED

DISCUSSION

MOELLER: What quantities of radioactive material would the iodine releases you described represent?

FURRER: If the two heaters were out of operation, which we don't believe would happen, the release of iodine would be some number of Ci. If the PASSAT heater has a failure, we would have a signal from the temperature controller. In a future plant the offgas stream will be switched to a second heater.

Kovach, J.L.: What is the probability of the heater failures that would result in an iodine release?

FURRER: The probability is very low. After three years of experimental work at the PASSAT DOG cleaning facility, we had only one failure at the heater in front of the iodine filter.

A MODEL OF IODINE-129 PROCESS DISTRIBUTIONS IN A NUCLEAR FUEL REPROCESSING PLANT

G. J. McManus
F. A. Duce
S. J. Fernandez
L. P. Murphy

Exxon Nuclear Idaho Co.
Idaho Falls, Idaho, USA

ABSTRACT

This paper documents the development, demonstration and verification of a model of iodine-129 pathways in a nuclear fuel reprocessing plant. Laboratory experimental results are presented on iodine-129 chemical forms and also on evaporator and solvent extraction behavior. In-plant sampling results for all accessable processes are also reported. A computer program using the developed model is documented. Although the ICPP is somewhat unique in its processes it is believed these results can be applied to other types of fuel reprocessing plants.

I. INTRODUCTION

All fuel reprocessing plants subject to EPA regulations must isolate at least 99.75% of the iodine-129 in the spent fuel from the environment. Therefore, all pathways in a nuclear fuel reprocessing plant containing greater than 0.25% of the original iodine-129 must be identified and characterized. This characterization must include all parameters influencing eventual recovery and fixation of the iodine-129 from process solutions, including ^{129}I concentration, chemical form, and volatility.

Other researchers have attempted to address this problem. Berg and Schottelhopf attempted to close the iodine-129 mass balance around the WAK (Karlsruhe)[1]. Yet because greater than 99% of the ^{129}I is volatilized at the WAK into the dissolver off-gas, the partition of the remaining ^{129}I into the downstream off-gas and liquid streams was uncertain due to the small amounts being measured. The release of greater than 99% of the iodine-129 into the dissolver off-gases may not be representative of non-Euorpean fuel reprocessing plants. European plants such at the WAK, use high temperature fumeless dissolving where oxygen is added directly to the dissolver solution. This oxygen would subsequently oxidize any iodide to I_2, which is then sparged from the dissolver into the off-gas.

However, in fuel reprocessing plants not using fumeless dissolution (Purex, electrolytic, etc.) pathways may be considerably different from those found in the European plants. This study was undertaken to measure the iodine-129 pathways in a more typical or "generic" fuel reprocessing plant.

The generic fuel reprocessing plant proposed by Davis[2] is shown in Figure 1. In this fuel reprocessing plant, the nuclear fuel is delivered to a head-end step (graphite burner, volixidizer, etc.); the iodine-129 may be partially released in this step (but much less than 99%). After dissolution, successive steps include solvent extraction, nitric acid recovery, and liquid waste management.

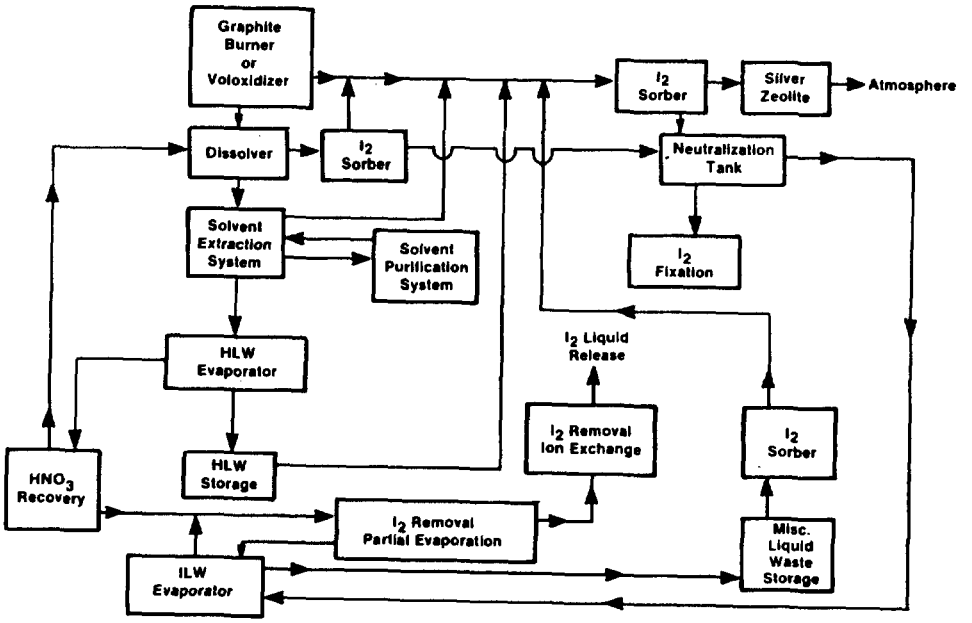

Figure 1. Generic Fuel Reprocessing Plant

ICPP-S-7884

To measure the iodine-129 pathways in a fuel reprocessing plant similar to that shown in Figure 1, a three phase program was undertaken: laboratory evaluation, in-plant sampling, and development of a computer model. The first phase was used to identify those processes most likely to be major pathways and to permit modeling of those unit operations impossible to measure at ICPP. This phase included a laboratory evaluation of the process chemistry, a review of past experience at the Idaho Chemical Processing Plant (ICPP), and simulation of individual process unit operations.

The second phase was the actual in-plant measurement of the iodine-129 pathways. The ICPP was chosen as a suitable site to measure these iodine-129 pathways because it does not use fumeless dissolution and both separation and waste management activities are performed at the same site. A block diagram of possible pathways at the ICPP is shown in Figure 2. All possible pathways identified by Davis[2] are present except the head-end step. However, since it is not clear at the present time that a head-end step will be required at future reprocessing plants, this may not be a significant deficiency.

The third phase was the compilation of the pathways analyses into a single computer program. This program must be sufficiently flexible to predict the effect of changes in process conditions on iodine-129 releases. Therefore, a fuel reprocessing plant that differs in some respects from ICPP can still be described by the results presented here.

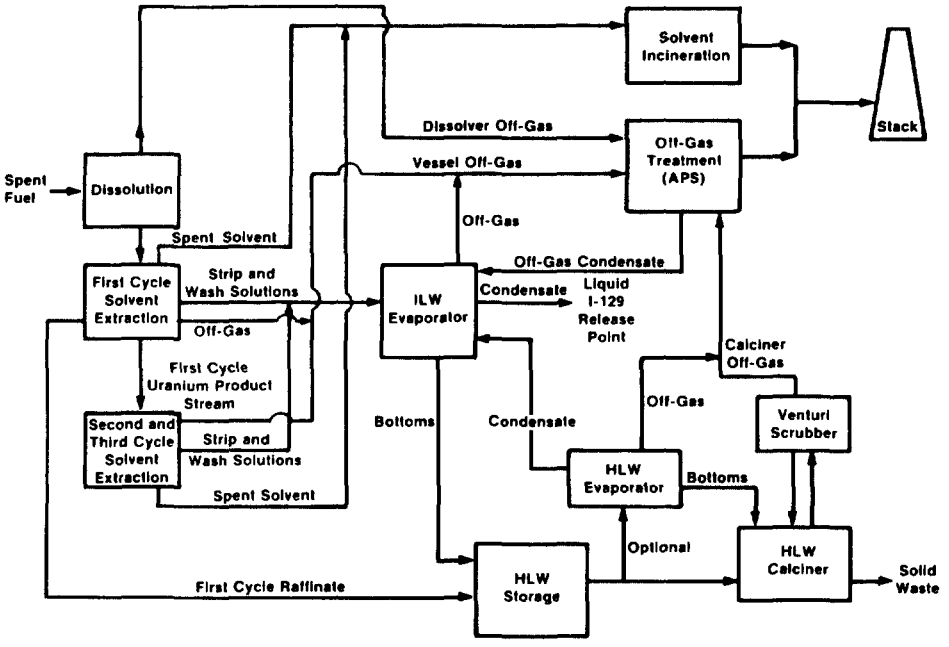

Figure 2. ICPP Pathways Block Diagram

ICPP-S-7882

II. LABORATORY EVALUATION

The purpose of the laboratory evaluation was to identify those processes most likely to be major pathways and to permit modeling of those unit operations impossible to measure in situ. To accomplish these goals, the laboratory evaluation was performed in three phases: 1) statistically correlate past off-gas and liquid iodine-129 releases with plant processes to identify the major release points of iodine-129; 2) determine the chemical forms of iodine-129 in the liquid process streams; and 3) determine the chemical and physical behavior of ^{129}I in different plant processes. Each of these phases is discussed in the following sections.

Statistical Correlation of Past Iodine-129 Releases

Liquid iodine-129 discharges for calendar years 1977-1979 and airborne iodine-129 releases for calendar years 1978-1980 were submitted to multivariate analysis to identify the most probable ^{129}I pathways. Multivariate analysis methods, such as factor analysis, can obtain information about a process' contribution to the ^{129}I release based on the radionuclides concentrations in a large number of samples. If one or more radionuclides originate from the same source as does the iodine-129, their variation as a function of time will be similar. By detecting this common variability, sources can be identified.

Multivariate analysis begins with the construction of a correlation matrix. This correlation matrix is constructed by calculating the linear correlation coefficients between each combination (taken two at a time) of nuclides in the data set. Correlation matrices for aqueous ^{129}I discharges were calculated (one each) for the years 1977-1979. Similarly, matrices for airborne iodine-129 releases were calculated (one matrix each) for the years 1978-1980. The eigenvalues of these matrices were

then calculated. The number of significant sources and their relative contributions were then calculated from these eigenvalues.

The eigenvalues for the airborne iodine-129 releases for the years 1978-1980 indicate only one major source with one or possibly two minor sources. Table I shows the major sources and the amount of the ^{129}I variation attributable to each source. From inspection of the airborne ^{129}I correlation matrices, ^{129}I correlated with ^{14}C, ^{3}H, ^{125}Sb ^{154}Eu, and ^{134}Cs in 1980; with ^{14}C, ^{144}Ce, and ^{90}Sr in 1979; and with ^{60}Co in 1978.

The correlation with ^{3}H, ^{14}C, and ^{125}Sb in 1980 and ^{14}C in 1979 indicates the Waste Calcining Facility (WCF) is the probable release mechanism and represents source 1 in Table I. Two additional facts that suggest source 1 is the WCF (calciner) are the following. First, 50% of all the iodine-129 was released from January to October when only the calciner operated. Secondly, the calciner was the only major process operating in 1979. The minor source (source 2 in Table I) is probably related to dissolution and uranium separation. This would account for the observed correlation of ^{129}I with the fission products ^{144}Ce, ^{134}Cs, and ^{154}Eu since these fission products are associated with dissolution and solvent extraction. Source 3 in Table I probably represents a summation of unaccountable minor sources and random analytical errors.

The eigenvalues for the liquid ^{129}I releases for the years 1977-1979 are similar to the airborne results in that only one significant source is indicated, with one or possibly two minor sources as shown in Table II. Examination of the correlation matrices shows that ^{129}I correlated with ^{106}Ru, ^{238}Pu, and ^{154}Eu in 1977; with ^{90}Sr, ^{137}Cs, ^{238}Pu, and ^{154}Eu in 1978; and with ^{152}Eu and ^{154}Eu in 1979.

TABLE I

MAJOR SOURCES OF AIRBORNE IODINE-129 RELEASES FOR 1978-1980 AND THEIR RELATIVE SIGNIFICANCE

Source	1978 % Variance	1979 % Variance	1980 % Variance
1	37	55	57
2	21	17	21
3	15	13	14

TABLE II

MAJOR SOURCES OF LIQUID IODINE-129 RELEASES FOR 1977-1979 AND THEIR RELATIVE SIGNIFICANCE

Source	1978 % Variance	1979 % Variance	1980 % Variance
1	44	40	47
2	23	18	24
3	33	42	29

The correlation with ^{106}Ru in 1977 and with $^{152, 154}Eu$ in 1978 and 1979 indicate that some process related to the extraction columns is involved. This conclusion is based on the high distribution coefficients for ruthenium, actinides and lanthanides in TBP (tributyl phosphate). Two additional facts that support this interpretation are the following. First, 90% of the iodine-129 released during 1978 was during July-October. This time period corresponds with the operation of the first-cycle extraction columns. Secondly, evaporator condensate samples were collected on 27 September 1980 (before first-cycle startup) and on 15 October 1980 (after first-cycle operation began). When analyzed for ^{129}I these samples contained $<1 \times 10^{-6}$ $\mu Ci\ ^{129}I/mL$ and 1.2×10^{-4} $\mu Ci\ ^{129}I/mL$ respectively. These results indicate that extraction activities were a significant source of iodine-129.

The other minor source (source 2 in Table II) is probably related to calciner operations. The most probable pathway of iodine-129 from the calciner to the aqueous release point would be condensation of iodine-129 from the calciner off-gas. Again, source 3 in Table II probably represents the sum of the contributions from minor, unaccountable sources and random analytical errors.

Iodine-129 Species Distribution

As noted in the previous section, the statistical correlations indicated that the caliciner is a significant source of the iodine-129 released to the atmosphere. For this to occur, a substantial amount of iodine-129 must be in the calciner feed. Therefore, experiments were performed to measure total ^{129}I and the chemical species distribution in calciner feed solutions.

Using a previously reported ^{129}I species separation procedure[3] five calciner solutions were analyzed. The samples were; (1) and (2) calciner scrub solutions; (3) a 5 to 1 mixture of high-level zirconium fluoride and high sodium concentration waste; (4) high-level zirconium fluoride waste; and (5) a 5 to 1 mixture of zirconium fluoride waste and high sodium concentration waste blended with recycled scrub solution. The scrub solutions were 2M HNO_3 used to scrub the WCF off-gas. The results of these analyses are shown in Table III.

TABLE III

RESULTS OF ^{129}I ANALYSIS OF WASTE CALCINER SOLUTIONS

Sample Number	Reduced ^{129}I (nCi/mL)	Oxidized ^{129}I (nCi/mL)	Percent Reduced ^{129}I
1	1.81±0.20	0.47±0.05	80±12
2	0.89±0.09	0.40±0.04	69±10
3	0.49±0.05	0.34±0.04	59±9
4	Total ^{129}I =	1.53±0.20	
5	1.14±0.20	0.58±0.06	66±5

It appears from these limited data that the iodide/total iodine ratio is a constant (2/3). At this point an attempt was made to develop a thermodynamic model of the calciner feed solution consistent with the determined I^-/total iodine ratio. The pertinent equilibrium equations and oxidation/reduction potentials are shown below in equations 1-5.

$$H_5IO_6 + H^+ + e^- = IO_3^- + 3H_2O \ (-1.7\ V) \quad (1)$$
$$IO_3^- + 5H^+ + 4E^- = HOI + 2H_2O \ (-1.14\ V) \quad (2)$$
$$HOI^- + H^+ + e^- = \tfrac{1}{2}\ I_2(aq) + H_2O \ (-1.15\ V) \quad (3)$$
$$HOI = H^+ + OI^- \quad (4)$$
$$\tfrac{1}{2}\ I_2\ (aq) + e^- = I^- \ (-0.83\ V) \quad (5)$$

These equilibrium equations were thought to be the most appropriate in the pH range (0 to -0.2) and oxidation-reduction potential (+800 to +850 mV) found in calciner feed solutions.

From equation 1-5 the preponderance area diagram shown in Figure 3 was constructed using well known graphical techniques[4]. The diagram plots logarithmic oxidation-reduction potential versus logrithmic H^+ activity (i.e., pE vs pH). Each area of the diagram is labeled with the single most predominant species for the pE and pH conditions of that area. Lines between areas graphically represent the pE and pH values at which species adjacent to the lines are in equal concentrations. Equilibrium equations, in logarithmic forms, for the equilibrium lines are also shown in Figure 3. The system pE and pH were measured and are shown on the diagram as a black square.

Solution of equilibrium Equation 2 with these data predicts that 73% of the total iodine is present as iodide ion. This is in excellent agreement with the experimental results obtained by the resin technique of 69 ± 9% iodide ion.

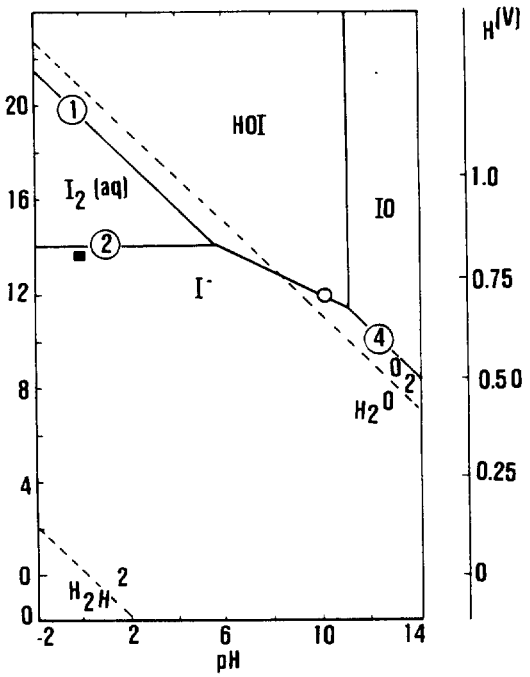

Figure 3. pE vs pH For Iodine System ICPP-S-4

Laboratory Simulation of First-Cycle Solvent Extraction Flowsheet

A series of laboratory experiments were performed to better determine the pathways of ^{129}I through a uranium recovery solvent extraction scheme. The experiments simulated the first-cycle extraction flowsheet shown in Figure 4. All tests were done in 250 mL glass separatory funnels with ^{125}I as a tracer. Six extraction tests were performed: three using a simulated coprocessing feed (coprocessing feed is similar to zirconium feed except it contains mercuric nitrate) and three using a simulated zirconium feed. Milligram quantities of stable iodine-127 (added as I^-) were added to one of the zirconium extractions and to two of the coprocessing extractions. The iodine-125 tracer was added to the feed and allowed to equilibrate overnight. Previous work has shown this equilibration time to be sufficient for isotopic exchange.[3] Equal amounts of aqueous feed and organic (10% TBP in tetradecane) were then mixed together in the separatory funnel for one to two minutes. After separating, the aqueous and organic phases were drawn off and counted separately on a Low Energy Photon Spectrometer (LEPS) to determine the iodine-125 distribution. Similar tests were done for the other four unit operations. The results of all six tests are presented in Table IV.

TABLE IV

Unit Operation	Aqueous Composition	Distribution Coefficient
Extraction (Zr)	Zr Waste	4
Extraction (coprocessing)	Zr Waste + Hg	4
Scrub	0.7M $Al(NO_3)_3$ + 0.3M $NH_4(OH)$	7.2
First Strip	0.005M HNO_3	<30
Second Strip	0.04M HNO_3	9.2
Cabonate Wash	0.1M Na_2CO_3	9.9

As shown in this table, the majority of the iodine remains in the organic and is not easily stripped. Therefore, there will be an iodine-129 buildup in the organic phase until equilibrium is reached. Based on the distribution coefficients shown in Table IV, equilibrium will be reached after the organic has been cycled 5-10 times. After equilibrium has been reached, 80-90% of the iodine-129 entering the extraction column will exit with the raffinate. The remaining iodine-129 leaving the extraction column is then distributed to second-cycle extraction, to the ILW waste evaporator, and to the solvent burner.

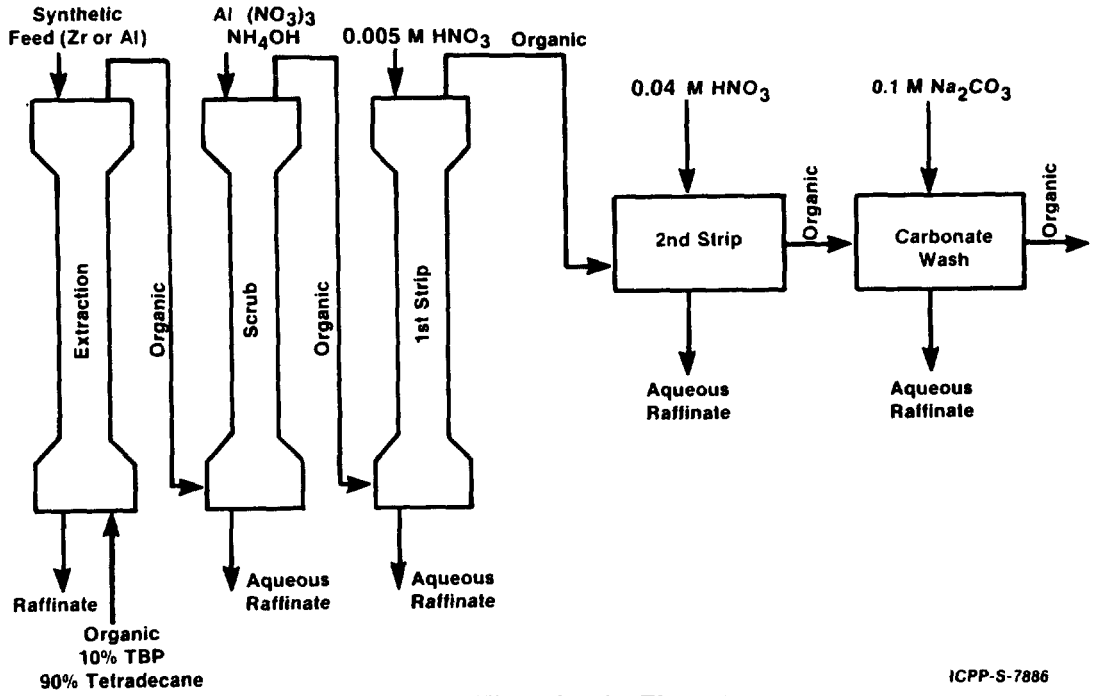

Figure 4. First Cycle Flowsheet

To determine the effect of chemical form on the iodine-129 distribution coefficient, the chemical species distribution before and after extraction was measured by the anion exchange method previously presented. The first cycle distribution coefficient varied from 8.6 for the reduced chemical forms to 0.83 for the oxidized forms. This means either that the iodine species distribution must be known to predict the solvent extraction behavior of iodine-129, or a range of distribution coefficients must be used in the model.

Laboratory Simulation of HLW Evaporator

Since statistical correlations identified the evaporation process as a liquid ^{129}I release pathway, a HLW evaporator was simulated in the laboratory. Using the apparatus shown in Figure 5 two types of HLW, each containing ^{125}I tracer, were investigated. Table V shows the composition of these two wastes.

Each of these two wastes was evaporated with different distillation rates and for each of these rates the iodine-125 in the condensate, bottoms, and off-gas was measured (Table VI). As indicated in Table VI, no more than 4% of the iodine was emitted to the off-gas during evaporation. The fraction of the iodine in the condensate is significantly higher for Type 2 wastes and increases slightly at higher distillation rates. Therefore, the major iodine-129 pathway leaving the HLW evaporator appears to be the condensate waste stream that leads to the ILW evaporator. The high solubility of the volatilized iodine suggests the formation of I_2 during HLW evaporation, but this question was not addressed in these experiments.

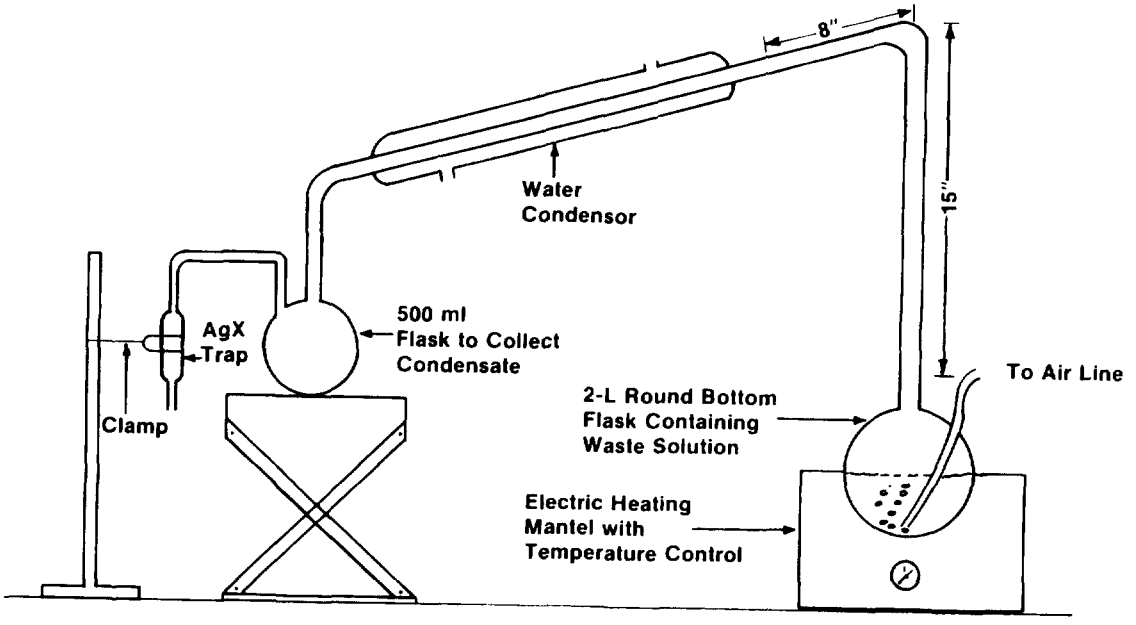

Figure 5. HLW Evaporator Simulation Apparatus

ICPP-S-7887

TABLE V

Species	Waste Type 1 (Molar Concentration)	Waste Type 2 (Molar Concentration)
H^+	1.26	1.40
Al^{3+}	0.51	0.65
$Fe^{2+,\ 3+}$	0.064	0.039
F^-	0.068	0.016
Cl^-	0.0008	0.0073
Na^+	0.0222	0.67
NO_3^-	3.34	4.40
SO_4^{2-}	0.041	0.76

TABLE VI

RESULTS OF HLW EVAPORATOR SIMULATION[a]

Feed Type	Distillation Rate (mL/min)	^{125}I In Condensate (%)	^{125}I In Bottoms (%)	^{125}I In Off-Gas (%)
1	1.13	58	16	2
1	1.43	45	39	1
1	2.93	54	23	1
2	1.39	38	23	4
2	1.46	64	24	4
2	2.90	84	19	1

[a] Percentages may not add to 100% due to analytical uncertainties

III. IN-PLANT SAMPLING

To verify the data from the laboratory studies, actual plant processes were sampled, including:

1) Waste solidification feed solutions, scrub solutions, and off-gas;
2) Dissolver off-gas;
3) First-cycle raffinates:
4) ILW evaporator (Process Equipment Waste or PEW) condensates, bottoms, and off-gas;
5) Other process off-gases.

The results of the in-plant sampling are presented in the following sections.

Waste Solidification (WCF) Sampling

From the previous laboratory analysis, it is apparent that more than 80% of the iodine-129 charged to the first-cycle solvent extraction processes remains in the aqueous raffinate and is eventually solidified in the calciner. In addition, the statistical correlations presented previously showed that the calciner is a major airborne release mechanism for iodine-129. Therefore, an iodine-129 mass balance was performed around the calciner to better characterize calciner emissions.

Two sample periods were used to perform the mass balance calculations. The first period was after four months of operation and the second was after one week. Each sample period consisted of raw feed and scrub solution samples and off-gas samples taken at calciner stations 3, 4, 5, and after the Atmospheric Protection System (APS) (Figure 6). The results of mass balance calculations for periods 1 and 2 are shown in Figures 7 and 8, respectively.

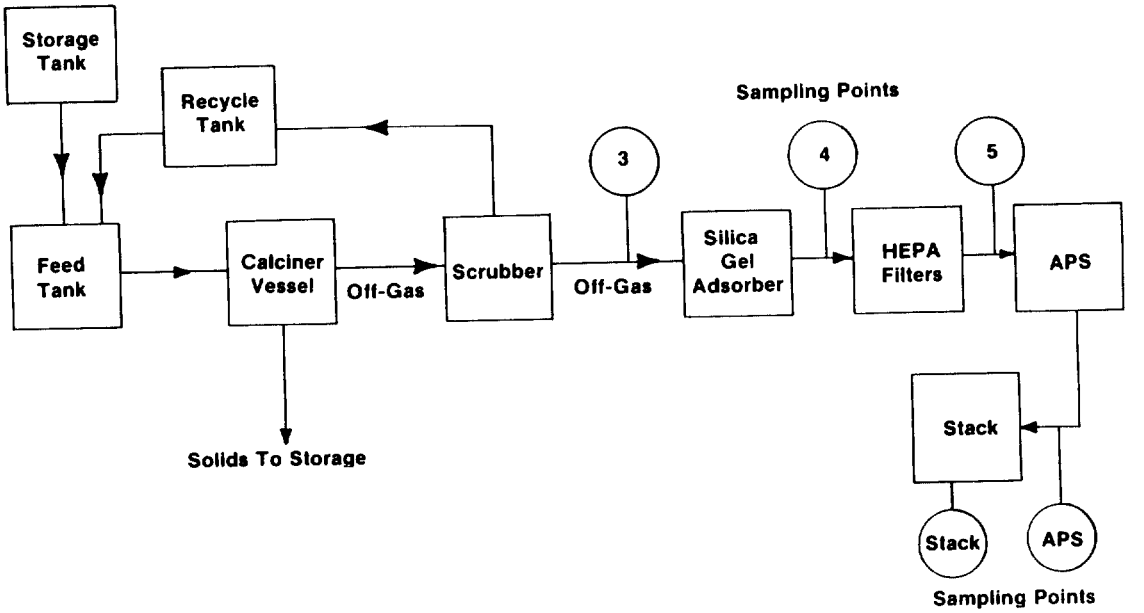

Figure 6. WCF Off-Gas System

ICPP-S-3861

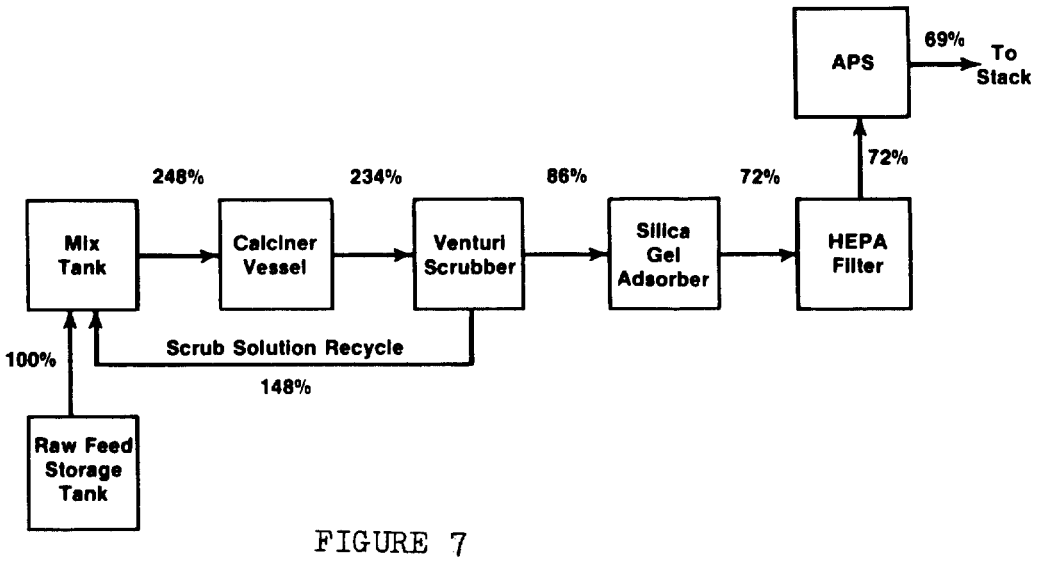

FIGURE 7

WCF MASS BALANCE AFTER 3 MONTHS OPERATION

ICPP-S-8517

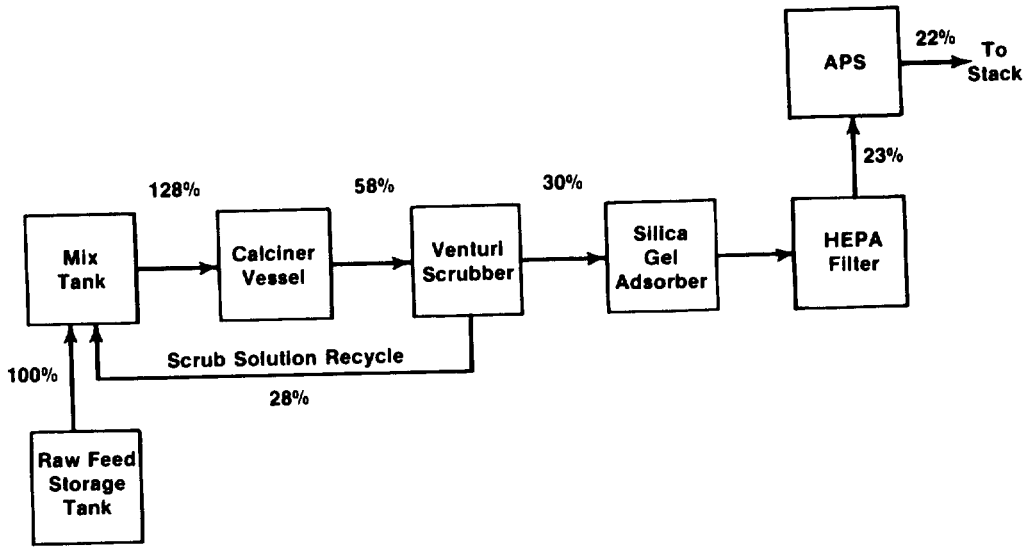

FIGURE 8

WCF MASS BALANCE AFTER 7 DAYS OPERATION

ICPP-S-8511

The following conclusions were drawn from the data presented in Figures 8 and 9.

1) Between 14% and 31% of the iodine-129 charged to the calciner as blended feed is released to the atmosphere.

2) Iodine-129 builds up in the recycled scrub solution. This is illustrated by the difference in scrub solution concentration between sample period 2 (after one week of operation) and sample period 1 (after four months of operation). This indicates that iodine-129 releases will increase as a calciner run progresses.

3) The combined removal efficiency of the silica gel absorbers, HEPA filters and the APS for iodine-129 is less than 30%, and of the three removal systems, the silica gel absorber is the most efficient control device in the off-gas cleanup system. The transmission of iodine-129 through the calciner vessel appears to increase as a calciner run progresses.

In addition to the mass balance performed for total ^{129}I, the chemical forms of the ^{129}I released to the off-gas were measured. The procedure for performing these measurements is described elswhere[5]. The results of this sampling is shown in Table VII. The significance of the large organic fraction shown in this table is that plateout may be only a minor component of the overall decontamination factor of the off-gas cleanup systems.

TABLE VII

WCF GASEOUS ^{129}I SPECIES DISTRIBUTION

Chemical Form	Fraction Emitted From WCF (%)
I_2	15
HOI	21
Organic	64

Dissolver Off-Gas Sampling

To test the previously presented prediction that the dissolver off-gas was only a minor release point for ^{129}I, in-plant off-gas samples were taken. Both the zirconium fuels dissolution and aluminum fuels dissolution processes were sampled. A diagram of the two off-gas system sampled and the sampler locations are shown in Figure 9.

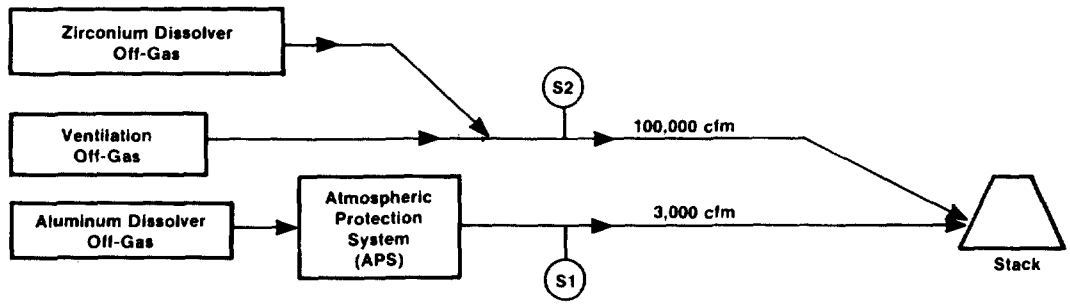

Figure 9. Dissolver Off-Gas Sampling Points

ICPP-S-7885

The location of the aluminum dissolver sampler is shown in Figure 9 as S1. The sampling method has been presented previously[6]. Briefly, two samples were collected on TEDA impregnated charcoal beds with a sample flowrate of 1 L/min. The first sample was taken over a 6.7-hour period; the second sample was collected for 52.8 hours. The average ^{129}I concentration that would be expected if 100% of the ^{129}I was volatilized was calculated and then compared to the amount of iodine-129 found on the charcoal beds. The results are shown in Table VIII. As can be seen from this table, less than 1 percent of the ^{129}I in the spent fuel charged to the aluminum dissolver is volatilized onto the process off-gas.

TABLE VIII

RESULTS OF ALUMINUM DISSOLVER OFF-GAS SAMPLING FOR ^{129}I

Sample	^{129}I Collected (nCi)	Measured ^{129}I Off-Gas Concentration (μCi/cc)	Maximum Possible ^{129}I Off-Gas Concentration (μCi/cc)	Percent ^{129}I Volatilized
1	<0.05	$<1.25 \times 10^{-10}$	1.66×10^{-8}	<0.75
2	<0.05	$<1.58 \times 10^{-11}$	1.66×10^{-8}	<0.10

A slightly different procedure was used for sampling the zirconium off-gas, indicated as position S2 on Figure 9. Longer sample periods and larger sample volumes were required because of the larger amounts of dilution air at S2 (2000:1 dilution versus 60:1 at S1). In addition to charcoal beds, two samples were subsequently collected using silver zeolite beds in the same sampler configuration. After sampling, the beds were homogenized and the ^{129}I counted directly on a LEPS. As was done with the aluminum off-gas, the average amount of iodine-129 that would be released from the zirconium dissolver if 100% of the ^{129}I was volatilized was calculated and then this amount was compared to that found on the samples (Table IX). As can be seen from Table IX, less than 5% of the iodine-129 charged to the zirconium dissolver is volatilized into the off-gas. Therefore, as the sampling of both aluminum and zirconium dissolution suggests, fuel dissolution is not a major iodine-129 released point to the atmosphere.

TABLE IX

RESULTS OF ZIRCONIUM DISSOLVER OFF-GAS SAMPLING FOR IODINE-129

Sample	Bed Type	Sample Duration (min)	Sample Flowrate (L/min)	Measured Off-Gas Concentration (μCi/cc)	Maximum Possible Off-Gas Concentration (μCi/cc)	Percent ^{129}I Volatilized
Background	Charcoal	5640	14.5	2.97×10^{-10}	----	----
1	Charcoal	4633	11.8	$<4 \times 10^{-12}$	4.44×10^{-10}	<0.9
2	Charcoal	4420	12.3	$<4 \times 10^{-12}$	2.75×10^{-10}	<1.5
3	Charcoal	4420	12.6	6.2×10^{-12}	3.92×10^{-10}	1.6
4	Charcoal	6957	11.8	6.3×10^{-12}	4.03×10^{-10}	1.6
5	Silver Zeolite	4320	11.8	2.45×10^{-11}	4.77×10^{-10}	5.1
6	Silver Zeolite	14130	14.8	4.8×10^{-12}	5.30×10^{-10}	0.9
7	Charcoal	16130	14.8	1.74×10^{-11}	4.06×10^{-10}	4.3

Uranium Recovery Process Stream Samples

To verify the laboratory solvent extraction results, actual first-cycle process stream samples were collected. However, due to the high radiation levels only a limited number of streams were sampled. The streams that were sampled and their ^{129}I content are shown in Table X. The two organic feed samples were taken three days apart and indicate that the ^{129}I concentration does reach an equilibrium value. From the organic feed concentration in Table X and the distribution coefficients measured in the laboratory (Table IV), a predicted carbonate wash raffinate concentration of 0.006μCi/L was calculated. This is in reasonable agreement with the measured value of 0.0089μCi/L in Table X. Assuming an average value of 0.016μCi/L for the solvent burner feed solution and an average flowrate of 5L/min, the solvent burner would not release more than 1% of the total ^{129}I processed to the stack.

TABLE X

RESULTS OF THE ^{129}I ANALYSIS FOR FIRST-CYCLE PROCESS STREAMS

Sample Description	Iodine-129 Concentration (μCi/L)
Solvent Burner Feed Solution	0.004
Solvent Burner Feed Solution	0.048
Organic Feed Solution	0.0562
Organic Feed Solution	0.0568
Carbonate Wash Raffinate	0.0089

In-Plant Sampling of ILW Evaporator

Because any aqueous iodine-129 that reaches the environment from the ICPP must pass through the ILW (Process Equipment Waste or PEW) evaporator, a sampling and analysis program around the PEW was performed. Samples of the feed, condensate, and bottoms were analyzed. Two sets of samples were collected: one when only the WCF was operating and one when only the uranium recovery process was operating. The results of both sample periods are summarized in Table XI; the source of iodine-129 to the PEW during each sample period is summarized in Table XII. These tables indicate that when the WCF is in operation the APS condenser accounts for 87% of the iodine-129 sent to the PEW; when the WCF is shutdown it accounts for only 13%. In addition, the amount of iodine-129 sent to the PEW from the APS condenser is an order of magnitude higher during WCF operation than during the uranium recovery process. There-

fore, during WCF operation, the major aqueous release of iodine-129 is due to condensation of calciner off-gas.

This may also explain why the organic fraction of the ^{129}I released from the WCF is high. The inorganic ^{129}I chemical forms would be preferentially condensed leaving behind the organic ^{129}I. Another plausible explanation is possible reactions with unburned kerosene in the calciner vessel. It is also clear that much more ^{129}I is released from the bottoms by the ILW evaporator than from the HLW evaporator. This may be due to the greater organic content of the PEW feed solutions. This conclusion was supported by the fact that the evaporator iodine off-gas emissions were almost entirely comprised of organic iodides[5].

TABLE XI

RESULTS OF IODINE-129 ANALYSIS OF PEW EVAPORATOR FEED SOLUTION, CONDENSATE, AND BOTTOMS

Operation	Off-Gas (Percent of Total)	Condensate (Percent of Total)	Bottoms (Percent of Total)
WCF	<10	>90	<1
URANIUM PROCESSING	<10	>90	<1

TABLE XII

SOURCES OF IODINE-129 IN PEW

Operation	Fraction ^{129}I from APS Condenser (%)	Fraction ^{129}I from Stored Waste (%)
WCF	87	13
URANIUM PROCESSING	13	87

Other Processes Off-Gas Sampling

In addition to the off-gas sampling already described, three other off-gas streams were sampled; 1) the APS process off-gas during plant shutdown, 2) ventilation off-gas during plant shutdown, and 3) the vessel off-gas (VOG) system. Insignificant amounts of ^{129}I (<0.25% of inventory during processing) were measured in the process off-gas and ventilation off-gas lines during plant shutdown.

The results of the vessel off-gas sampling showed that the only time detectable quantities of iodine-129 were released was during first-cycle raffinate transfers. This is to be expected because of the atomizing effect of the airlifts used in these transfers. Even though the iodine-129 in the VOG is detectable during transfers (2.9×10^{-12} μCi/cc), the detected ^{129}I accounts for an insignificant fraction of the ^{129}I released from the stack (<0.25%).

IV. COMPUTER MODEL OF IODINE-129 PATHWAYS

Using the data from the laboratory evaluation and in-plant sampling sections of this paper, a computer program that models the ^{129}I pathways was written. The program consists of a series of subroutines based on the major plant processes. These processes include: dissolution and first-cycle extraction, second-cycle extraction, HLW calcination, HLW and ILW evaporation. These subroutines were then combined into the program shown in Appendix I.

Model Verificaton

To verify the accuracy of the computer program four different operating period, representative of each major plant process at the ICPP, were selected. These time periods, not used for in-plant sampling were:

1) Simultaneous operation of zirconium dissolution, first-cycle extraction, and waste calcination;
2) Simultaneous coprocessing dissolution and first-cycle extraction;
3) Simultaneous electrolytic dissolution, first-cycle extraction and HLW evaporation;
4) Only HLW calcination.

The results shown in Table XIII were obtained using the process flowsheet values for flowrates and flow ratios and the laboratory determined values for the distribution coefficients. These results compare the sum of the calculated gaseous and liquid ^{129}I discharges to the sum of the measured gaseous and liquid ^{129}I discharges. The uncertainty in these releases was also calculated based on the total ^{129}I charged to the plant during these periods. This value is of interest since the EPA regulations are based on the total ^{129}I generated in the nuclear fuel cycle. The least uncertainty was during the period when only the WCF was operating. This may occur because all subroutine parameters were determined by in-plant sampling.

The results obtained when the dissolution/first-cycle subroutine is employed are least accurate, with uncertainties ranging from 12-25%. There are three possible explanations. 1) A conservative 5% of the ^{129}I input to the dissolvers is assumed to be released into the off-gas. Since this 5% represents an upper limit, the off-gas release may be overestimated and the input to the solvent extraction columns may be underestimated. 2) The distribution coefficients for the first-cycle solvent extraction column vary from 0.8 for oxidized iodine species to 8 for re-

TABLE XIII

UNCERTAINITY IN PREDICTED ENVIRONMENTAL RELEASES

Processes Operating	Uncertainty Based on Release (%)[a]	Uncertainty Based on Input (%)[b]
Zr Dissolution First-Cycle Extraction Waste Calcination	-11.6%	-4.0%
Al + Zr Dissolution First-Cycle Extraction	+25%	+3.5%
Electrolytic Dissolution First-Cycle Extraction HLW Evaporation	+8.8%	+3.6%
Waste Calcination	+0.5%	+0.4%

[a] Uncertainity Based = $\frac{\text{Calculated - Measured}}{\text{Calculated}} \times 100\%$

[b] Uncertainity Based = $\frac{\text{Calculated - Measured}}{\text{Feed to Plant}} \times 100\%$

duced species. Therefore, small changes in the iodine species distribution will cause large changes in the first-cycle distribution coefficients. Best agreement between predicted and measured environmental releases was obtained with distribution coefficients in the range of 3-4, in agreement with the laboratory experiments presented previously. 3) Historically, the solvent extraction process varies significantly from flowsheet values. These deviations from flowsheet values would result in increased uncertainties.

Overall, it appears the computer program (listed in Appendix I) can predict total environmental ^{129}I releases within 10-25%.

V. CONCLUSIONS

The following conclusions were reached as a result of the work described here. First, two-thirds of the iodine-129 found in the aqueous waste streams is iodide, with the remaining one-third in higher oxidation states. This species distribution can be explained based on the pH and oxidation-reduction potential of dissolver solutions. Only a small fraction (2-5%) of the iodine-129 entering the plant in the spent fuel elements is released into the off-gas during dissolution. The remaining iodine-129 is distributed through the plant processes with waste solidification being the major atmospheric release point and ILW evaporation being the major liquid release point. Only 14-31% of the ^{129}I charged to the HLW calcination process as blended feed is released to the atmosphere. This is due to the recycled scrub solutions that remove 45-65% of the volatilized iodine-129. However, this collected ^{129}I is revolatilized when these scrub solutions are solidified.

A flow diagram of iodine-129 transport through a nuclear fuel reprocessing plant was constructed using the ^{129}I process distribution computer program listed in Appendix I. The results are shown in Figures 10 and 11. Figure 10 illustrates transport without HLW evaporation and Figure 11 illustrates transport with HLW evaporation. Both cases assumed a first-cycle extraction distribution coefficient of 4. From these two figures it can be seen that the HLW evaporation process will determine if the major ^{129}I release point is the off-gas or liquid waste streams.

In conclusion, it appears the computer program listed in Appendix I can accurately predict environmental releases within 10-25%.

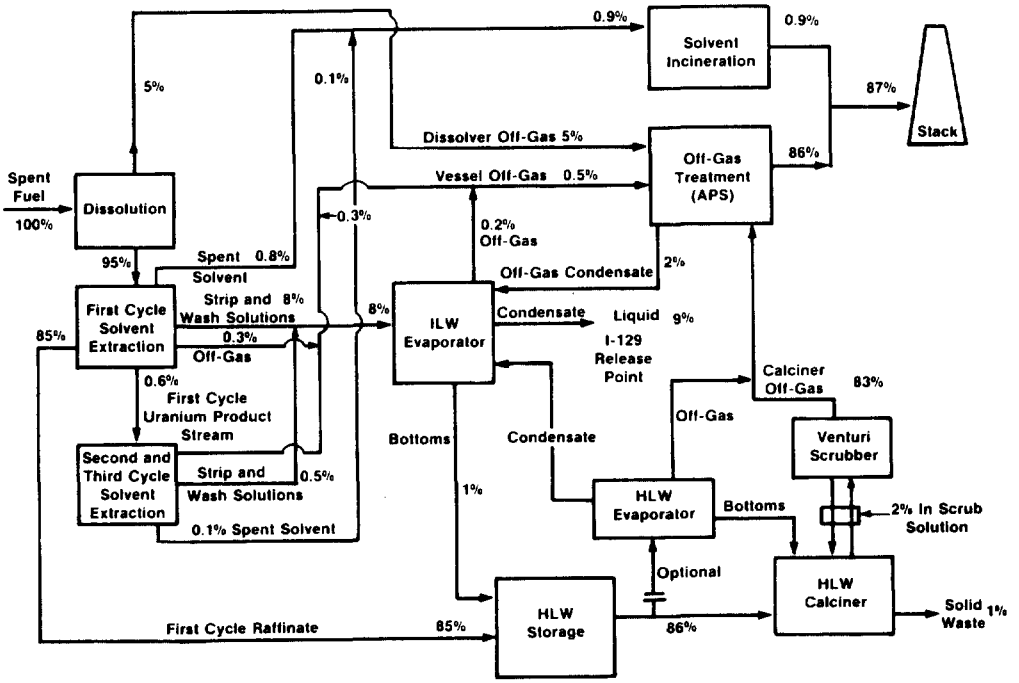

FIGURE 10. ^{129}I TRANSPORT THROUGH FUEL REPROCESSING PLANT WITHOUT HLW EVAPORATION

ICPP A-7936

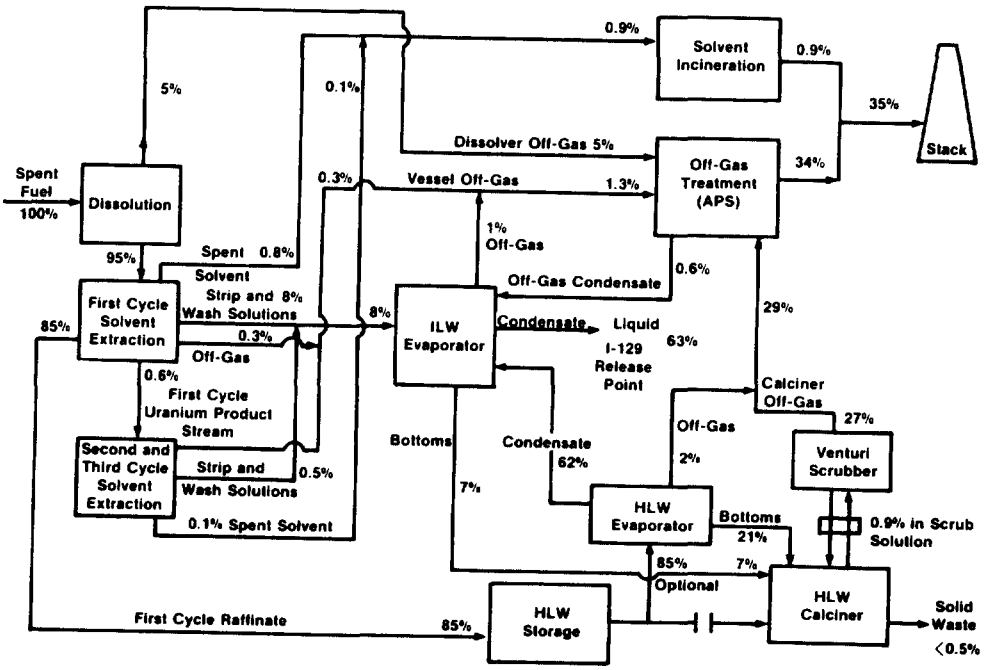

FIGURE 11. ^{129}I TRANSPORT THROUGH FUEL REPROCESSING PLANT WITH HLW EVAPORATION

VI. REFERENCES

1. R. Berg and H. Schuttlekopf, "Measurement of the Distribution of ^{129}I in and its Discharge from the Karlsruhe Reprocessing Plant", paper presented at a symposium on Radioactive Effluents from Nuclear Fuel Reprocessing Plants", Karlsruhe, W. Ger., November 1977.

2. W. Davis, "A Model of Iodine Transport and Reaction Kinetics in a Nuclear Fuel Reprocessing Plant", ORNL/NUREG 16, May, 1977.

3. G. D. Pierce and S. J. Fernandez, "Anion Exchange Differentiation of Iodine-129 Oxidation States in Waste Solidification Feed Solutions", paper presented at 34th Northwest Regional Meeting of the American Chemical Society, Richland, WA, June 13-15, 1979.

4. L. G. Sillen, "Graphical Presentation of Equilibrium Data", in Treatise on Analytical Chemistry, Part I, Theory and Practice, I. M. Kolthoff and P. J. Elving, Ed., New York: The Interscience Encyclopedia, Inc., 1959.

5. D. C. Hetzer, S. J. Fernandez, B. G. Motes, and L. P. Murphy, "Characterization of the Gaseous Iodine-129 Species in the Process Off-Gas System at the Idaho Chemical Processing Plant", paper presented at 35th Northwest Regional Meeting of the American Chemical Society, Salt Lake City, UT, June 1980.

6. L. P. Murphy, F. A. Duce, and S. J. Fernandez, Continuous Tritium, Carbon-14, Iodine-129, and Krypton-85 Monitor for Nuclear Facility Off-Gas, ENICO-1092, October 1981.

APPENDIX I

```
10 PRINT "INPUT THE FLOWRATE TO THE EXTRACTION COLUMN IN L/HR"
20 INPUT F9
30 F9=F9/3.785
40 PRINT "INPUT THE A/O RATIO FOR THE EXTRACTION COLUMN"
50 INPUT A1
60 PRINT "INPUT THE A/O RATIO FOR THE SCRUB COLUMN"
70 INPUT A2
80 PRINT "INPUT THE A/O RATIO FOR THE STRIP COLUMN"
90 INPUT A3
100 PRINT "INPUT THE A/O RATIO FOR THE SECOND STRIP"
110 INPUT A4
120 PRINT "INPUT THE A/O RATIO FOR THE CARBONATE WASH"
130 INPUT A5
140 PRINT "INPUT THE DIS. COEF. FOR THE EXTRACTION COLUMN"
150 INPUT E1
160 PRINT "INPUT THE DIS. COEF. FOR THE SCRUB COLUMN"
170 INPUT E2
180 PRINT " INPUT THE DIS. COEF. FOR THE STRIP COLUMN"
190 INPUT E3
200 PRINT " INPUT THE DIS. COEF. FOR THE SECOND STRIP"
210 INPUT E4
220 PRINT "INPUT THE DIS. COEF. FOR THE CARBONATE WASH"
230 INPUT E5
240 PRINT "INPUT THE # OF uCi OF I-129 SENT TO THE DISSOLVER/DAY"
250 INPUT F
260 PRINT "INPUT THE # OF OPERATING DAYS"
270 INPUT D
280 F1=F/24
290 N=D*24
300 Y4=0
310 S1=0
320 R1=0
```

```
330 P=0
340 M9=0
350 P1=0
360 Y3=0
370 K2=0
380 Z9=0
390 Y7=0
400 N=N-1
410 FOR Z=0 TO N
420 S=0.05*F1
430 F2=F1-S
440 F2=F2+Z9
450 R=(F2+Y4)/(E1/A1+1)
460 Y=R*E1/A1
470 Z9=Y*(A2/E2/(1+A2/E2))
480 Y=Y-Z9
490 Y2=Y*(A3/E3/(1+A3/E3))
500 Y1=Y-Y2
510 Y3=Y1*(A4/E4/(1+A4/E4))
520 Y1=Y1-Y3
530 P=Y1*(A5/E5/(1+A5/E5))
540 Y4=Y1-P
550 Y6=Y2+Y3
560 K=0.054*Y6
570 Y5=Y6-K
580 P2=Y5*0.85
590 S2=Y5*0.05
600 Y5=Y5*0.1
610 S1=S+S1+S2
620 R1=R+R1
630 P1=P+P1+P2
640 Y7=Y7+Y5
650 K2=K2+K
660 NEXT Z
670 PRINT " THE AMOUNT OF I-129 SENT TO THE STACK IN ";D;" DAYS"
680 PRINT "IS ";S1;" uCi, THIS CORRESPONDS TO AN AVERAGE"
690 S2=S1*2.45E-13/D
700 PRINT " CONCENTRATION OF ";S2;" uCi/cc"
710 PRINT "THE AMOUNT OF I-129 SENT TO THE PEW IN ";D;" DAYS IS"
720 PRINT P1;" uCi"
730 PRINT "THE AMOUNT SENT OUT IN THE FIRST CYCLE RAFFINATE IN"
740 PRINT D;" DAYS IS ";R1;" uCi. THE TOTAL VOLUME WAS ";F9*24*D;" GALS"
750 PRINT "THE CONCENTRATION OF THE I-129 IN THE RAFFINATE WAS"
760 PRINT R1/(F9*D*24*3.785);" uCi/L"
770 PRINT "THE AMOUNT OF I-129 SENT TO THE SOLVENT BURNER IN ";D;" DAYS"
780 PRINT "WAS ";K2
790 PRINT " THE AMOUNT OF I-129 SENT THE SECOND CYCLE IN ";D;" DAYS"
800 PRINT "IS ";Y7
810 GOSUB 2270
820 GOSUB 2510
830 GOSUB 2640
840 PRINT "IS THE 1ST CYCLE RAFFINATE TO BE CALCINED DIRECTLY 1=Y,2=N"
850 INPUT H
860 GOSUB H OF 960,870
870 PRINT "IS HLLW EVAPORATION DESIRED 1=YES,2=NO"
880 INPUT H
890 GOSUB H OF 1660,910
900 GOSUB 960
910 PRINT "SINCE NO CALCINATION OR HLLW EVAPORATION IS DESIRED THEN"
920 PRINT R1;" uCi OF I-129 FROM THE FIRST CYCLE IS SENT TO THE "
930 PRINT "TANK FARM"
940 GOSUB 2390
950 GOSUB 2610
960 REM ------------------CALCINER SUBROUTINE-----------------------
970 PRINT "INPUT THE % REMOVAL IN SCRUBBER"
980 INPUT K
990 K=K/100
1000 PRINT "INPUT THE SCRUB FLOWRATE IN GAL/HR"
1010 INPUT D9
1020 IF M9=9 THEN 1070
1030 J=F9
1040 I=R1/(F9*24*D*3.785)
1050 L=D
1060 GO TO 1080
1070 GOSUB 2940
```

```
1080 R=0
1090 X=0
1100 A=0
1110 E=0
1120 H=0.42
1130 P=0.755
1140 M=L*24/(1400/J)
1150 G=1400/J
1160 B=R1*1000/(D*24*3600)
1170 FOR T=1 TO M
1180 F=3600*B*G
1190 F=F*H
1200 A=F*K+E
1210 C=A*2.642E-7
1220 S=C*D9*1.051
1230 B=I*J+S
1240 E=0.8*A
1250 IF H=>1 THEN 1280
1260 H=H+0.0025
1270 IF H<1 THEN 1290
1280 H=1
1290 N=B-S
1300 N=N*1400*3600/J
1310 P=P+0.071
1320 IF P=>1 THEN 1340
1330 IF P<1 THEN 1350
1340 P=1
1350 O=N*P
1360 Q=O*0.97
1370 Y=O-Q
1380 X=X+Y
1390 R=R+Q
1400 NEXT T
1410 U=R/(L*86400)
1420 V=Q*J*2.0E-7
1430 W=V*2.1186E-8
1440 A=X/(L*86400)
1450 PRINT "AFTER ";L;" DAYS OF OPERATION THE CONCENTRATION OF THE"
1460 PRINT "SCRUB SOLUTION IS ";C;"nCi/mL"
1470 PRINT
1480 PRINT "AND THE SCRUB SOLUTION RECYCLE RATE IS "
1490 PRINT S;"nCi/sec"
1500 PRINT "AFTER ";L;" DAYS OF OPERATION THE AVERAGE I-129 "
1510 PRINT "FLOWRATE OUT THE STACK IS ";U;"nCi/sec"
1520 U=U*1.0E-3*3600*24*L
1530 PRINT "AND THE PRESENT FLOWRATE IS ";V;"nCi/sec"
1540 PRINT  '
1550 PRINT "ASSUMING AN AVERAGE STACK FLOW OF 100000 CFM THIS RESULTS"
1560 PRINT "IN A I-129 CONCENTRATION OF ";W;"nCi/cc"
1570 PRINT
1580 PRINT "THE AVERAGE AMOUNT OF I-129 SENT TO THE PEW FROM THE APS"
1590 PRINT "DURING THE ";L;" DAYS THE CALCINER WAS OPERATING WAS";
1600 PRINT A;"nCi/sec"
1610 S2=A*1.0E-3*3600*24*L
1620 GOSUB 2380
1630 GOSUB 2590
1640 PRINT
1650 REM----------------------HLLW EVAPORATOR SUBROUTINE---------------
1660 REM C IS I-129 CONCENTRATION IN nCi/L"
1670 C=R1*1000/(F9*D*24)
1680 REM INPUT FLOWRATE OF CONDENSATE F
1690 PRINT "INPUT THE RATE OF DISTILLATION IN GAL/HR"
1700 INPUT F
1710 REM INTIAL VOL CHARGED TO THE EVAPORATOR V
1720 PRI "INPUT THE INTIAL VOLUME OF FEED CHARGED TO THE EVAPORATOR IN"
1730 PRINT "GAL"
1740 INPUT V
1750 REM INPUT HR BETWEEN BATCHS H
1760 PRINT "INPUT THE NUMBER OF HOURS BETWEEN BATCHS"
1770 INPUT H
1780 REM INPUT # OF DAYS OF OPERATION D
1790 PRINT "INPUT THE NUMBER OF BATCHS BETWEEN BOTTOM TRANSFERS"
1800 INPUT N
1810 G=F*H
1820 B9=V-G
1830 REM INPUT # OF DAYS OF OPERATION D
1840 PRINT "INPUT THE # OF DAYS THE EVAPORATOR IS IN OPERATION"
```

```
1850 INPUT D
1860 V9=B9*D*24/(N*H)
1870 K=0
1880 J=V*C
1890 FOR L=1 TO N
1900 E=0
1910 REM CALCULATES % REMOVAL PER BATCH
1920 FOR T=1 TO H
1930 B=V-T*F
1940 A=F/B
1950 Y=1-EXP(-1.26*A)
1960 E=E+Y
1970 IF E>0.98 THEN 2000
1980 NEXT T
1990 REM CAL I-129 THAT LEFT THE EVAPORATOR IN THE CONDENSATE
2000 I=J*E
2010 REM SUMS AMOUNT I-129 DISTILLED PER BATCH
2020 K=K+I
2030 REM CALCULATES AMOUNT I-129 REMAINING IN THE EVAPORATOR
2040 J=J-I
2050 J=J+G*C
2060 NEXT L
2070 M=H*N
2080 O=D*24/M
2090 REM CALCULATES THE AMOUNT OF I-129 SENT TO THE PEW
2100 P=O*K*1.0E-3
2110 G1=0.02*P
2120 GOSUB 2560
2130 P=P-G1
2140 REM CALCULATES THE AMOUNT OF I-129 SENT TO THE CALCINER
2150 Q=((N-1)*G+V)*C*O*1.0E-3-P-G1
2160 PRINT "THE AMOUNT OF I-129 SENT TO THE PEW IN"
2170 PRINT D;" DAYS WAS ";P;" uCi"
2180 GOSUB 2340
2190 PRINT "THE AMT, OF I-129 SENT TO THE CALCINER IN ";D;" DAYS IS"
2200 PRINT Q;" uCi"
2210 PRINT V9;" GALS OF WASTE ENDED UP IN THE BOTTOMS"
2220 PRINT "THIS CORRESPONDS TO AN AVE. I-129 CONCENTRATION IN THE"
2230 PRINT "BOTTOMS OF ";Q/V9;" uCi/GAL"
2240 M9=9
2250 RETURN
2260 END
2270 REM--------------------PEW SUBROUTINE--------------------
2280 REM 1ST CYCLE CONTRIBUTION
2290 D1=P1
2300 RETURN
2310 REM 2ND CYCLE CONTRIBUTION
2320 D1=D1+O2
2330 RETURN
2340 REM HLLW EVAPORATOR CONTRIBUTION
2350 D1=D1+P
2360 RETURN
2370 REM CALCINER CONTRIBUTION
2380 D1=D1+S2
2390 PRINT "INPUT THE AMOUNT OF I-129 THAT GOES TO THE OFF-GAS, COND,"
2400 PRINT "AND THE BOTTOMS"
2410 INPUT G,C,R
2420 G1=G/100
2430 IF H=2 THEN 2560
2440 C1=C/100
2450 R1=R/100
2460 E1=D1*G1
2470 E2=D1*C1
2480 E3=D1*R1
2490 PRINT E2;"uCi OF I-129 WAS SENT TO THE INJECTION WELL"
2500 RETURN
2510 REM------------STACK SUBROUTINE-------------------------
2520 P5=S1+K2+Y4
2530 RETURN

2540 P5=P5+S2
2550 RETURN
2560 P5=P5+G1
2570 IF H=2 THEN 2440
2580 RETURN
```

```
2590 P5=P5+U
2600 P5=P5+E1
2610 PRINT ' THE TOTAL AMOUNT OF I-129 SENT UP THE STACK FROM ALL '
2620 PRINT 'PROCESSES WAS ';P5
2630 END
2640 REM ------------------2ND-CYCLE SUBROUTINE-----------------
2650 O2=0
2660 S2=0
2670 PRINT 'INPUT THE A/O RATIOS FOR THE IIA,IIB,IIIA,IIIB COLUMNS'
2680 INPUT A2,A3,B2,B3
2690 PRINT 'INPUT THE DIS. COEF. FOR THE IIA,IIB,IIIA,IIIB COLUMNS'
2700 INPUT E2,E3,E4,E5
2710 F=Y7
2720 PRINT 'INPUT # OF DAYS OF OPERATION'
2730 INPUT N
2740 F1=F/N
2750 N=N-1
2760 FOR Z=0 TO N
2770 R=F1*A2/(A2+E2)
2780 Y2=F1-R
2790 R2=Y2*(A3/E3/(1+A3/E3))
2800 Y3=Y2-R2
2810 R3=R2*B2/(E4+B2)
2820 Y4=E4*Y3
2830 R4=Y4*(B3/E5/(1+B3/E5))
2840 Y5=E5*R4
2850 O2=O2+R+R3+R4
2860 S2=S2+Y3+Y5
2870 NEXT Z
2880 PRINT O2;' uCi OF I-129 WAS SENT TO THE PEW FROM THE 2ND CYCLE'
2890 PRINT S2;' uCi OF I-129 WAS SENT TO THE SOLVENT BURNER FROM THE'
2900 PRINT 'THE 2ND CYCLE'
2910 GOSUB 2310
2920 GOSUB 2540
2930 RETURN
2940 REM--------------------CALCINATION OF HLLW BOTTOMS-------
2950 PRINT 'INPUT THE # OF DAYS THE CALCINER IS RUNNING'
2960 INPUT L
2970 I=Q/V9/3.785
2980 PRINT 'INPUT THE RAW FEED FLOWRATE IN GAL/HR'
2990 INPUT J
3000 RETURN
3010 PRINT 'INPUT THE RAW FEED FLOWRATE IN GAL/HR'
3020 INPUT J
3030 RETURN
```

DISCUSSION

Anon: Can you tell us the reason for the small release of iodine in the dissolver off-gas?

McManus: You mean versus the high release that has been found in Germany and France? I think it has to do with the temperature of our dissolution process. It is a lower temperature than is used in Europe, and that influences the amount that is released in dissolution.

Anon: What is the temperature?

McManus: Between 40 and 60 degrees.

CARBON DIOXIDE - KRYPTON SEPARATION AND RADON REMOVAL FROM NUCLEAR FUEL REPROCESSING OFF-GAS STREAMS*

P.M. Hirsch, K.Y. Higuchi, and L. Abraham
General Atomic Company
San Diego, California

Abstract

General Atomic Company (GA) is conducting pilot-plant-scale tests that simulate the treatment of radioactive and other noxious volatile and gaseous constituents of off-gas streams from nuclear reprocessing plants. This paper reports the results of engineering-scale tests performed on the CO_2/krypton separation and radon holdup/decay subsystems of the GA integrated off-gas treatment system.

Separation of CO_2 from krypton-containing gas streams is necessary to facilitate subsequent waste processing and krypton storage. Molecular sieve 5A achieved this separation in dissolver off-gas streams containing relatively low krypton and CO_2 concentrations and in krypton-rich product streams from processes such as the krypton absorption in liquid carbon dioxide (KALC) process.

The CO_2/krypton separation unit is a 30.5-cm-diameter x 1.8-m-long column containing molecular sieve 5A. The loading capacity for CO_2 was determined for gas mixtures containing 250 ppm to 2.2% CO_2 and 170 to 750 ppm krypton in either N_2 or air. Gas streams rich in CO_2 were diluted with N_2 to reduce the temperature rise from the heat of adsorption, which would otherwise affect loading capacity. The effluent CO_2 concentration prior to breakthrough was less than 10 ppm, and the adsorption capacity for krypton was negligible. Krypton was monitored on-line with a time-of-flight mass spectrometer and its concentration determined quantitatively by a method of continuous analysis, i.e., selected-ion monitoring.

Radon-220, a gaseous decay product of the U-232 contaminant in thorium recycle fuels, was treated by holdup and decay on a column of synthetic H-mordenite. The Rn-220 concentration was monitored on-line with flow-through diffused-junction alpha detectors. Single-channel analyzers were utilized to isolate the 6.287-MeV alpha energy band characteristic of Rn-220 decay from energy bands due to daughter products.

The decontamination factor (DF) was determined as a function of bed height for a 34.6-cm-diameter column. The experimental results yielded a mathematical expression to describe the dependence of DF on bed height. A column about 3.66 m (12 ft) long is recommended for achieving the design DF of 1000.

A DF in excess of 1000 was demonstrated in either N_2, air, or CO_2 carrier gas streams. Regeneration of bed material to remove moisture, followed by pretreatment of the adsorbent with carrier gas, significantly improved the performance of the bed. Substantial retention of particulate daughter products of Rn-220 was demonstrated, although those not retained within the bed need to be trapped in a downstream high-efficiency particulate air (HEPA) filter.

---

*Prepared under contract DE-AT03-76SF71053 for the San Francisco Operations Office of the Department of Energy.

Introduction

Engineering-Scale Off-Gas Treatment System

General Atomic Company (GA) has completed the detailed design and installation of a (radioactively) cold engineering-scale facility for the treatment of off-gas from the reprocessing of spent nuclear fuel. Engineering-scale component tests have been performed to simulate the treatment of fission and decay products and nonradioactive gaseous constituents inherent to nuclear fuel reprocessing.[1,2,3] The radon removal test results were derived from studies made with the radon holdup/decay subsystem of the GA engineering-scale off-gas treatment system.

The GA off-gas treatment system is designed to process simulated radioactive or other noxious volatile and gaseous constituents in both dissolver off-gas (DOG) and burner off-gas (BOG) streams. Dissolver off-gas is common to several nuclear fuel cycles, e.g., light water reactors (LWRs), high-temperature gas-cooled reactors (HTGRs), and liquid metal fast breeder reactors (LMFBRs), whereas BOG streams are specific to only HTGR fuel reprocessing. Gaseous fission products such as H-3, C-14, Kr-85, I-129, and Rn-220 are released during reprocessing. These fission, activation, or decay products can be removed before the gas effluent is released into the atmosphere. In addition, other gaseous components in the off-gas stream, such as CO, SO_2, and NO_X, can be removed or converted into harmless molecular forms if necessary for environmental and/or process control considerations.

The GA off-gas treatment system is divided into BOG and DOG subsystems. The BOG subsystem includes units for removal of SO_2, HTO, I_2, radon, krypton, and CO_2 and a unit for CO and HT oxidation. The DOG subsystem includes units for removal of NO_X, I_2, H_2O, radon, CO_2, and krypton. The processes used in this engineering-scale system are based on prior laboratory-scale development at various sites under the sponsorship of the U.S. Department of Energy (DOE) or its predecessor agencies. The GA engineering-scale off-gas treatment system is funded under the Consolidated Fuel Reprocessing Program, which is managed by Oak Ridge National Laboratory (ORNL) for DOE.

Carbon Dioxide/Krypton Separation

The off-gas produced during reprocessing of nuclear fuels contains trace amounts of krypton, which can be removed before the off-gas is released into the atmosphere. For LWR, LMFBR, and HTGR fuel, the spent fuel is reprocessed by dissolution in HNO_3. The resulting DOG (for HTGR fuel) contains about 200 ppm Kr-85 (half-life = 10.7 yr) and 250 ppm CO_2, and the balance is air. The air constituent typically contains 1.14 ppm normal isotopic krypton and 330 ppm CO_2. For HTGR fuel, the support structure and moderating graphite material must be burned off prior to dissolution. The BOG contains about 10 to 15 ppm Kr-85, which is initially concentrated by the krypton absorption in liquid carbon dioxide (KALC) process. The resulting off-gas contains about 1.5% krypton, 2.5% xenon, 5% O_2, and 91% CO_2. The CO_2 must be separated from the krypton before storage because the radiolytic interaction of Kr-85 with CO_2 can cause the formation of ozone, creating a potentially explosive gas mixture.

In the cold engineering-scale tests, natural isotopic krypton was separated from CO_2 using an adsorption column filled with molecular sieve 5A (W.R. Grace & Co., Davison Chemical Division). This process was based on prior laboratory-scale studies performed by C.W. Forsberg at ORNL[4]. The separation occurs owing to the different adsorption characteristics of krypton and CO_2 on the molecular sieve material.

The krypton concentration in the column effluent was monitored on-line by a time-of-flight mass spectrometer and quantitatively analyzed by selected ion monitoring. The krypton breakthrough from the CO_2/krypton separation bed was studied under simulated post-KALC BOG and DOG conditions and the CO_2 decontamination factor (DF) and CO_2 capacity of molecular sieve 5A determined.

Radon Removal by Adsorption/Decay

Radon-220 is a decay product of the U-232 contaminant in recycle fuels originating from thorium-uranium fuel cycles. Radon-220 is a gas with a short half-life at ambient temperature, and it diffuses rapidly, resulting in contamination of the surfaces it touches. Because of the short half-life of Rn-220 (56 s), significant decontamination can be achieved by increasing the Rn-220 residence time in the off-gas treatment system. Laboratory-scale tests conducted by Allied Chemical Corporation at the Idaho National Engineering Laboratory (INEL) have shown that the synthetic molecular sieve H-mordenite is capable of delaying the transport of Rn-220 for several half-lives, thus achieving DFs on the order of 10^3.[5] The success of these experiments has made it desirable to investigate Rn-220 adsorption on a larger scale. Through operation of an engineering-scale system, performance and scale-up design data can be obtained.

In the GA engineering scale studies, Rn-220 was generated from U_3O_8 containing approximately 20 ppm U-232. The radon was transported in a carrier gas stream, which then passed through the radon holdup/decay bed (an adsorber column containing H-mordenite). The Rn-220 concentration was monitored at the inlet and outlet of the adsorber column.

The system chosen for radon analysis is different from that used at INEL. Rather than a batch method of gamma radiation detection, an on-line continuous method of alpha detection was used. The 6.287-MeV alpha particle emitted by Rn-220 was selectively monitored through a system of diffused-junction alpha detectors and sophisticated electronics which discriminate between the Rn-220 alpha particles and the other alphas emitted by daughter products of Rn-220. The solid daughter products resulting from the decay of Rn-220 during holdup on the H-mordenite either adsorb onto the bed material or are removed by the carrier gas. It was unnecesary to determine the absolute Rn-220 concentration levels because only the DF, a relative measurement, was desired. Therefore, identically calibrated alpha detector units possessing equivalent detection efficiencies were utilized to measure the ratio of inlet to outlet Rn-220 concentration, i.e., the DF.

The DF of the radon holdup/decay bed was determined as a function of bed height for a 0.305-m (1-ft) diameter column. The experimental data in concert with a mechanistic analysis of the system yielded a mathematical expression to describe the dependence of DF on bed height. The effects of N_2, air, and CO_2 carrier gas on DF were studied. Regeneration of the bed material to remove moisture and pretreatment of the adsorbent with carrier gas increased the Rn-220 removal efficiency of the bed. The daughter products of Rn-220 were detected in trace quantities in the bed effluent.

PART I: CARBON DIOXIDE - KRYPTON SEPARATION

Experimental Method

Figure 1 is a schematic of the CO_2/krypton separation subsystem of the GA engineering-scale off-gas treatment system. This subsystem is capable of simulating post-KALC BOG streams and DOG streams. The CO_2/krypton separation subsystem, like the other subsystems within the off-gas treatment system, can be isolated to allow

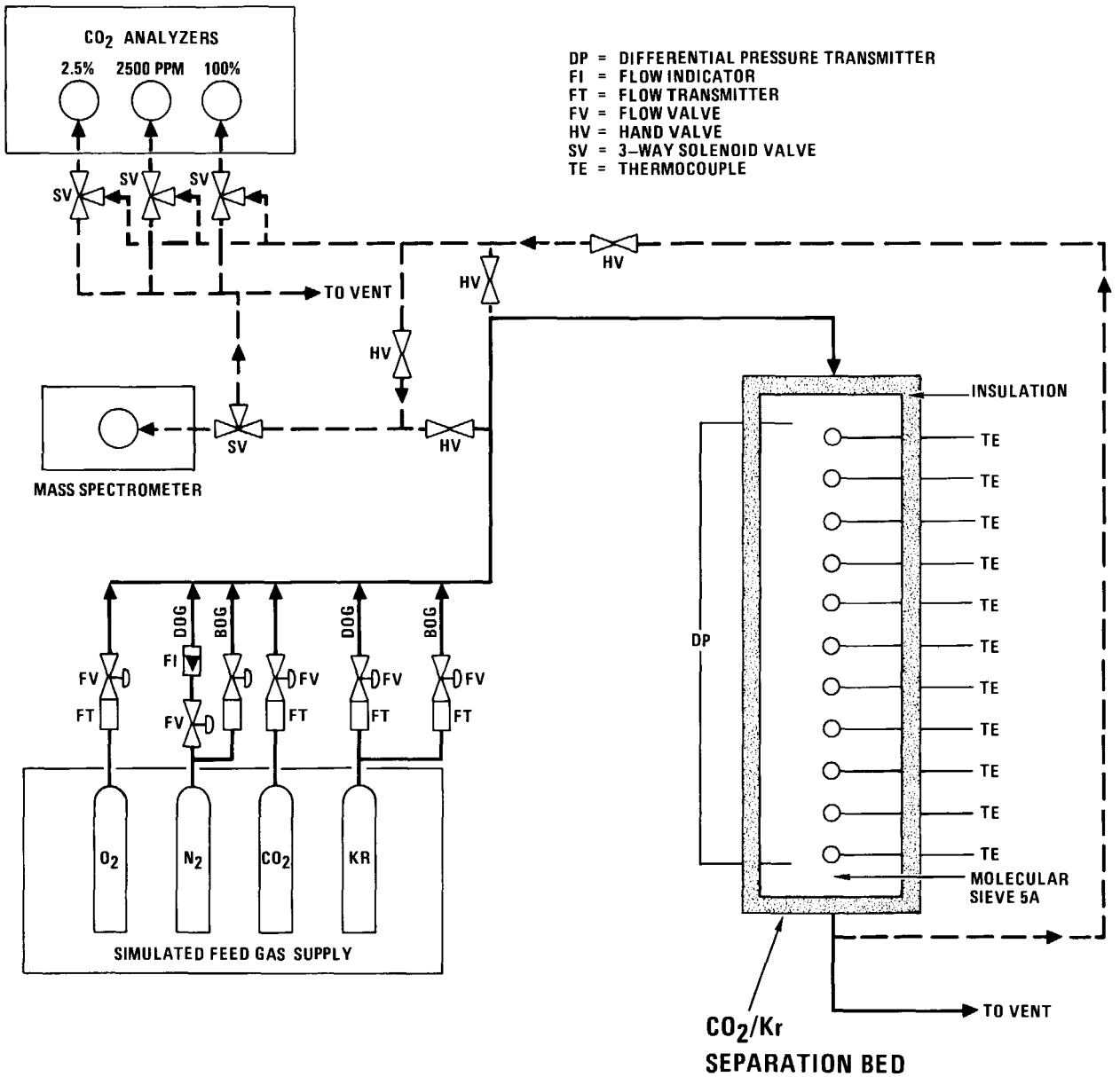

Figure 1. Schematic of the CO_2/krypton separation subsystem.

independent testing. The individual components of the CO_2/krypton separation subsystem are described below.

Separation Vessel Design

The CO_2/krypton separation vessel is fabricated from 316L stainless steel pipe with a 324-mm o.d. and a 5 mm-thick wall (12 in. Sch 10S). The vessel is 1.8 m (71 in.) long and is packed with 8- to 12-mesh 5A molecular sieve adsorbent supported by a 40-mesh 304 stainless steel screen.

Eleven thermocouples are placed 150 mm apart along the bed centerline to measure the CO_2 adsorption temperature gradient. The thermocouples are Chromel-Alumel (K-type) insulated with MgO powder and Inconel 600 sheaths. An expansion compensator (Hyspan Precision Products Incorporated) is located immediately downstream of the vessel to protect the system from stress during adsorbent regeneration. A Rosemount model 1151 DP differential pressure transmitter is provided to measure the pressure drop across the bed. The transmitter range is 0 to 37.4 kPa (0 to 150 in. H_2O), and it has an accuracy of ±0.2% of full scale.

Adsorbent

The adsorbent (Davison 5A molecular sieves) is a crystalline metal aluminosilicate with a three-dimensional interconnecting network structure of silica and alumina tetrahedra. The basic structure of the molecular sieve is represented by the 4A, or sodium, form. The 5A is produced by substituting calcium cations for the sodium cations. The calcium cations, being divalent, will replace two sodium cations and open the structure to apertures of about 5 Å. Most of the adsorption takes place inside the pores. The uniformity of the size of the pores enables large molecules (over 5.5 Å) to be "sieved" out. However, since CO_2, krypton, and N_2 have effective diameters of about 3 Å, the sieving effect is minimal.

The calcium ions induce strong, localized, positive charges in the crystal lattice. Therefore, polar molecules or induced polar molecules will adsorb more than less polar molecules. Since CO_2 has an electric quadrupole moment, whereas the monatomic krypton is nonpolar, the CO_2, and krypton molecules are separated on the basis of polarity.

Simulated Feed Gas Supply

The feed gas supply system is capable of generating either simulated post-KALC BOG or DOG compositions. Figure 1 shows the piping and instrumentation. The BOG N_2 dilution supply is regulated by a Brooks 0-to 50-lpm model 5815 thermal mass flow controller. This controller maintains a preset flow to within ±0.2% and has an accuracy of ±1% of the full-scale reading when the gas is measured at 21.1°C (±5.6°C) and 274 kPa (±104 kPa). The DOG N_2 supply is regulated by a Masoneilan Micro Pak flow control valve in conjunction with a Brooks model 1110 rotameter and model 5522 flow transmitter. The rotameter accuracy is ±1% of full scale.

The BOG and DOG CO_2 supply is regulated by a Brooks 0- to 1000-sccm model 5815 thermal mass flow controller. The BOG krypton supply is regulated by a 0- to 20-sccm Brooks model 5815 thermal mass flow controller and the DOG krypton supply by a 0- to 100-sccm Brooks model 5815 thermal mass flow controller. The DOG O_2 supply is regulated by a Brooks 0- to 100-lpm model 5815 thermal mass flow controller.

Gas Analysis System

The gas analysis system consists of three Beckman model 864 infrared spectrophotometers for CO_2 analysis and a CVC MA-3 time-of-flight mass spectrometer for krypton analysis. This mass spectrometer is intended for use in the mass range 1 to 300 amu with unit resolution greater than 150 and usable resolution to 250.

Carbon Dioxide Analysis. The CO_2 concentration is analyzed at the inlet and outlet of the CO_2/krypton separation bed. The analyzers measure CO_2 in three ranges: 2500 ppm, 2.5%, and 100% full scale, with an accuracy of ±1% of the full-scale value. The analyzers are calibrated with certified standard gas mixtures prepared by Matheson. The sample point locations and specific analyzers are selected by hand valve and solenoid switching.

Krypton Analysis. The krypton concentration is measured on-line at the inlet and outlet of the CO_2/krypton separation bed with a time-of-flight mass spectrometer using a select-ion method of analysis. With the time-of-flight principle, a sheet of positive ions of various mass-to-charge (m/e) ratios is accelerated to a high level of kinetic energy and directed through a field-free drift tube toward an ion detector. The positive ions are formed by bombarding the sample gas with a stream of electrons created by thermionic emission of a heated filament. Because all the ions receive equal energy, their drift velocities depend on the m/e ratio; i.e., the lighter ions travel to the ion detector faster than the heavier ions. Because all the ions leave the starting position almost simultaneously and all drift the same distance to reach the detector, those of equal mass separate into sheets displaced from other masses. As each sheet of ions strikes the detector, the ions dislodge secondary electrons, which are directed into a multiplier, where gains of up to 10^7 can be achieved. This process takes place 30,000 times/s. The resultant peak heights that are observed are linearly related to ion abundance and hence to relative species concentration in the sample gas.

Process Control and Data Acquisition

The N_2 and CO_2 gas flow rates are regulated by a Diogenes (Rosemount, Incorporated) process controller. The output signals from the flow indicators, CO_2 analyzers, mass spectrometer, thermocouples, and pressure sensors are monitored by a Hewlett Packard data acquisition system that continuously scans and displays the test data on a cathode ray tube (CRT). The data can also be printed and/or stored in a floppy disc file at specified time intervals.

Results

The first series of runs was carried out to study the adsorption characteristics of krypton and CO_2 under simulated post-KALC BOG conditions. The heat of adsorption of CO_2 on molecular sieve 5A is high, and its adsorption capacity is significantly reduced at elevated temperatures. Therefore, the temperature rise was limited to 25°C by diluting the krypton/CO_2 flow with N_2 to achieve a total flow rate of about 47 slpm. This flow rate represents an N_2 dilution factor greater than 70. The krypton breakthrough curve for this simulated diluted BOG stream is shown in Fig 2. The krypton broke through in about 34 min and attained a steady-state outlet concentration equal to the inlet concentration of 410 ppm. The CO_2 was essentially fully adsorbed onto the bed at a feed stream composition of 1.2%. The CO_2 concentration in the adsorber effluent was less than 10 ppm. The maximum bed temperature rise was approximately 20°C, which is in agreement with the CO_2 heat of adsorption data supplied by the manufacturer of molecular sieve 5A.

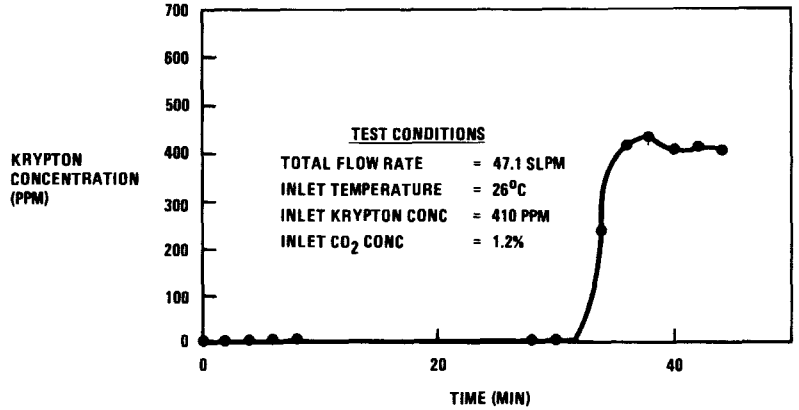

Figure 2. Nitrogen-diluted KALC effluent; CO_2/krypton separation on molecular sieve 5A.

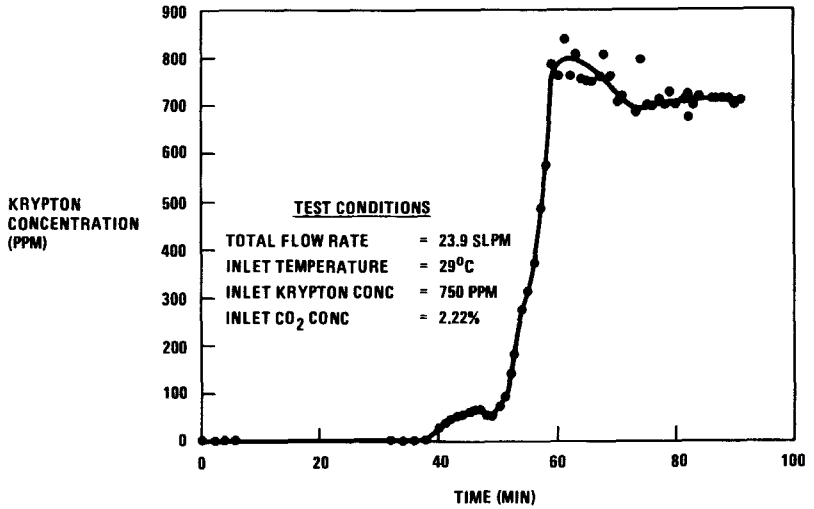

Figure 3. Nitrogen-diluted KALC effluent; krypton breakthrough on molecular sieve 5A.

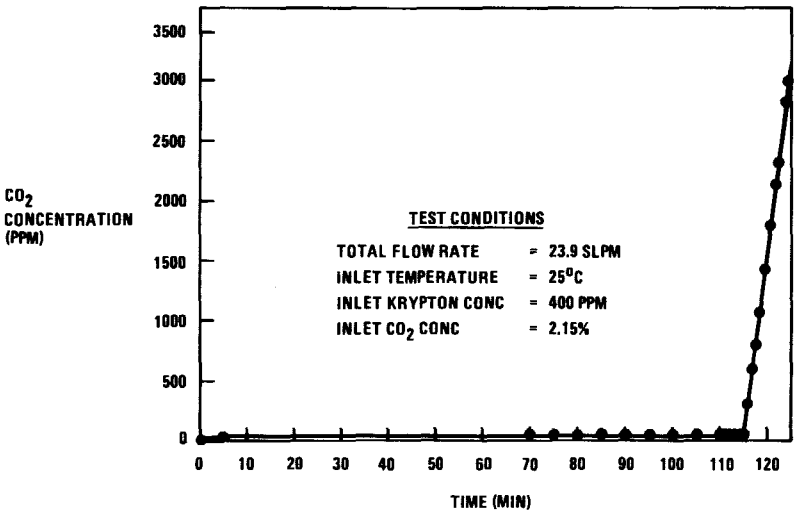

Figure 4. Nitrogen-diluted KALC effluent; CO_2 breakthrough on molecular sieve 5A.

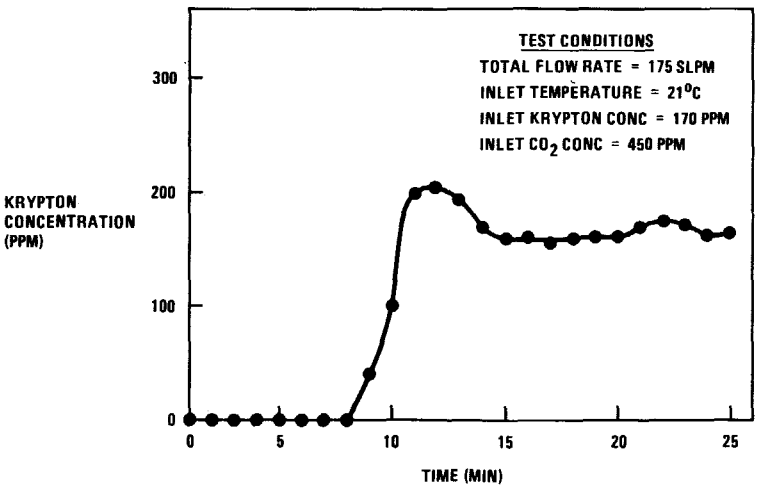

Figure 5. Simulated dissolver off-gas; krypton breakthrough on molecular sieve 5A.

An additional run was carried out with the N_2 gas flow rate reduced in half to study its effect on krypton breakthrough (Fig 3). (Prior to this and all succeeding runs, the CO_2/krypton separation bed was regenerated at 200°C with N_2 back-purge gas until the effluent CO_2 concentration was less than 10 ppm.) Krypton breakthrough started after 45 min, and a bed temperature rise of 35°C due to CO_2 adsorption was observed. Even at the higher CO_2 concentration of 2.22%, the concentration in the bed effluent was less than 10 ppm.

A CO_2 breakthrough run was carried out to determine the CO_2 adsorption capacity of molecular sieve 5A under simulated post-KALC conditions. The CO_2 breakthrough began after 116 h, as shown in Fig 4. After 122.5 h, a power failure occurred which terminated the run. It was not possible to repeat this run; however, by extrapolating the initial breakthrough curve to 2.15% CO_2, an estimate of the CO_2 adsorption capacity was made. The value obtained was 0.0968 g CO_2/g molecular sieve 5A, which is in excellent agreement with the manufacturer's data of 0.098 g CO_2/g molecular sieve 5A.

The DOG run series was carried out at a total flow rate of 250 lpm, compared with 47.1 lpm for the simulated N_2-diluted BOG runs. As expected, the krypton breakthrough occurred very rapidly owing to the relatively high flow rate. Both N_2 and air carrier gas were studied to simulate probable dissolver operating conditions. Figure 5 shows a typical DOG krypton breakthrough. The time to krypton breakthrough was 9 min, which was average for the DOG runs. The CO_2 concentration in the effluent from the CO_2/krypton separation bed was less than 10 ppm. The CO_2 adsorption capacity is expected to be the same as that obtained under simulated N_2-diluted BOG conditions, because the CO_2 concentrations in the feed are about equal.

Conclusions and Recommendations

Molecular sieve 5A was an effective adsorbent for separating CO_2 from simulated post-KALC BOG streams and DOG streams containing krypton. The CO_2 adsorption capacity of the molecular sieve material was approximately 0.097 g CO_2/g molecular sieve 5A, which is in agreement with the manufacturer's data. The effluent from the CO_2/krypton separation bed contained less than 10 ppm CO_2 for more than 100 h prior to breakthrough for an inlet CO_2 concentration of 2.2%.

The resultant krypton-rich N_2 effluent needs to be separated in another type of adsorption column for further concentration of krypton prior to krypton waste storage. A Canadian study[6] has shown that removal of krypton from N_2 gas streams by selective adsorption is technically feasible.

As an alternate engineering scale-up approach, the amount of N_2 dilution to post-KALC BOG streams can be reduced by redesigning the separation column to incorporate in-vessel cooling by an extended-surface internal heat exchanger. In this configuration, the heat generated by CO_2 adsorption can be more effectively removed from the column material, thus reducing the necessary N_2 dilution rate in addition to increasing the adsorption capacity for CO_2 owing to its increased partial pressure.

PART II: RADON REMOVAL

Experimental Method

Figure 6 shows a schematic of the radon holdup/decay subsystem of the GA engineering-scale off-gas treatment system. This subsystem, like all others within

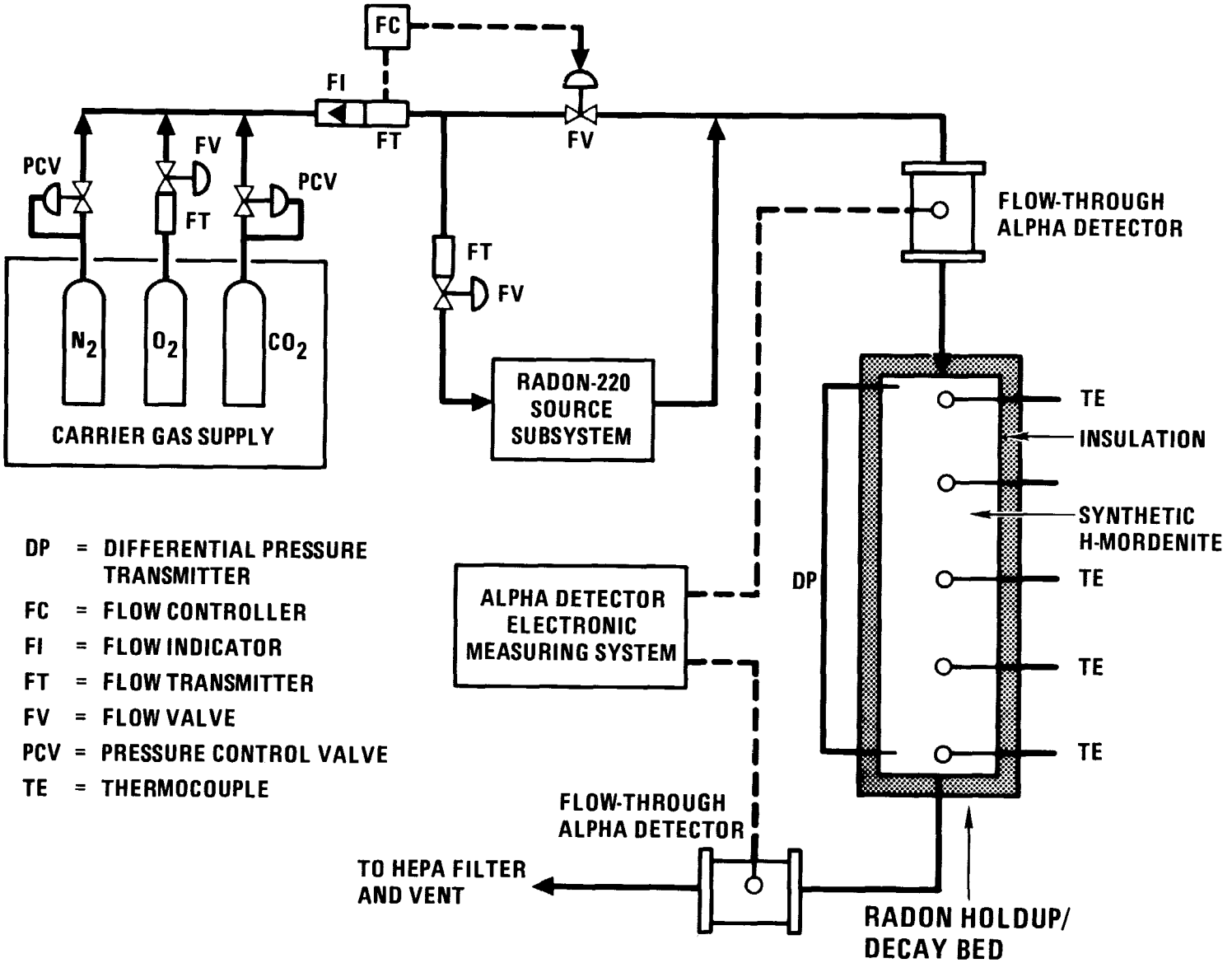

Figure 6. Schematic of the Rn-220 holdup/decay subsystem.

the off-gas treatment system, is capable of being isolated from the integrated system to allow independent testing. The individual components of the radon removal subsystem are described below.

Radon Holdup/Decay Vessel Design

The radon holdup/decay vessel is fabricated from 356-mm-o.d., 4.8-mm-thick (14-in. Sch 10S) 316L stainless steel pipe and is rated at 500°C at 50 psig. The vessel accepts a variable-depth adsorption bed of 3 m (118 in.) maximum length. The adsorbent is supported by a 40-mesh 304 stainless steel wire screen. A port is provided at the top of the vessel for vacuum removal of the contaminated bed material.

Five thermocouples are evenly distributed along the bed centerline for measuring the temperature gradient. The thermocouples are Chromel-Alumel (K-type), insulated with MgO powder and Inconel 600 sheaths. An expansion compensator (Hyspan Precision Products Incorporated) is located immediately downstream of the vessel to protect the system from stress during adsorbent regeneration. A Rosemount model 1151 DP differential pressure transmitter is provided to measure the pressure drop across the bed. The transmitter range is 0 to 7.5 kPa (0 to 30 in. H_2O) with an accuracy of ±0.2% of full scale.

Adsorbent

The adsorbent (Zeolon 900H) is a hydrogen-substituted synthetic mordenite manufactured by Norton Company. Zeolon 900H is an aluminosilicate characterized by a system of parallel channels with uniform diameters of about 10 Å. This material is highly acid resistant and has a silica-to-alumina ratio of 10:1. The adsorbent is a 3.2-mm (1/8-in.) diameter extrudate and is 4.8 to 7.9 mm (3/16 to 5/16 in.) in length.

Carrier Gas Supply

The carrier gas is either pure N_2, simulated air (80% N_2, 20% O_2), or pure CO_2. The total carrier gas flow rate is regulated at 10 scfm by a Fisher model 513 microflute flow control valve in conjunction with a Brooks model 1110 rotameter and model 5522 flow transmitter. The rotameter accuracy is ±1% of full scale. The oxygen supply is regulated by a Brooks model 5815 thermal mass flow controller. This controller maintains a preset flow to within ±0.2% with an accuracy of ±1% of the full-scale reading when the gas is measured at 21.1°C (±5.6°C) and 274 kPa (±104 kPa).

A side stream is diverted from the main carrier gas stream to the radon source subsystem, where it acts as a sweep gas to carry radon to the holdup/decay column. The side stream is maintained at 2 scfm by a Brooks model 5815 thermal mass flow controller. The side stream is adequate for transporting the relatively small amount of Rn-220 released from the source material. The radon-containing stream is rejoined with the main carrier gas downstream of the Fisher flow control valve. The flow control valve compensates for the pressure differential between the main carrier gas line and the sidestream passing through the radon source subsystem. The column effluent is conducted into a vent line and passed through an absolute filter bank for removal of particulates. The filtered carrier gas stream is then diluted with ventilation air supplied by a 6000-scfm blower prior to discharge through the pilot plant stack.

Rn-220 Source Subsystem

The radon source subsystem consists of the radon source material and auxiliaries required for safe containment of the radioactive materials within the system. A description of the components shown in Fig. 7 is given below.

Encapsulated Uranium Disc Assembly. The primary containment for the Rn-220 source material was designed and fabricated by Mott Metallurgical Corporation. The encapsulated uranium disc assembly is designed to provide safety in handling of the U_3O_8 sample during assembly and disassembly of the radon generator. The U_3O_8 was enclosed within a cavity (5.08 cm in diameter by 7.92 mm deep) formed between two porous 316 stainless steel discs. The discs were 2-μ sintered metal filters (5.40-cm o.d. by 2.38 mm thick). The bottom disc was welded to a stainless steel retainer flange, forming a cavity for the U_3O_8. The uranium sample was transferred to the cavity in a glove box. The cavity was then sealed by press-fitting the upper disc so that it rested on a small ledge machined into the flange.

Rn-220 Source Material. The Rn-220 source material consists of 2.097 g U_3O_8 containing 1.733 g uranium. The material is in the form of a black, loose, granular powder containing some fines. The uranium composition on a weight basis is given below:

U-234 = 95.938%
U-238 = 3.91%
U-235 = 0.1040%
U-236 = 0.048%
U-232 = 19.7 ppm (alpha pulse height analysis performed on 9/7/78).

The activities of the U-234 and U-232 are about 10.2 and 0.73 mCi, respectively.

Isolation, Shielding, and Safety Interlocks. The encapsulated uranium disc assembly is sealed between two 2-in. welding neck flanges by two gaskets (Flexitallic Gasket Company). Two manually operated ball valves are welded onto the upstream and downstream flanges. The entire assembly is radially shielded by 2 in. of lead and axially shielded by 1/2 in. of lead.

Upstream of the inlet ball valve and downstream of the outlet ball valve are high-efficiency particulate air (HEPA) filters that capture any particulates that escape from the uranium disc assembly. The HEPA filters are Gelman polysulfyn cartridge model 12791, which have better than 99.97% retention for 0.3-μm particles. On the upstream and downstream sides of the absolute filters are solenoid-operated, fail-close stainless steel block valves (ASCO model 8210 C88). The solenoid valves are interfaced with the motor control center so that they automatically close upon failure of the pilot plant stack blower. The operator is alerted to this condition by a red-light visual alarm. The solenoid valves also automatically close upon power failure, thereby isolating the Rn-220 from the main system.

Radon Detection System

Theoretical Background. Figure 8 shows the decay chain for U-232 and Th-232. In converting thorium to uranium, uranium isotopes are produced in various abundances. Table I gives the five principal isotopes and their typical mass fractions. Alpha emission is predominant in the decay scheme of each of these isotopes and spans a broad energy range. It is assumed, however, that only Rn-220 and its decay products can enter the transport lines. Radon is a gas at ambient temperature, whereas its precursors are nonvolatile solids.

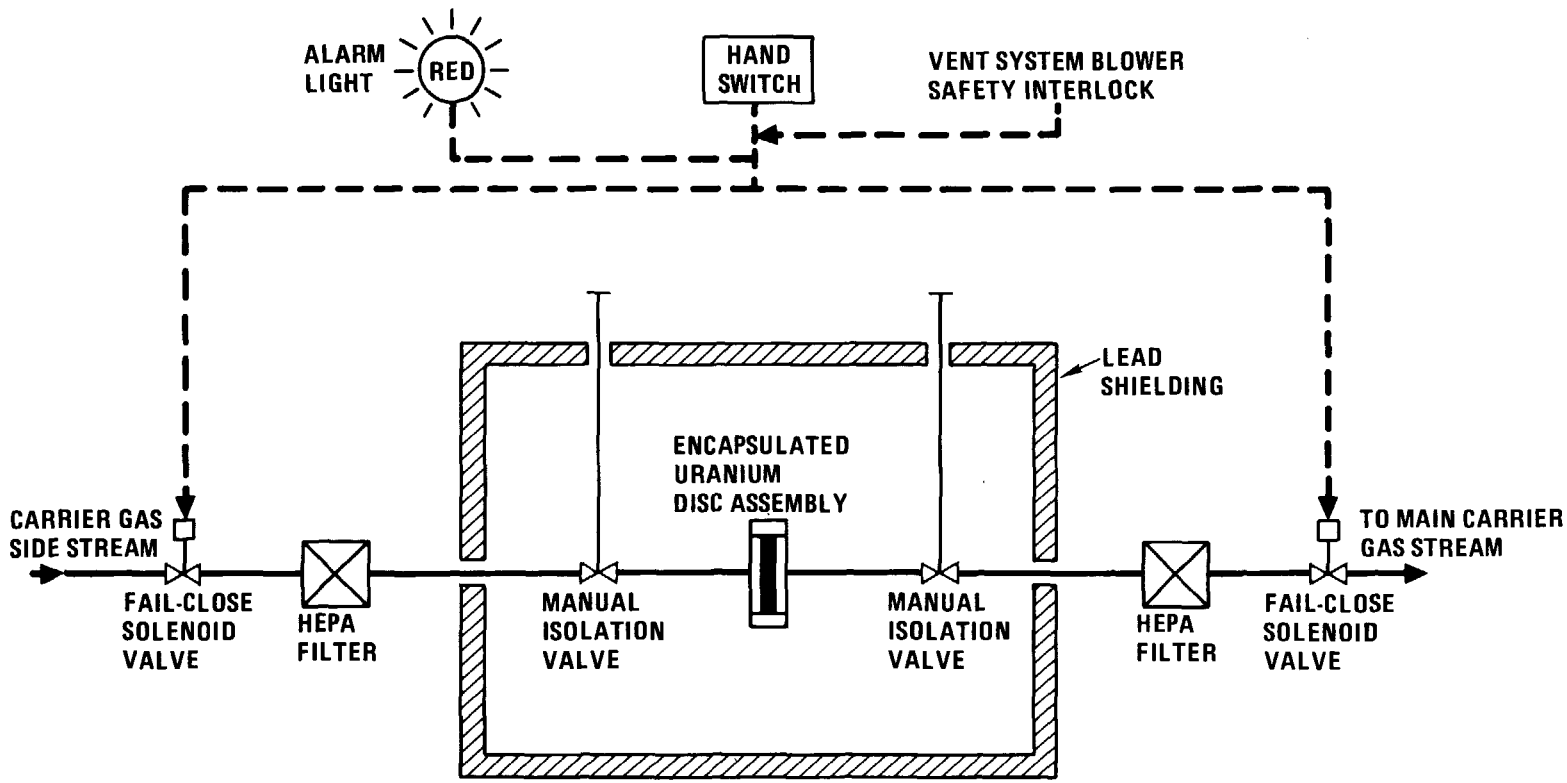

Figure 7. Schematic of the Rn-220 source subsystem.

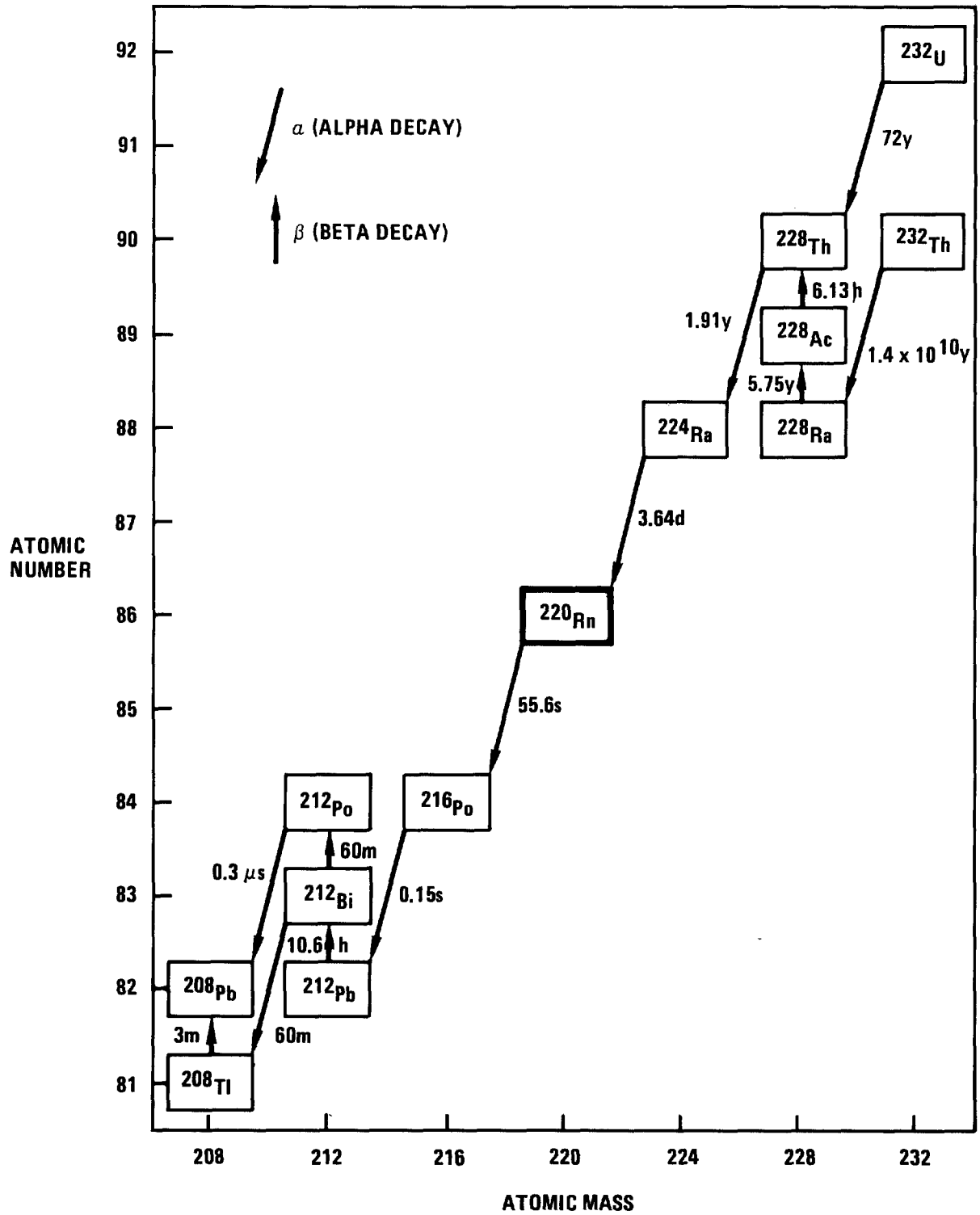

Figure 8. U-232 and Th-232 decay chain.[5]

Table I. Mass fractions of the principal uranium isotopes[7,8].

Isotope	Typical Mass Fraction
U-232	0.00038
U-233	0.83
U-234	0.14
U-235	0.025
U-236	0.003

Table II. The alpha spectrum of Rn-220 and its daughter products[9].

Nuclide	Alpha Energy (MeV)	Alpha Intensity (%)
Rn-220	6.287	~99.7
	5.747	0.3
Po-216	6.78	100
Bi-212	6.049	25
	6.088	10
Po-212	8.78	100

Table II lists the alpha spectra for Rn-220 and its daughter products. The 6.287-MeV alpha particle accompanies the decay of Rn-220 approximately 99.7% of the time. It is possible, therefore, to distinguish Rn-220 from its daughter products by using an electronic system capable of discriminating alpha particles of varying energies. This may be achieved with an alpha detector in series with a single-channel analyzer tuned to the 6.287-MeV alpha energy band emitted by Rn-220. In addition to alpha particles, beta and gamma radiation is also present. The use of an electronic discriminator makes certain that the beta and gamma radiation and all alpha particles whose energy is less than 6.287 MeV are not counted. Similarly, ignoring all particles whose alpha energy exceeds that produced by Rn-220 excludes nuclides emitting more energetic alpha particles from the count. Figure 9 illustrates these concepts.

Flow-Through Alpha Detectors. The flow-through alpha detector assemblies and associated electronics were designed and supplied by Harshaw Chemical Company, Crystal and Electronics Product Department. Figure 10 shows a block diagram of the alpha detector. The detector assembly consists of a flanged, stainless steel chamber fitted with an array of four silicon, diffused-junction, alpha particle detectors. The flow channel contains a series of baffles arranged to maximize the spectral resolution in the analysis.

A diffused-junction detector can be thought of as an ionization chamber in which the gas has been replaced with a semiconducting solid. The semiconductor is a partially depleted, phosphorous-diffused, p-type silicon nuclear radiation detector. Discrimination between alpha particles is based upon the differences in the specific ionization of the particles. The number of ions collected determines the height of the electronic pulse, as illustrated in Fig. 9.

Detector Electronics. The small output signal generated by the diffused-junction detectors requires sophisticated electronics, as shown in Fig. 10. The individual components are as follows:

1. Preamplifier. A low-noise, charge-sensitive preamplifier (Harshaw model NB-25) intended for use with silicon detectors. The charge created in the detectors by radiation energy is converted to an amplified voltage. The preamplifier is located near the flow-through alpha detector assemblies to minimize external electrical interference.

2. Mercury switch pulse generator. A pulse generator (Harshaw model NP-10A) designed to closely simulate the output pulse characteristics of nuclear radiation detectors. It is primarily used for calibrating and testing the associated pulse-handling instruments, i.e., amplifier, single-channel analyzer, scaler, and linear rate meter.

3. Detector bias supply. A high-voltage power supply (Harshaw model NV-30) that provides up to ±300 V dc for operation of solid-state detectors.

4. Amplifier. A research-grade linear amplifier (Harshaw model NA-25) for accepting the output signal from the preamplifier.

5. Single-channel analyzer. A single-channel pulse height analyzer (Harshaw model NC-22) for discriminating the output pulses from the linear amplifier The energy threshold and band width can be selected to allow measurement of the 6.287-MeV Rn-220 alpha particles.

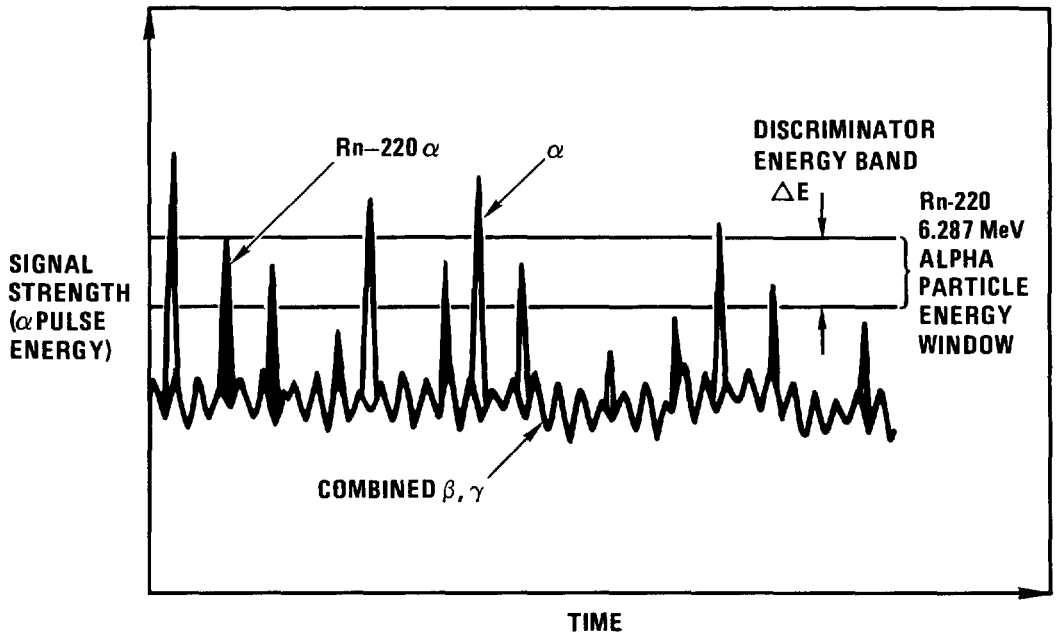

Figure 9. Rn-220 alpha pulse, energy discrimination.

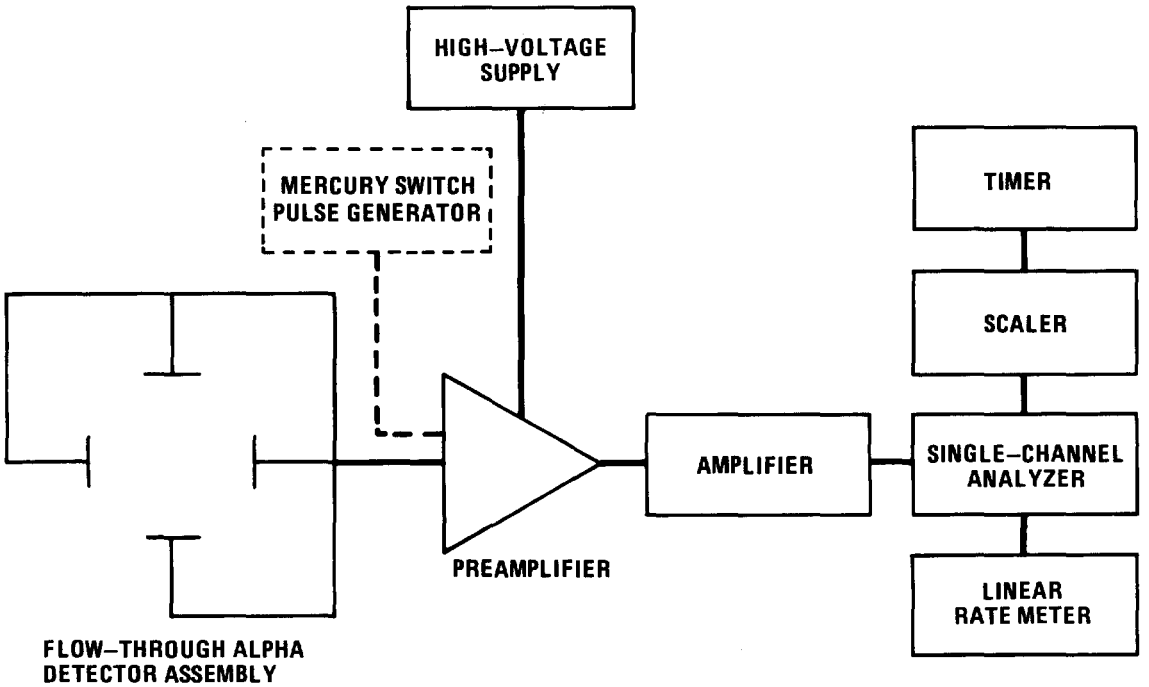

Figure 10. Block diagram of the alpha particle electronic measuring system.

6. Linear rate meter. A linear rate meter (Harshaw model NR-30) driven by the single-channel analyzer. It is capable of measuring alpha count rates from 10 to 10^5 cps in twenty ranges.

7. Scaler. A high-rate pulse counter (Harshaw model NS-12) capable of a maximum continuous count rate of 20 MHz with a resolution of 50 ns. The maximum count capacity is 10^6 with reset capability.

8. Timer. A digital preset timer (Harshaw model NT-27) for control of the scaler. Timing is from 0.1 s to 990 min in 1% increments.

Process Control and Data Acquisition

The main carrier gas and side-stream flow rates are regulated by a Diogenes (Rosemount, Incorporated) process controller. The output signals from the flow indicators, linear rate meter, thermocouples, and pressure sensors are monitored by a Hewlett Packard data acquisition system that continuously scans and displays the test data on a CRT. The data can also be printed and/or stored in a floppy disc file at specified time intervals.

Results

The goals of the radon holdup/decay test series were as follows: (1) to empirically determine the H-mordenite bed length necessary to achieve the design criterion DF of 10^3; (2) to determine the effects of N_2, air, and CO_2 carrier gas on DF at a fixed bed length; (3) to determine the effects of bed regeneration and pretreatment with carrier gas on radon removal efficiency; and (4) to determine whether particulate daughter products of Rn-220 are effectively trapped within the H-mordenite bed.

The first series of runs was carried out to determine the effect of holdup/decay bed length on removal efficiency. Nitrogen carrier gas was chosen because it does not adsorb on H-mordenite. The H-mordenite was used as received; i.e., it was neither regenerated nor pretreated with N_2. The total carrier gas flow rate was 17 Nm^3/h (10 scfm) at a face velocity of 3 m/min through the bed. A 3.4-Nm^3/h (2-scfm) side stream was bypassed through the radon generator subsystem, as shown in Fig. 6.

The column lengths studied were 1.07 m (3.5 ft), 1.52 m (5.0 ft), 2.29 m (7.5 ft), and 3.05 m (10.0 ft). Table III presents the test conditions for runs 1 through 4. The diffused-junction detectors were cleaned with absolute ethanol and dried with high-purity nitrogen before each run. A background noise count was taken at the inlet and the outlet of the radon holdup/decay bed immediately prior to introducing radon into the carrier gas. At the completion of each run, a background count was taken to account for any daughter products that accumulated on the diffused-junction detectors. The average value of these two alpha count rates was used to correct the data obtained during actual radon measurement for background noise and detector contamination. Immediately after introducing radon into the system, a Rn-220 alpha energy spectrum was measured at the bed inlet to set the detection band so that overlapping daughter peaks such as Bi-212 and Po-212 could be discriminated. This procedure was carried out before each run.

Figures 11 through 14 plot the total adjusted inlet and outlet Rn-220 alpha counts versus time. The accuracy of the alpha detectors was severely affected by electrical interference introduced by other pilot plant activities. Therefore, the runs were carried out after normal working hours, limiting their duration. The Rn-220 removal efficiency is expected to decrease slowly during a long-term run owing to adsorption of Rn-220 daughter products and small quantities of moisture onto the

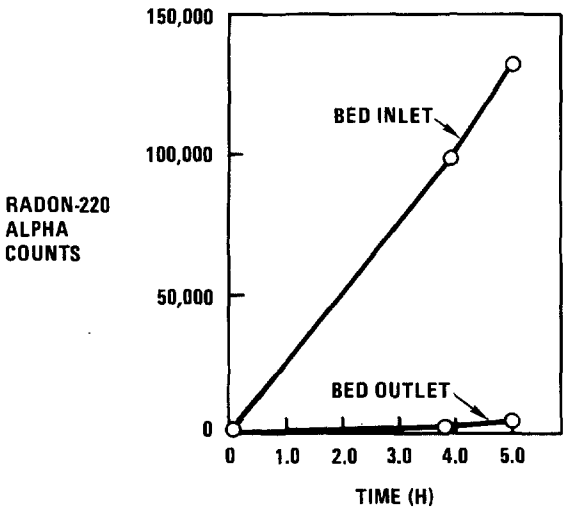

Figure 11. Cumulative Rn-220 alpha counts for the inlet and outlet of a 1.07-m (3.5-ft) holdup/decay bed

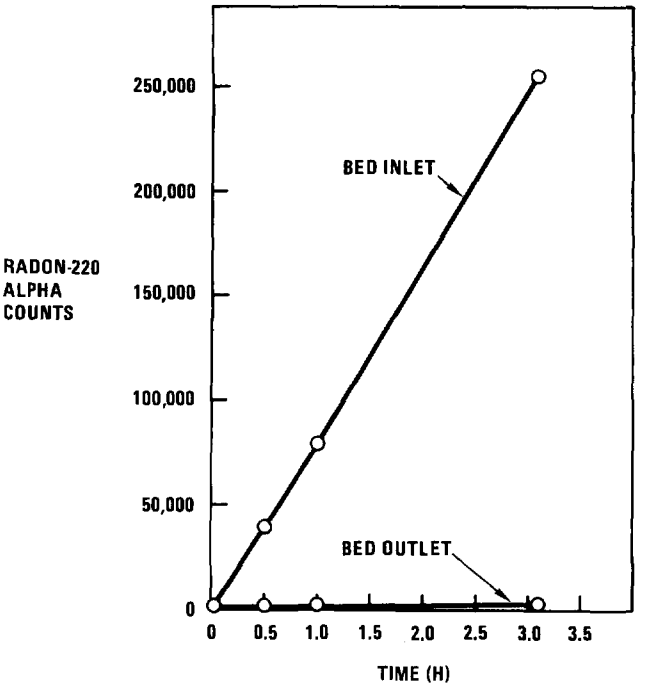

Figure 12. Cumulative Rn-220 alpha counts for the inlet and outlet of a 1.52-m (5.0-ft) holdup/decay bed.

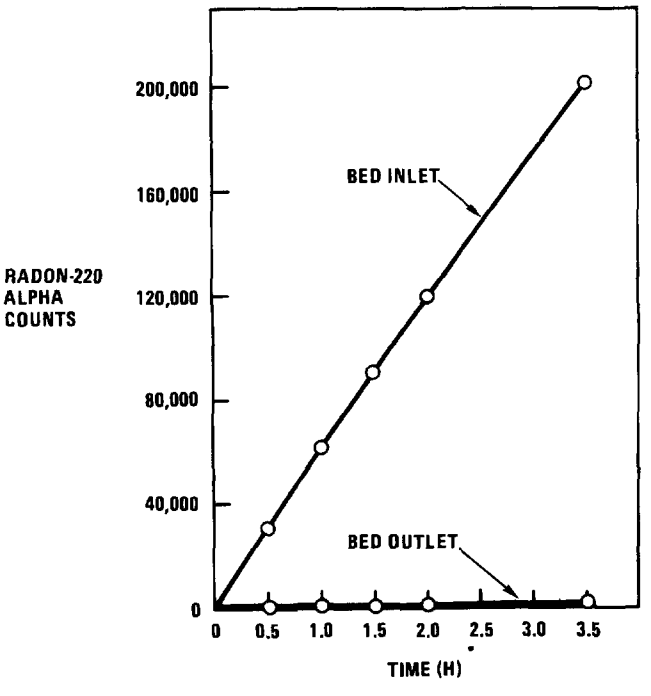

Figure 13. Cumulative Rn-220 alpha counts for the inlet and outlet of a 2.29-m (7.5-ft) holdup/decay bed.

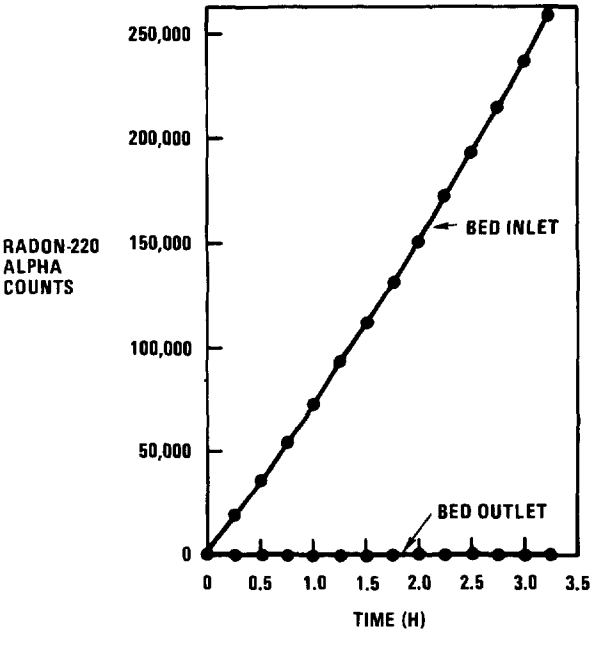

Figure 14. Cumulative Rn-220 alpha counts for the inlet and outlet of a 3.05-m (12-ft) holdup/decay bed.

bed material. The cumulative DFs, i.e., the total inlet Rn-220 alpha counts divided by the total outlet Rn-220 alpha counts over the duration of the run, are presented in Table III and shown graphically in Fig. 15 for the bed lengths studied.

A mechanistic analysis of the removal of short-lived isotopes by holdup and decay in an adsorbent bed yields a general equation which takes into account three mechanisms of mass transport: (1) molecular diffusion in the gaseous phase; (2) eddy diffusion; and (3) intraparticle mass transfer resistance[10]. The equation at steady-state is:

$$\frac{C}{C_o} = \exp\left\{-\frac{LV_s}{2D}\left[\left(1 + \frac{4D\rho K\lambda}{V_s{}^2}\right)^{1/2} - 1\right]\right\} , \qquad (1)$$

where C_o = concentration of the radioactive isotope in the feed to the adsorption bed,
C = concentration of the radioactive isotope in the effluent from the adsorption bed,
D = effective diffusion coefficient,
K = effective adsorption coefficient,
L = length of adsorption bed,
V_s = superficial carrier gas velocity,
λ = decay constant for the radioactive isotope,
ρ = bulk density of the adsorbent.

Combining constant terms, Eq. 1 can be rewritten as:

$$DF = \exp(k'L) = k^L , \qquad (2)$$

where

$$DF = C_o/C , \qquad (3)$$

and

$$k' = \frac{V_s}{2D}\left[\left(1 + \frac{4D\rho K\lambda}{V_s{}^2}\right)^{1/2} - 1\right] \qquad (4)$$

is a constant for the fixed run conditions.

This simple expression can be used to fit the data given in Table IV. Figure 16 shows a plot of log DF versus L. A least-squares analysis yields a value of 2.15 for the constant k when L is measured in feet. Figure 15 shows the curve determined by the least-squares analysis. This curve predicts a 2.74-m (9-ft) bed length to achieve a DF of 10^3, which is in good agreement with the results found for CO_2 carrier gas in previous laboratory-scale experiments.[5]

The DOG at the inlet to the radon holdup/decay bed is primarily air, whereas the BOG at the radon holdup/decay bed inlet is primarily CO_2. It was therefore necessary to determine the DF of Rn-220 in both air and CO_2 carrier gas so that the results could be applied to the design of a full-scale facility.

The carrier gas can have an effect on the adsorption properties of Rn-220 owing to competition with Rn-220 for adsorption sites. Nitrogen and oxygen do not have a

Table III. Rn-220 holdup/decay test conditions and results.

Run No.	Bed Length [m (ft)]	Carrier Gas	Total Flow Rate [Nm^3/h (scfm)]	Radon Source Subsystem Flow Rate [Nm^3/h (scfm)]	Holdup/Decay Bed ΔP [kPa (in. H_2O)]	Cumulative Rn-220 DF
1	1.07 (3.5)	N_2	17.5 (10.3)	3.4 (2.0)	0.069 (0.3)	31
2	1.52 (5.0)	N_2	7.7 (10.4)	3.4 (2.0)	0.49 (1.9)	180
3	2.29 (7.5)	N_2	17.5 (10.3)	3.4 (2.0)	0.90 (3.6)	290
4	3.05 (10.0)	N_2	17.4 (10.2)	3.4 (2.0)	1.4 (5.5)	830
5	3.05 (10.0)	CO_2	16.8 (9.91)	3.4 (2.0)	1.4 (5.5)	$\geq$1000
6	3.05 (10.0)	Air	17.5 (10.3)	3.4 (2.0)	1.4 (5.5)	$\geq$3800

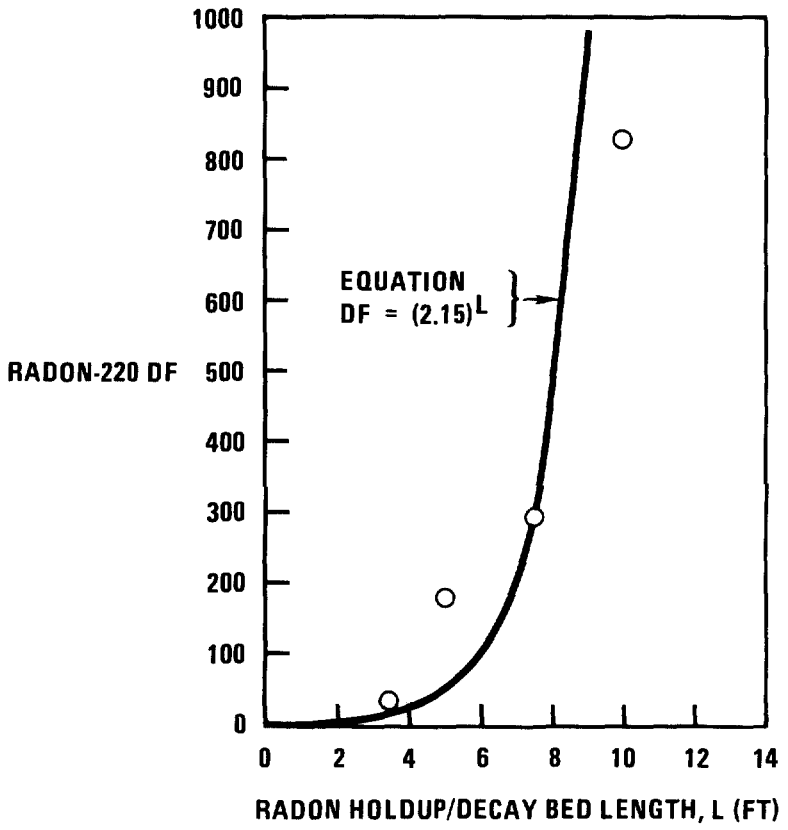

Figure 15. Rn-220 decontamination factor versus radon holdup/decay bed length.

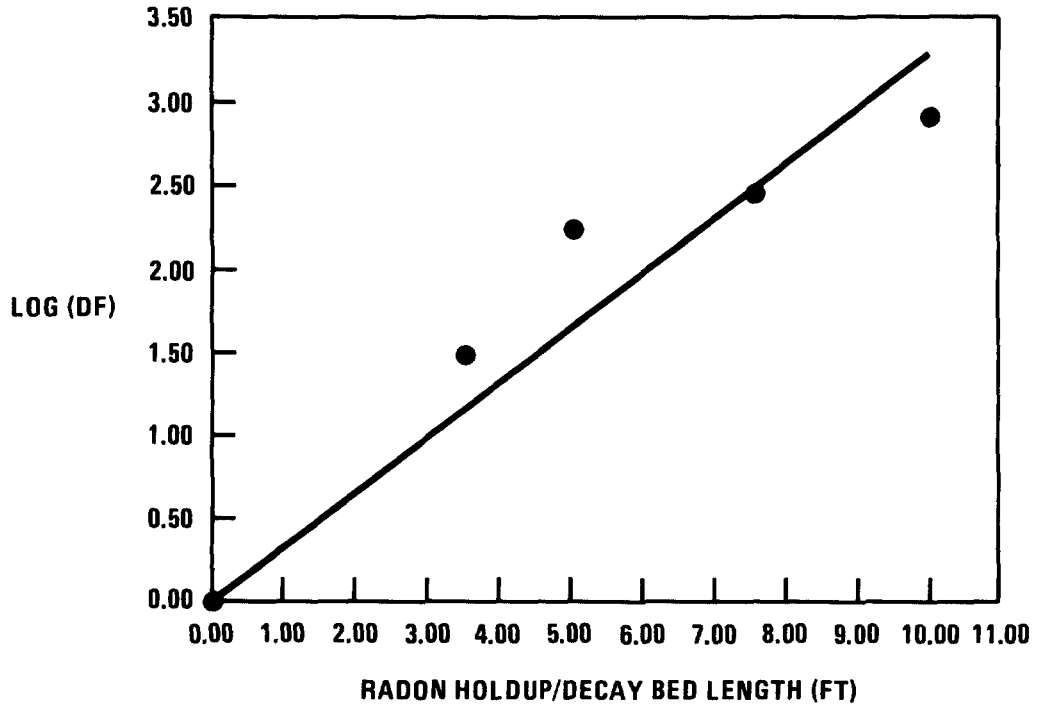

Figure 16. Plot of log DF versus radon holdup/decay bed length.

significant affinity for H-mordenite, and Rn-220 should have the same adsorption behavior in each of these carrier gases. Carbon dioxide, however, adsorbs strongly on H-mordenite, and the behavior of Rn-220 in this gas may differ from that in N_2 and air.

Table III shows the test conditions for runs 5 and 6. Prior to each run, the 3.05-m (10-ft) holdup/decay bed was regenerated with dry N_2 at 200°C for about 24 h. For run 5, the H-mordenite was pretreated with a steady 17-Nm^3/h (10-scfm) flow of CO_2 for 48 h before introducing Rn-220 into the feed. A 55°C bed temperature gradient was observed, indicating that CO_2 was being strongly adsorbed. Pretreatment was considered complete when the H-mordenite regained ambient temperature. Radon-220 was introduced into the carrier gas and measured at the inlet and the outlet of the radon holdup/decay bed for 4 h. No measurable Rn-220 was detected at the outlet of the bed over the duration of the run after adjusting for background counts. The maximum measurable DF, based on the background counts at the outlet alpha detector, was slightly greater than 1000. Therefore, the actual DF for a 3.05-m (10-ft) bed with CO_2 as the carrier gas was at least 1000.

Prior to run 6, the H-mordenite was pretreated with a 17-Nm^3/h (10-scfm) flow of dry simulated air (80% N_2, 20% O_2) for 3 h before introducing Rn-220 into the feed stream. The Rn-220 concentration was measured at the bed inlet and the outlet for 3 h. No measurable Rn-220 was detected at the outlet of the bed over the duration of the run after adjusting the measured counts for background noise. The maximum measur-able DF, based on the background counts at the outlet alpha detector, was about 3800. Therefore, the actual DF for a 3.05-m (10-ft) bed with air as the carrier gas was at least 3800.

During the air and CO_2 carrier gas studies, trace amounts of Rn-220 daughter products were detected in the radon holdup/decay bed effluent. These particulates can be removed from the off-gas stream by installing a HEPA filter at the outlet of the bed.

Conclusions and Recommendations

A series of Rn-220 removal tests was carried out with the radon holdup/decay subsystem of the GA engineering-scale off-gas treatment system. The removal efficiency was studied in N_2, air, and CO_2 carrier gas streams to simulate dissolver and burner off-gas compositions.

In N_2 carrier gas, the Rn-220 DF obeyed the relation $DF = (2.15)^L$, where L is the length of the holdup/decay bed in feet. Although this expression represents a statistical fit of a small number of data points, it is in good agreement with the results found for CO_2 carrier gas in previous laboratory-scale experiments[5].

A DF in excess of 1000 was demonstrated in air and CO_2 carrier gas streams for a bed length of 3.5 m (10 ft). However, a 3.66-m (12-ft) bed is recommended to ensure that the design DF of 1000 is attained.

The H-mordenite adsorbent for Rn-220 removal must be regenerated prior to its use, because adsorbed water reduces its effective radon removal efficiency.[5] For BOG streams, the adsorbent must be pretreated with CO_2 to protect against the initial flow perturbation and heat generation caused by the adsorption of CO_2.

Trace amounts of Rn-220 daughter products in the bed effluent can be removed from the off-gas stream. Installation of a HEPA filter at the outlet of the bed is recommended to trap these particulates.

Acknowledgment

The authors extend their appreciation to John W. McLean for his technical support in conducting the experiments and maintaining the equipment.

References

1. Abraham, L., and P.M. Hirsch, "Consolidated fuel reprocessing program interim development report: off-gas treatment system," DOE Report GA-A16292 (June 1981).

2. Hirsch, P.M., "Consolidated fuel reprocessing program: off-gas treatment system NO_X converter component tests," DOE Report GA-16559 (January 1982).

3. Hirsch, P.M., "Selected conversion of NO_X by catalytic reduction with ammonia," Environ. Prog. 1, 24-29 (February 1982).

4. Forsberg, C.W., "Separation of radioactive krypton from carbon dioxide and oxygen with molecular sieves," Oak Ridge National Laboratory Report ORNL/TM-5826 (October 1977).

5. Hohorst, F.A., "Containment of Rn-220 via adsorption on molecular sieves for HTGR-OGCS," Idaho National Engineering Laboratory Report ICP-1114 (May 1977).

6. Ruthven, D.M., J.S. Devgun, and F.H. Tezel, "Removal of Kr from N_2 by selective adsorption," in Proceedings of the Sixteenth DOE Nuclear Air Cleaning Conference, Vol. 1, p. 177 (February 1981), CONF-801038.

7. Hamilton, C.J., et al., "HTGR spent fuel composition and fuel element block flow," DOE Report GA-A13886, Vol. II (July 1976).

8. Zane, G., et al., "Large high-temperature gas-cooled reactor medium-enriched uranium spent fuel element definitions and block flows," DOE Report GA-A14980, Vol. II (August 1978).

9. Weast, R.C. (ed.), Handbook of Chemistry and Physics, The Chemical Rubber Company, Cleveland (1967).

10. Underhill, D.W., "A mechanistic analysis of fission-gas hold-up beds," Nucl. Appl. 6, 544 (1969).

DISCUSSION

HOHORST: What absolute concentrations of ^{220}Rn were used in, for example, curies·meter $^{-3}$?

HIRSCH: The U_3O_8 sample that was used for these tests contained approximately 20 ppm U-232. This was the only such source available in the USA for Rn-220 generation. The actual Rn-220 release from the U_3O_8 sample depends on Rn-220 generation, diffusion, and decay within the U_3O_8 particles. The actual release from these particles is indeterminable. Therefore, we did not obtain absolute Rn-220 concentrations, but rather measured the relative concentration at the bed inlet and outlet to calculate the DF. Since the amount of Rn-220 produced by a reprocessing plant on a yearly basis is extremely small, (in the mg range) the large size of the Rn holdup/decay bed is more than adequate to treat all the Rn-220.

LITTLE: CO_2 removal using 5A sieves appears effective. However, the use of N_2 for dilution to prevent heat buildup is counter productive. How does this dilution affect the final collection of the Kr product?

HIRSCH: Alternatives to nitrogen dilution may consist of either modifying the CO_2/Kr separation bed by installation of internal heat exchangers or by operating the CO_2/Kr separation bed at much colder temperatures to counteract the heat generation by CO_2 adsorption. The effectiveness of these processes has yet to be determined. With respect to nitrogen dilution, the resultant Kr-rich N_2 effluent needs to be separated in another process for further concentration of Krypton prior to Krypton waste storage. A Canadian study given in reference 6 has shown that removal of krypton from N_2 gas streams by selective adsorption is technically feasible.

RINGEL: Will it be technically feasible to separate a larger amount of CO_2 from a smaller amount of Kr by adsorption of the CO_2?

HIRSCH: The Kr concentration in KALC overhead product is high enough to allow separation of Kr from CO_2 with a relatively larger concentration by adsorption. The flow rate from KALC is about 0.5 LPM. It will not require much bed material to capture the CO_2 for long periods of time. In addition, the separation bed can be regenerated and re-used.

ADSORPTION OF GASEOUS RuO_4 BY VARIOUS SORBENTS. II

Lj. Vujisić and R. Nikolić
Department of Chemistry
Boris Kidrič Institute of Nuclear Sciences-Vinča
Belgrade, Yugoslavia

Abstract

Sorption of gaseous RuO_4 on impregnated Alcoa Alumina H-151 impregnated charcoal, silica gel and HEPA filter was investigated. The results obtained on various sorbents are compared and discussed in connection with possibilities to use chosen material in air cleaning systems.

I. Introduction

Ruthenium, in nuclear facilities, transforms to volatile compounds rather easily and because of its elusive and variable chemical and gama- ray spectral characteristics it is rarely detected in waste gases. However, Ru-103 and Ru-106 have generally been observed among the principal radionuclides precipitated by rainfall and pollen[1].

Among volatile radioactive species removal of ruthenium tetroxide from waste gases is greatest problem. In the last years large number of papers have been published concerning its adsorption. Unfortunately, many investigators seem to have avoided purification of RuO_4 from other volatile compounds during its generation. Because of usually unknown RuO_4 initial concentration it is impossible to make complete balance of RuO_4 in adsorption experiments. That is one of the reasons why decontamination factor and adsorption characteristics for the same materials differ in various papers concerning RuO_4 adsorption.

Among many investigated materials for RuO_4 adsorption the best results were obtained with silica gel. However, there is dis-

agreement in results obtained on silica gel as adsorbent for RuO_4 given by different authors. Descreapances in the results may be caused by different characteristics of silica gel and by different experimental conditions. Most experiments were done at high temperature and long residence time which are not normal operating conditions of filtration systems.

In this paper special attention was paid to generate very pure RuO_4 of known concentration and to find suitable adsorption material for RuO_4 under normal ventilation conditions (25°C, residence time 0.3 sec). Adsorption materials investigated in the present work were blue silica gel (Merck), Alcoa Alumina H-151 and Alcoa Alumina H-151 impregnated with: $CrCl_3$, $K_2Cr_2O_7$, Na_2CrO_4, $CoCl_2$ and $Co(NO_3)_2$.

II. Experimental

Anhydrous ruthenium tetroxide was prepared from ruthenium chloride by following procedure. First, ruthenium chloride was fumed with concentrated sulfuric acid to remove the chlorides. Solution of $^{106}RuCl$ (product of Amersham) was also treated with sulfuric acid and the chlorides were removed by repeated evaporation of sulfuric acid solution. Aliquots of ruthenium sulfate solutions labelled with ^{106}Ru were added to the solutions of inactive ruthenium sulfates in 50% sulfuric acid and heated to 60°C in an all glass apparatus. Solid sodium bismuthate was added to oxidize ruthenium to ruthenium tetroxide and slow stream of dry nitrogen was passed through the apparatus. Ruthenium tetroxide vapor, carried by the stream of nitrogen, was dried with anhydrous magnesium perchlorate and collected in an U shaped glass tube, which was immersed into a trap containing solid carbon dioxide.

In order to obtain certain concentration of ruthenium tetroxide in the gas stream for adsorption experiments the U shaped tube was immersed in NaCl-ice bath and stream of dry nitrogen was passed through it. Temperature of the bath and flow rate of nitrogen were determined in preliminary experiments for several desired RuO_4 concetrations. Concentration and purity of ruthenium tetroxide were determined spectrophotometrically. For spectrophotometric measurements ruthenium tetroxide was collected in dilute perchloric acid and spectra of these solutions were registrated immediately after the gas

generation. The spectra were typical for ruthenium tetroxide solutions in perchloric acid[2].

Adsorption of ruthenium tetroxide was followed by measurements of gama radioactivity of sorbent samples on a scintillation counter. Concentration of ruthenium tetroxide in the gas stream and concentration of ruthenium species retained with sorbents were calculated from known initial specific radioactivity of generated ruthenium tetroxide. Therefore in order to calculate ruthenium concentration in this way, in adsorption experiments, it is necessary to obtain very pure ruthenium tetroxide, labelled with ^{106}Ru isotope.

Adsorption of ruthenium tetroxide by various sorbents was first investigated under nearly stationary conditions. Ruthenium tetroxide was carried by a very slow stream of dry nitrogen (0.2 dm^3/h) through a series of glass tubes containing various sorbents which are normaly used in filtration systems of nuclear facilities. From these experiments the most convenient sorbents for ruthenium tetroxide were chosen for further investigation. Sorbents for investigation of ruthenium tetroxide adsorption were placed in a glass column with 5 cm inner diameter. Apparatus for investigation of ruthenium tetroxide adsorption is schematically presented in the Figure 1.

The column was filled with three separate beds of various sorbents. The first bed was the test bed followed by the two safety beds. Two separate safety columns were also placed after the adsorption column.

Ruthenium tetroxide of desired concentration was passed through the adsorption column with air stream of 360 dm^3/h flow rate, Residence time was, in all experiments, 0.3 sec. Relative humidity of the air was $60\pm5\%$ and the temperature of the air stream and the test bed was 22-25°C.

III. Results and Discussion

In preliminary experiments of ruthenium tetroxide adsorption by various sorbents[3] it was shown that silica gel is promissing material for adsorption of ruthenium tetroxide in filtration system of nuclear facilities, when the adsorption is carried out under normal filtration conditions (25°C, 60% R.H., residence time

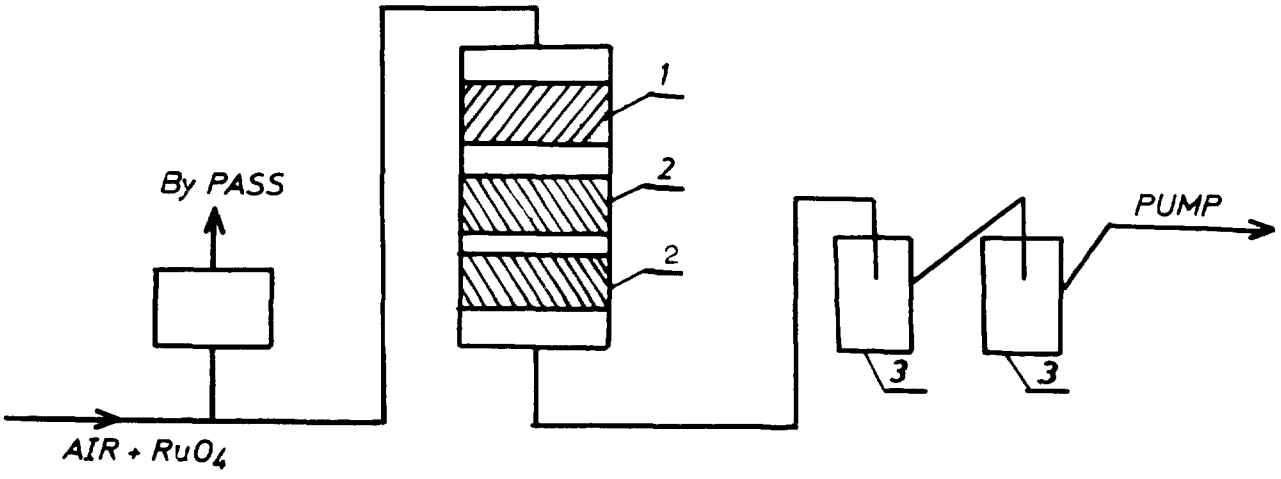

Figure 1. Schematic diagram of the apparatus for investigation of adsorption of RuO_4; (1) test bed, (2) safety beds, (3) safety columns.

0.3 sec.).

For investigation of ruthenium tetroxide adsorption blue silika gel, produced by Merck, grain size 1-1.6 mm containing 2% of moisture was chosen. Chemical analysis of the silica gel, used in these experiments, show that it contains iron, cobalt, nickel and chromium. During adsorption of ruthenium tetroxide on this silica gel from the wet air stream black deposit on silica gel have been formed immediately. Retention of ruthenium tetroxide in these experiments was better than 99.8%. Detailed information about experimental conditions and results of ruthenium tetroxide sorption on blue silica gel are given in previous paper[3].

There are some assumptions[4] that ruthenium tetroxide is physically adsorbed on silica gel. If that is the case one could expect adsorbed ruthenium species to be eluted from silica gel by water or acids. However, if Merck's blue silica gel after adsorption of ruthenium tetroxide is immersed in 50% H_2SO_4 only less than 0.1% of adsorbed ruthenium is dissolved. Therefore, it can be assumed that ruthenium tetroxide is chemically adsorbed on silica gel. Probable mechanism of adsorption is gradual reduction of ruthenium tetroxide by

polyvalent metal ions, contained in silica gel, into a stable RuO_2. If this conclusion is correct than good adsorption of ruthenium tetroxide by other sorbents which are impregnated or contain polyvalent metal ions can be expected. It is known[5] that iron wool and Fe_2O_3 powder are also fairly good sorbents for RuO_4, but from some practical reasons they are not convenient for use in an off gas filtration systems (filling and refilling of adsorption columns). To avoid failure due to indefinite grain size of iron materials Alcoa Alumina H-151, which contains 0.1% of Fe_2O_3 and have definite grain size was chosen as a base material for sorption of RuO_4.

Alcoa Alumina H-151 is inexpensive, chemically stable and inflammable. It also may have advantage in comparison with silica gel because it adsorbs water poorly while capacity of silica gel for RuO_4 is reduced by significant water adsorption.

Sorption of RuO_4 was investigated on Alcoa Alumina H-151 without further treatment and Alcoa Alumina H-151 impregnated with: 0.1M $CrCl_3$, 0.1M $K_2Cr_2O_7$, 0.1M Na_2CrO_4, 0.1M $CoCl_2$ and 0.1M $Co(NO_3)_2$. The residence time in all the experiments was 0.3 sec, temperature of the air stream and the test bed was 22-25°C, and relative humidity of the air stream was $60 \pm 5\%$. The results obtained on these sorbents are presented in Table I. In the same table the results for sorption of RuO_4 on silica gel[3] under the same condition are given for comparison.

From the Table I it can be seen that unimpregnated Alcoa Alumina H-151 adsorbs RuO_4 very poorly although it was expected that it would be very good adsorber since it contains 0.1% of Fe_2O_3. In addition to it, safety beds with Merck's silica gel and the safety columns did not retain ruthenium species after they passed the Alcoa Alumina H-151 bed. Similar effect was observed earlier with other sorbents[6].

From Table I it can also be seen that all the sorbents investigated retain RuO_4 to some extent. With exception of silica gel and Alcoa Alumina H-151 impregnated with $Co(NO_3)_2$ significant losses of ruthenium from the system are observed with all the sorbents. A tentative explanation for this behavior might be that with strong reducing agents RuO_4 is directly reduced to RuO_2 with evalution of oxygen which prevents further reduction of RuO_4 in the gas stream. Similar behavior was observed with activated charcoal and HEPA

Table I. Results of RuO_4 adsorption on various sorbents; temperature 22-25°C, relative humidity 60±5%, residence time 0.3 sec.

impregnant	C(mg/m^3)	Q_o(mg)	R(%)	Q_1(mg)
Alcoa Alumina H-151				
	6.0	1.67	1.20	1.61
$CrCl_3$	7.2	2.66	44.4	1.46
$K_2Cr_2O_7$	10.2	3.04	21.8	2.34
Na_2CrO_4	4.0	1.85	22.3	1.38
$CoCl_2$	2.8	1.04	39.6	0.58
$Co(NO_3)_2$	0.9	0.34	99.9	0.0
Blue Silica Gel[3]				
	10.0	0.50	99.9	0.0
	9.7	0.97	99.9	0.0
	9.7	1.45	98.5	0.0
	9.4	1.65	98.2	0.0
	10.2	2.04	98.0	0.0
	10.0	2.92	97.3	0.0

C - concentration of RuO_4 in the air stream,
Q_o - generated amount of RuO_4,
R - retention of RuO_4 by the test bed,
Q_1 - no nadsorbed amount of RuO_4 in the system.

filters[3,6]. Difference between sorption properties of Alcoa Alumina H-151 impregnated with $Co(NO_3)_2$ and $CoCl_2$ may be explained by oxidative properties of NO_3 ions and possibilities of various complex formation between ruthenium and nitrates[7].

IV. Conclusion

Results of RuO_4 adsorption on charcoal, silica gel and Alcoa Alumin H-151 unimpregnated and impregnated by chromium and cobalt salts show that probably the most important fact is the way

of reduction of RuO_4. If reduction of RuO_4 goes directly to RuO_2 or metal ruthenium than oxygen is evolved. Hence, oxidative atmosphere is formed which prevents further reduction of RuO_4. Oxidative atmosphere might also be formed when other oxidative substances are present in the gas stream. For instance, in nuclear power plants, various iodine species which are present in the waste gases stream may also interact with ruthenium volatile species causing losses of ruthenium in filtration systems and difficulties in detection of ruthenium species on the filters.

Satisfactory adsorption material for ruthenium tetroxide can only be a sorbent on which reduction of ruthenium tetroxide goes slowly and gradually through formation of ruthenium compounds in which ruthenium is in various lower oxidation states.

Acknowledgements: Performed under contract of Serbian Fund for Scientific Activities.

References

1. G.G.Eichholz, Prog.Nucl.Energy, 2, 29 (1978).
2. R.E.Connic, C.R.Hurley, J.Am.Chem.Soc., 74, 5012 (1952).
3. R.Nikolić, Lj.Vujisić, Jahrenstagung Kerntechnik, Düsseldorf, 1981, p.323
4. M.Klein, C.Weyers, W.R.A.Goossens, IAEA-SR-72/03, 1982.
5. A.Donato, W.Bocola, Energ.Nucl. (Milan), 18, 353 (1971).
6. R.Nikolić, Lj.Vujisić, unpublished data.
7. F.A.Cotton, G.Wilkinson, Advanced Inorganic Chemistry, Interscience Publishers, 1962., p.820.

DISCUSSION

KLEIN, M.: Do you think the difference in the trapping mechanism for Ru could be: (1) in the case of silica gel, RuO_4 is first adsorbed and then reduced so that the Ru remains on the bed (2) in the case of impregnated Alcoa alumina, RuO_4 is reduced in the gas phase into aerogels of Ru oxides which are not efficiently trapped by either a silia gel bed or an Alcoa alumina bed?

Vujisic: The mechanism of RuO_4 adsorption on silica gel is slow and gradual reduction occurs on it. But in the case of Alcoa alumina 4-151 (either unimpregnated or impregnated with Cr and Co salts, except Co $(NO_3)_2$) it reduces directly and a lot of oxygen is liberated. So, this oxidative atmosphere prevents further reduction of RuO_4 on the sorbent material.

TEST RESULTS IN THE TREATMENT OF HTR REPROCESSING OFF-GAS

H. Barnert-Wiemer
B. Bendick
B. Juergens
A. Nafissi
H. Vygen
Kernforschungsanlage Juelich GmbH,
Juelich, Fed. Rep. of Germany
W. Krill
Nukem GmbH, Hanau, Fed. Rep. of Germany

Abstract

The AKUT II-facility (throughput 10 m^3/h, STP) for the clean up of the burner off-gas has been tested with synthetic off-gas and with off-gas from cold burner tests. The results are reported.

During dissolution of the burner ash in nitric acid an off-gas is formed whose main component is air and which, besides the gaseous fission products, contains NO_x. Before the separation of the gaseous fission products NO_x and/or O_2 are removed by reaction with H_2 or NH_3. For these reactions catalysts were used. Because of the known disadvantages of catalytic systems, like reduction in efficiency by poisoning or thermal influence, the alternative method of thermal, flameless reduction was tested.

The reactions were carried out in a stainless steel and a quartz reactor. Throughput, reaction temperature, O_2-, NO_x-, H_2-, and NH_3-concentrations respectively were varied. The goal of these tests was to remove O_2 and NO_x to below 1 ppm behind the reactor and NH_3 to below the detection limit of 50 ppm.

It was found that at a reaction temperature of 750°C in the stainless steel reactor these goals can be reached for both H_2 and NH_3 as reducing agents. In the quartz reactor only the O_2-H_2-reaction takes place. Obviously stainless steel acts as a catalyst for all other reactions.

I. Burner Off-Gas

The composition of the burner off-gas

The burner off-gas consists mainly of CO_2 with varying amounts of CO and impurities in the ppm-range (Table I), of which I_2, Xe, Cs, and part of the Kr are fission products. The water vapor contains also 10^{-2} ppm fission product T in the form of tritiated water. The rest of the impurities stems from the oxygen used for burning and from the graphite. O_2 should not be present in the off-gas in the percent range except for burner disturbances. When the O_2 concentration reaches 5 % the burner is shut down automatically.

CO_2	85 Vol %
CO	15 Vol %
(O_2	< 5 Vol %)
H_2O	1000 ppm
Xe	42 ppm
Kr	18 ppm
J_2	1 ppm
Cs-Aerosols	50 mg/m³
N_2	50 ppm
Ar	550 ppm
CH_4	30 ppm
C_mH_n	30 ppm
SO_2	6 ppm
Cl_2	2 ppm
NO_x	1 ppm
NH_3	0,5 ppm

Table I: Typical Composition of the Burner Off-Gas

The AKUT II-facility

To clean up the burner off-gas the AKUT II-facility [1,2] has been built. The facility is operated with synthetic off-gas and with off-gas from the JUPITER facility [3].

The AKUT II-facility with a nominal throughput of 10 m³/h [STP] is divided into a low pressure section ($p \leq 1,5$ bar) for the removal of impurities other than Kr and a high pressure section ($p \leq 100$ bar) for the enrichment and separation of Kr (Figure 1).

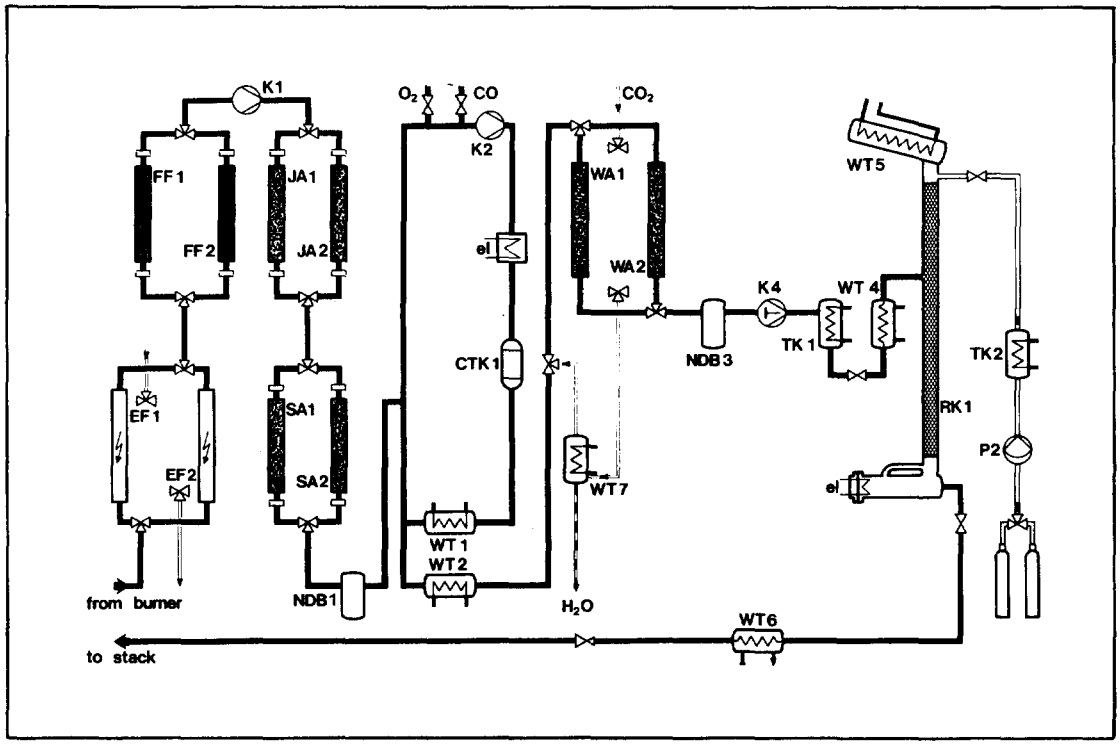

Figure 1: Schematic Flowsheet of the AKUT II-Facility

The low pressure section comprises electrostatic precipitators (EF 1+2), HEPA-filters (FF 1+2), adsorption beds for I_2 and Cl_2 (IA 1+2), SO_2 (SA 1+2), and H_2O (WA 1+2) and a recycle system with a catalytic oxidizer (CTK 1) for the conversion of CO and O_2 to CO_2 (Table II).

AKUT II Component	Bed		Material		Operation			Regeneration		
	Volume [l]	Height [mm]	Name	Manufacturer	Pressure [bar abs.]	Temperature [°C]	Nominal Gas Velocity [m/s]	Pressure [bar abs.]	Temperature [°C]	Gas Velocity [m/s]
I_2-Adsorber (IA 1 + 2)	6.5	650	AC 6120	Süd-Chemie, München	1.4	25	0.21	–	–	–
SO_2-Adsorber (SA 1 + 2)	6.5	650	Zeolon 900 Na	Norton, Wesseling	1.3	25	0.23	1.1	250	0.24
Oxidizer (CTK 1)	12	2 x 40	1922 K (0.15 % Pd)	Kali-Chemie, Hannover	1.2	250-650	Space Velocity: 12.5 m^3 (STP)/lh	–	–	–
H_2O-Adsorber (WA 1 + 2)	6.5	650	3 A Molecular Sieve	Merck, Darmstadt	1.2	25	0.25	1.1	350	0.28

Table II: AKUT II, Adsorption and Catalyst Beds

For the enrichment of Kr the gas is compressed (K 4), liquefied (TK 1 and WT 4), and fed into the distillation column (RK 1).

The two sections have been operated separately. The following analyzers were used for monitoring concentrations:

Halogens: Oxidant Monitor Type 924-9 by Mast Co., Davenport, Iowa

SO_2: Model 953 by Beckman, Munich, and a model 299 by Perkin-Elmer, Überlingen, with a 20 m gas cell

H_2O: AQUANAL by K. Gerhard, Blankenbach

CO: URAS by Hartmann und Braun, Frankfurt and a model 299 by Perkin-Elmer, Überlingen, with a 20 m gas cell

O_2: MAGNOS by Hartmann und Braun, Frankfurt, and a Type OA 137 by Servomex, Ratingen

Test results

Three test phases can be distinguished: first the components were tested separately. Then the low pressure section was tested as a whole before it was connected to the JUPITER facility.* In table III the tested flows and concentrations in the feed and the

*With JUPITER off-gas 5 test runs were made with a duration between 4,5 and 7 hours

resulting effluent concentrations are listed.

	Synthetic Off-Gas		JUPITER Off-Gas	
	Feed	Effluent	Feed	Effluent
Flow	5 – 10 m^3/h (STP)		3.5 – 9.5 m^3/h (STP)	
Concentrations:				
CO_2	82.5 – 97.5 %	~ 100 %	40 – 99 %	~ 100 %
CO	2.5 – 17.5 %	< 20 ppm	0 – 60 %	< 100 ppm
O_2	–	0.35 %	0 – 1.5 %	0.3 – 1.5 %
H_2O	775 – 2500 ppm	2 ppm	600 – 2500 ppm	3 ppm
SO_2	7 – 19 ppm	0.1 ppm	0.05 – 5 ppm	0.02 ppm

Table III: AKUT II, Test Conditions

The I_2-adsorber tests were not completed because the iodine analyzer broke down. They will have to be repeated after repair of the analyzer, but no surprises are expected because the material AC 6120 has been tested sufficiently at other institutions [4].

The SO_2 adsorption material Zeolon 900 Na has been tested at General Atomic Company [5] and has been put into the AKUT II-facility for intermediate use. During the tests it reached the expected decontamination factors (Table III). For two reasons laboratory tests are under way to find a chemical rather than a physical adsorbent:

a) on physical adsorbents other components such as water vapor (containing tritiated water vapor) are coadsorbed, which are released to the stack during regeneration of the adsorbent. Besides Zeolon 900 Na has a rather low dynamic adsorption capacity for SO_2 (30 mg/g at a face velocity of 0.08 m/s) [5]

b) the radioactive isotope S 36 with a lifetime of 88 days is formed during irradiation from the chlorine present in the graphite. It might be necessary to store SO_2 till this isotope has decayed.

Table IV contains the preliminary data of the chemical adsorbents tested so far. The tests were made with a high SO_2 concentration of 2300 ppm to shorten the run time. In previous tests with 18 ppm SO_2 in the feed with all adsorbents less than 0.1 ppm SO_2 in the effluent were reached at ambient temperature. A rise of temperature up to 400°C produced no significant improvement. The utilisation of the active component has been a few percent at best so far but tests for optimisation are going on.

The next component downstream of the SO_2-adsorbers is the catalytic oxidizer (Table II). The catalyst (0.15 wt.-% Pd on Al_2O_3) can be operated as low as 200°C, but since the CO-O_2 reaction

Adsorption Material	Active Comp.	Percentage of Act. Comp. wt-%	Bulk Packing Densitiy kg/l	Cost DM/kg	Time till Breakthrough min
Merck Nr. 5953	MnO_2	40–60	0.91	432.–	155
Kali-Chemie Br 1601	MnO_2	8	0.9	26.–	50
Kali-Chemie Br 1598	MnO_2	8	0.48	23.–	18
Süd-Chemie G-72 D	ZnO	90	1.05	10.20	35
Süd-Chemie G-3	Fe_2O_3/Cr_2O_3	80/9	1.0	9.40	32
Süd-Chemie ODL-N-140	CuO	22	0.75–1.0	35.–	35

Table IV: Chemisorption of SO_2

Bed volume: 136 ml
Bed height: 150 mm
Gas flow: 100 l/h [STP]

Superficial face velocity: 0.03 m/s
SO_2 concentration: 2300 ppm SO_2 in CO_2
Temperature: 20°C

breaks down completely between 190° and 200°C it is advisable to keep a safety margin. We do not operate lower than 250°C.

The gas recycle of the oxidizer system, which dilutes the off-gas to a concentration far below the CO-O_2 explosion limit, was operated at 150 ± 20 m^3/h [STP].

The CO concentration behind the catalyst is < 20 ppm (detection limit of the Perkin Elmer IR-analyzer model 299 with 20 m gas cell) and independent of the CO feed concentration when the O_2 surplus is $\geq$ 0.33 %. During the JUPITER tests the Perkin Elmer IR-analyzer was not available, so that a less sensitive analyzer was used where the detection limit was 100 ppm CO.

The JUPITER off-gas shows a fluctuation of flow, O_2 and CO concentration even at steady state conditions. The typical variation would be between 10 and 11 m^3/h [STP], 10 and 13 % CO, and 0 - 0.2 O_2 in a 3 minute rythm (corresponding to the feed of crushed fuel elements into the burner). The CO fluctuations were controlled well in the oxidizer system, but sudden CO increases $\geq$ 5 % caused O_2 surplusses up to 1.5 %. Work is under way to improve the control system and also to reduce the pressure drop across the connecting

ducts, because the AKUT II blower (K 1) could only suck 9,5 m^3/h [STP] due to a too high pressure drop.

If in the off-gas hydrocarbons are present these are reduced in the oxidizer to H_2O and CO_2.

Water vapor is removed in the H_2O-adsorbers (WA 1+2). In the laboratory 3 A, 4 A, and 5 A molecular sieves have been tested. No difference was detected in capacity, breakthrough curve or decontamination factor. The 3 A molecular sieve was chosen for AKUT II. Figure 2 shows the breakthrough curves for identical molecular sieves and identical loading conditions for the laboratory adsorber of 34 mm diameter and the AKUT II adsorber of 113 mm diameter. Rather unexpectedly the breakthrough time and with it the length of the mass transfer zone were much longer for the adsorber with 113 mm diameter compared to the adsorber with 34 mm diameter.

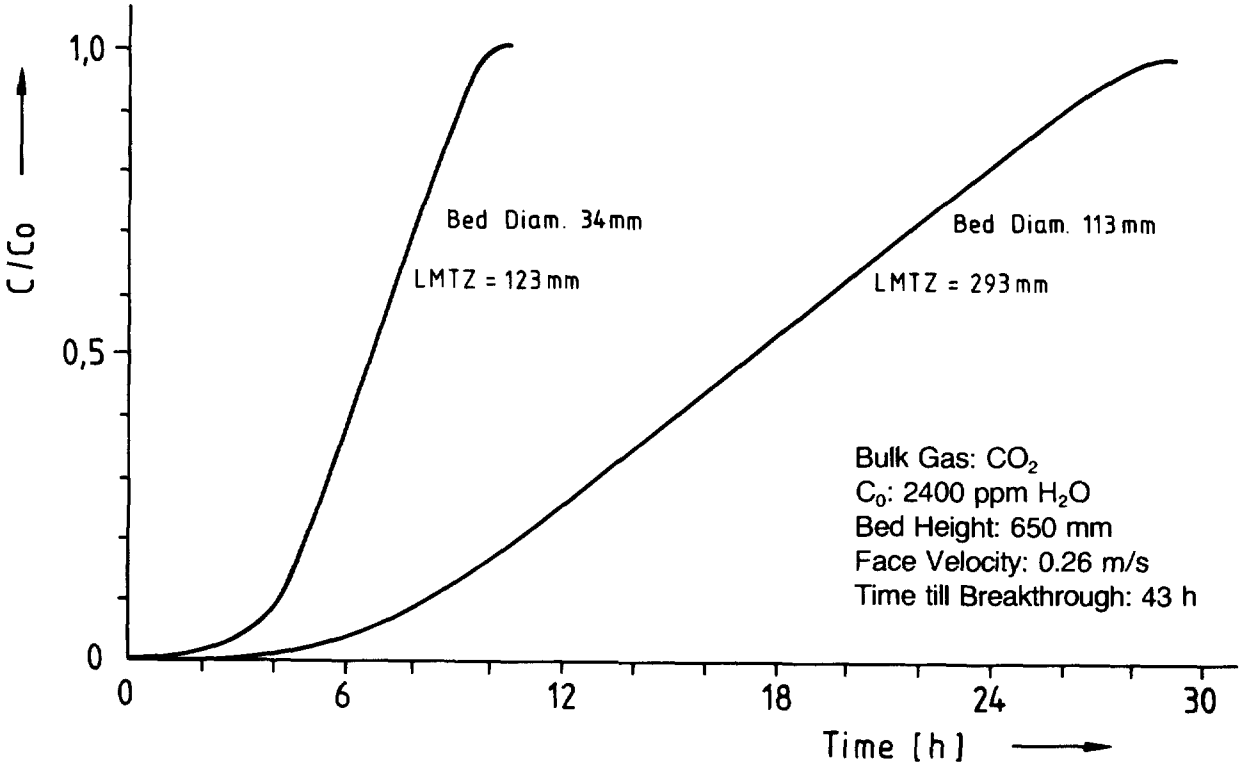

Figure 2: Adsorption of H_2O on 3 A Molecular sieve (Merck), ratio of effluent concentration c and feed concentration c_o versus time

The H_2O effluent concentration was 2 - 3 ppm and in the tested range independent of the feed concentration (Table III). The capacity of 190 g H_2O/kg MS corresponds to the data given in literature (6).

Behind the water adsorbers the off-gas was released into the hot cell off-gas ducts.

The distillation column RK 1 has been tested separately with pure CO_2 to gain the flooding curves.

The overall length of the column is 5.8 m and the inner diameter is 40 mm. The total height of the packing (wire spirals 5 x 5 mm) is 4.7 m. It is divided into four parts with liquid distributors between them.

The diameter of the column was designed such that the vapor velocity at nominal throughput was 50 % of the flooding velocity. The flooding velocities were calculated with the empirical equation given in Perry's Handbook [7]

$$\frac{U_t^2 a_p \rho_g}{g\varepsilon^3 \rho_l} \mu_l^{0.2} = \text{function } \frac{L}{G}\sqrt{\frac{\rho_g}{\rho_l}} \qquad (1)$$

U_t = superficial gas velocity, ft./sec.
a_p = total area of packing, sq. ft./cu. ft. bed
ε = fractional voids in dry packing
g = gravitational constant, 32.2 ft./sec.^{2}
$\rho_{l,g}$ = gas and liquid densities, lb./cu. ft.
L = liquid-mass rate, lb./(sec.)(sq. ft.)
G = gas-mass rate, lb./(sec.)(sq. ft.)
μ_l = liquid viscosity, centipoise

For comparison the flooding curves were also calculated with the equation given by Sawistowski [8]

$$\ln \frac{U_F^2 a \rho_G}{g\varepsilon^3 \rho_L} \left(\frac{\mu_L}{\mu_W}\right)^{0.2} = -4 \left(\frac{L}{G}\right)^{1/4} \left(\frac{\rho_G}{\rho_L}\right)^{1/8} \qquad (2)$$

where U_F = flooding velocity of the gas phase based on total column cross-section
a = surface area of packing per unit volume of column
g = acceleration due to gravity
ε = void fraction of the packing
ρ_L = density of the liquid
ρ_G = density of the gas
μ_L = viscosity of the liquid
μ_W = viscosity of water at 20°C (approx. 1 centipoise)
G = mass rate of flow of the gas phase
L = mass rate of flow of the liquid phase

In Figure 3 the vapor velocities at flooding points for L/V = 1, i.e. for total reflux, at temperatures between - 10° C and + 20°C are shown. The calculated curves are based on equation (1) (dot - dash - line) and equation (2) (dashed line). The diagram also contains our data (solid line). The difference between the vapor velocities calculated by equation (1) and our data is only between 8 % at 12°C and 1 % at - 10°C. This is very satisfactory, considering the fact that equation (1) was derived from data on air-water-systems where e.g. the ρ_L/ρ_G ratio is 1000 compared to the CO_2 system where ρ_L/ρ_G = 6.5 at 10°C.

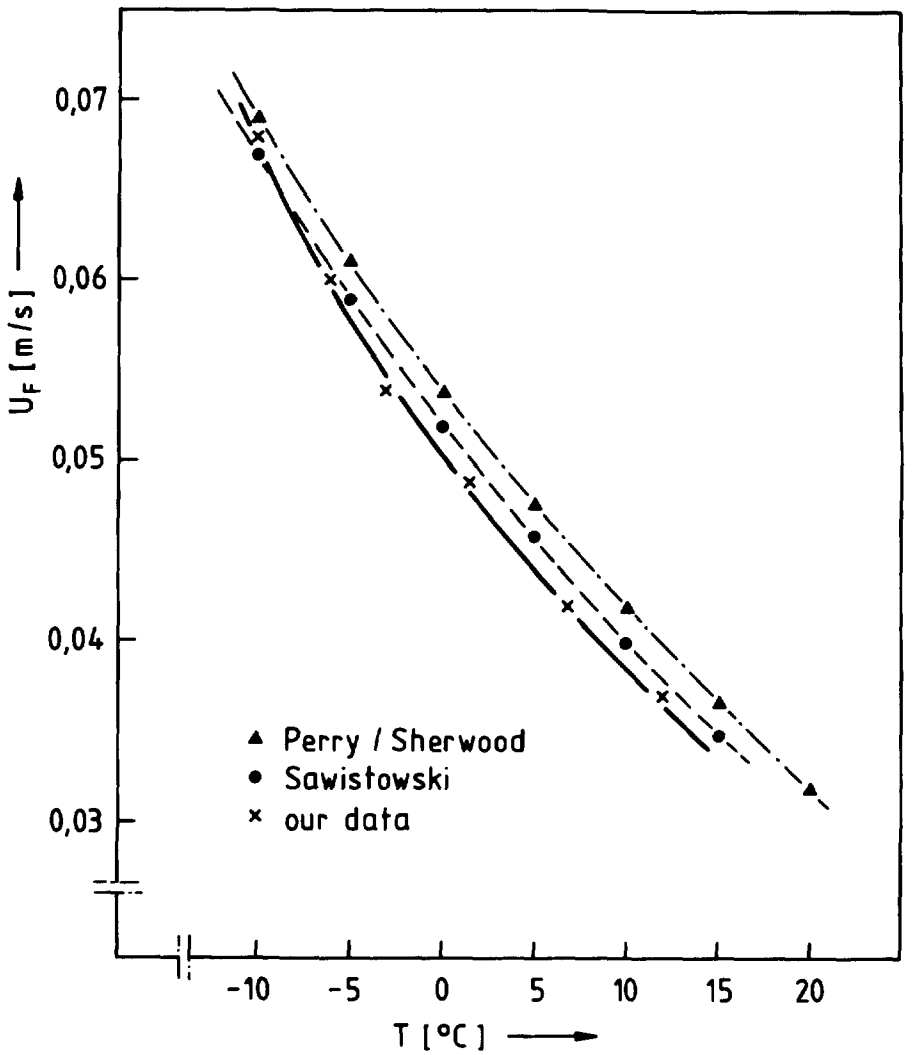

Figure 3: Vapor velocities at flooding points versus temperature for L/V = 1

The pressure drop (Δp) through the column is plotted versus the vapor velocity (U_D) for several temperatures in Figure 4. The curves show the typical lower break at the loading velocity and the typical upper break at the flooding velocity.

The values for the vapor velocity and the pressure drop at the flooding points (U_F and Δp_F) at various temperatures (T) are inserted in the diagram. (U_F was plotted versus T in Figure 3.)

Work planned for the AKUT II-facility in near future is

- to get the low pressure section ready for the next JUPITER campaign, planned for september
- to run the distillation column at L/V ratios other than 1 and to determine the efficiency of the column for CO_2-N_2, CO_2-O_2, and CO_2-Kr systems.

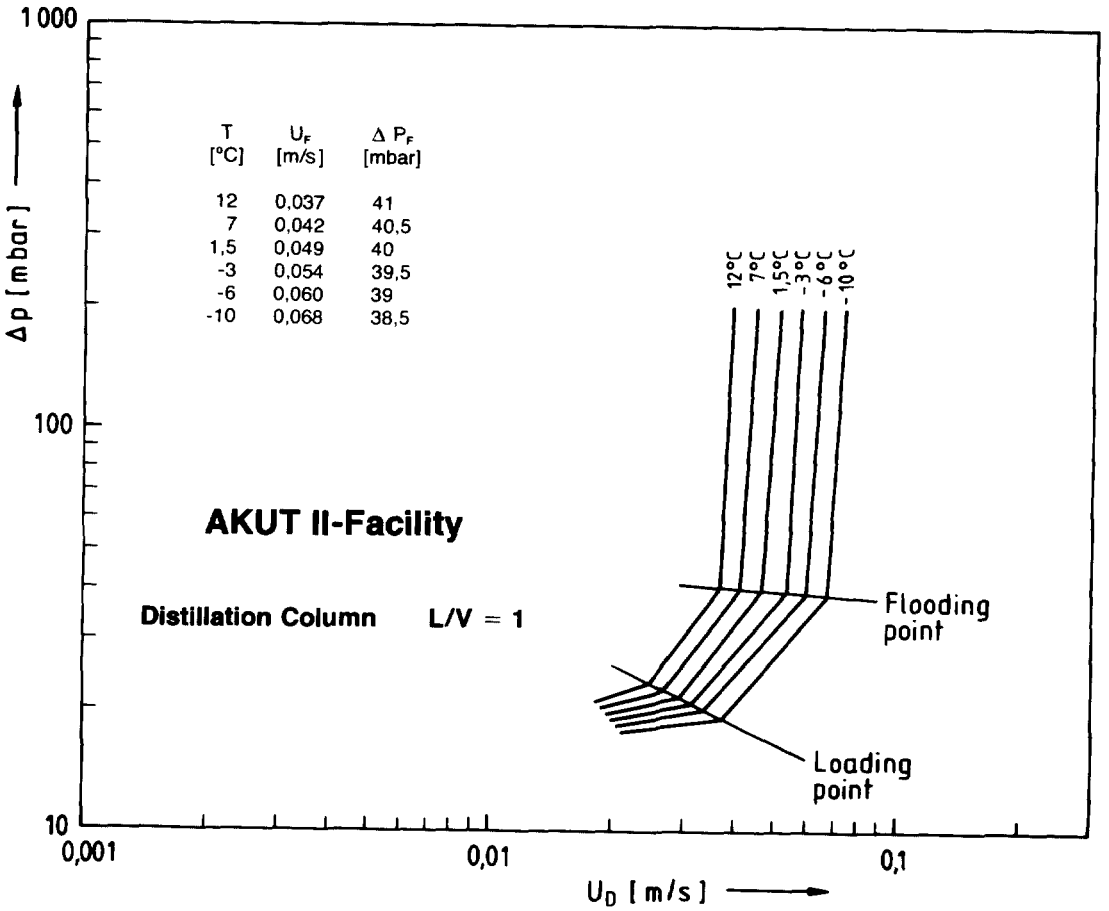

Figure 4: The Pressure Drop Δp through the Distillation Column versus Vapor Velocity U_D at Various Temperatures

II. Dissolver Off-Gas

Introduction

During dissolution of nuclear fuel in concentrated nitric acid nitrogen oxides are formed which are released into the process off-gas system together with the gaseous fission products. A typical composition of the dissolver off-gas is shown in table V.

N_2	75.4 Vol.%
O_2	20.3 Vol.%
H_2O	1.5 Vol.%
Xe	1.06 Vol.%
Ar	0.9 Vol.%
NO_x	0.5 Vol.%
Kr	0.16 Vol.%
H_2, J_2, CO_2, C_nH_m	< 0.1 Vol.%

Table V: Typical Composition of the Dissolver Off-Gas

The goal of the experiments reported herein was the removal of O_2 and NO_x from the dissolver off-gas to below 1 ppm to protect the cryogenic Krypton-separation unit following downstream.

The main work on removal of O_2 and/or NO_x has been done on catalytic reduction:

O_2 and NO_x together have been reacted with H_2 over noble metal catalysts [9,10]. To remove NO_x alone, it was reduced with NH_3 over mordenite [11,12].

Since the use of catalysts includes some drawbacks like poisoning and dust formation, it was decided to check the possibilities of thermal reduction. As reducing agents both H_2 and NH_3 were tested [13].

The reaction equations for the O_2-NO_x-H_2 and the O_2-NO_x-NH_3 systems are listed in table VI. The stoichiometric amount of H_2 was determined by equations I and II and of NH_3 by equations VI and VII. The NH_3, which is formed according to equation III and the NH_3

$O_2 + 2\,H_2$	$\rightarrow$	$2\,H_2O$	(I)
$2\,NO + 2\,H_2$	$\rightarrow$	$N_2 + 2\,H_2O$	(II)
$2\,NO + 5\,H_2$	$\rightarrow$	$2\,NH_3 + 2\,H_2O$	(III)
$NO_2 + H_2$	$\rightarrow$	$NO + H_2O$	(IV)
$2\,NH_3$	$\rightarrow$	$N_2 + 3\,H_2$	(V)

$2\,NH_3 + 3/2\,O_2$	$\rightarrow$	$N_2 + 3\,H_2O$	(VI)
$4\,NH_3 + 4\,NO + O_2$	$\rightarrow$	$4\,N_2 + 6\,H_2O$	(VII)
$4\,NH_3 + 3\,NO_2$	$\rightarrow$	$7/2\,N_2 + 6\,H_2O$	(VIII)
$4\,NH_3 + 5\,O_2$	$\rightarrow$	$4\,NO + 6\,H_2O$	(IX)
$2\,NH_3$	$\rightarrow$	$N_2 + 3\,H_2$	(V)
$2\,NO + 5\,H_2$	$\rightarrow$	$2\,NH_3 + 2\,H_2O$	(III)

Table VI: Reaction Equations for the O_2-NO_x-H_2 and the O_2-NO_x-NH_3 Systems

surplus in the O_2-NO_x-NH_3 system dissociate according to equation V into N_2 and H_2. This leads to the second goal of our tests besides the removal of O_2 and NO_x below 1 ppm: to introduce no NH_3 into the off-gas.

Table VII contains the different gas mixtures, the various gas streams and concentration ranges, and the reactor materials that were tested successively.

Tested Gas Mixtures

N_2 – O_2 – H_2
N_2 – NO – H_2
N_2 – O_2 – NO – H_2
N_2 – O_2 – NO – H_2 – H_2O
N_2 – O_2 – NO – H_2 – I_2

N_2 – O_2 – NO – NH_3
N_2 – O_2 – NO – NH_3 – H_2O

Tested Gas Compositions

N_2 : 600, 800, 1000 l/h (20°C, 1.1 bar)
O_2 : 0.5, 1 %
NO : 750, 1500 ppm
H_2O : 0, 10000 ppm
H_2 : 23 to 140 % surplus
NH_3 : – 40 to + 60 % surplus
I_2 : 0 to 3000 ppm

Tested Reactor Materials

Stainless Steel Nr. 1.4571 (DIN)
Quartz

Table VII: Tested Gas Mixtures, Gas Compositions, and Reactor Materials

Test Equipment

Figure 5 shows the design of the thermal reactor fabricated from stainless steel Nr. 1.4571 (DIN). Five thermocouples in protective tubes are located at various heights. Three resistance heater jackets were controlled independently to establish a fairly even temperature profile throughout the reactor.

The quartz reactor had the same dimensions as the metal reactor, but was equipped with only 2 thermocouples, T 2 and T 6.

Figure 6 shows the test assembly. the gases were supplied from gas cylinders, with the exception of iodide and water vapor. Iodine was liberated from a sodium iodide solution by reaction with ammonium ferro sulfate. Water vapor was added by directing part of

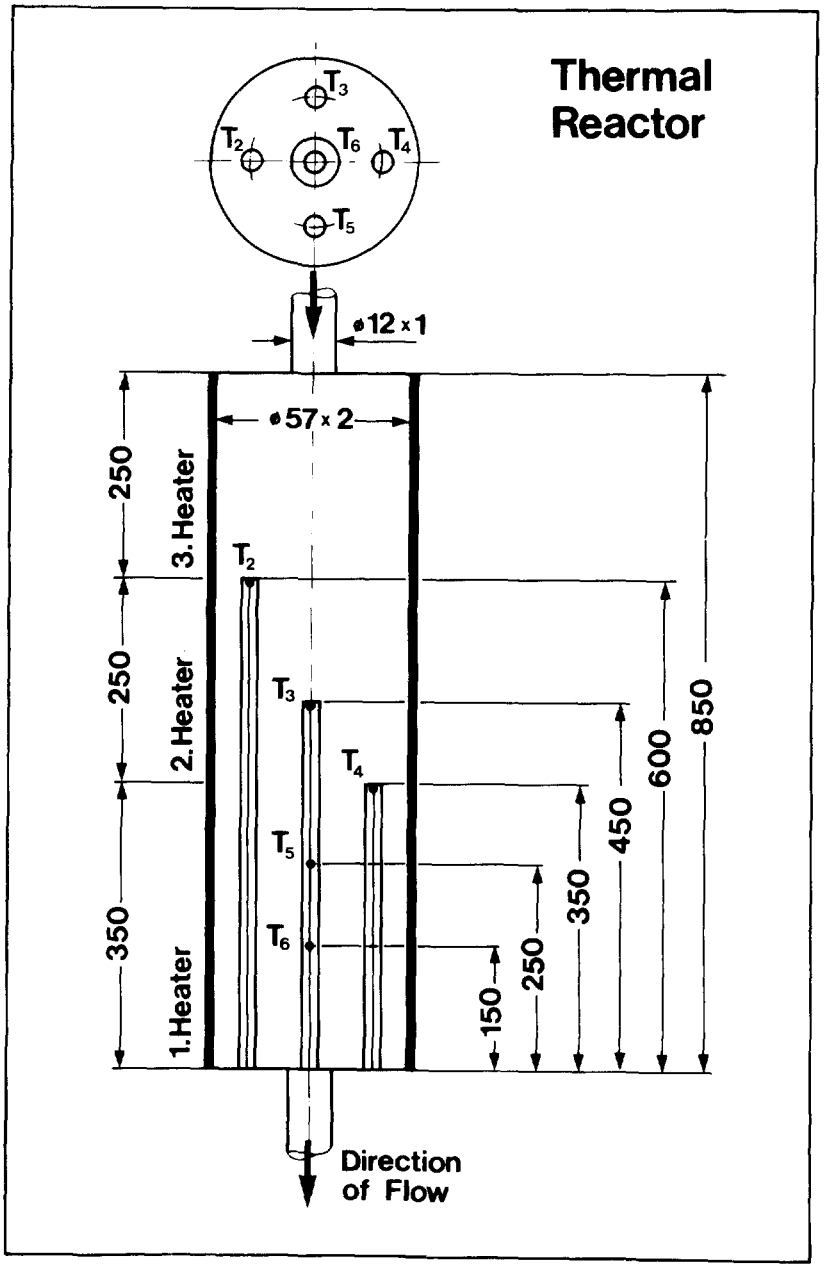

Figure 5: Design of the Thermal Reactor

the N_2 stream through a water tank. Entrained water aerosols were separated in a demister. All gases were blended upstream of reactant gas supplies. Before the gas entered the reactor it was heated in a preheater wrapped with a heating tape. The gas entered the reactor in all tests with a temperature of 420°C. The reactor temperature was varied between 420°C and 750°C. Behind the reactor the gas was cooled to ambient temperature in a water cooled heat exchanger, where part of the water vapor condensed.

The gas was analysed for iodine and ammonia discontinuously, all other analyses were continuous. For O_2 concentrations above 1000 ppm a MAGNOS (Hartmann & Braun), for O_2 concentrations below 1000 ppm an ELCOFLUX C5 (Dr. Thiedig & Co) were used. H_2 was measured with CALDOS analyzers by Hartmann & Braun, and NO_x with a

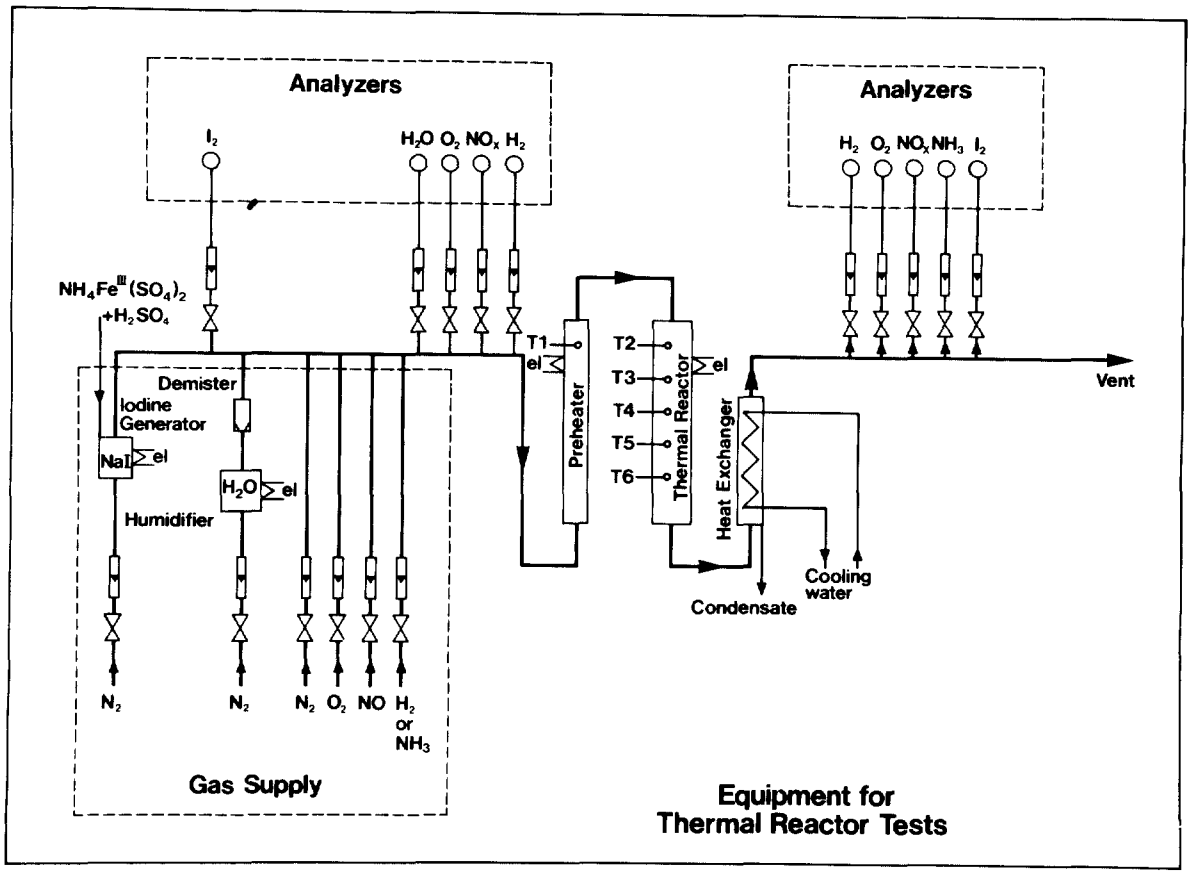

Figure 6: Test Assembly

LUMINOX 201 by BOC and a model 951 by Beckman. For water analysis an AQUANAL by K. Gerhard KG was used. NH_3 was absorbed in boric acid and titrated. I_2 was absorbed in an aqueous potassium carbonate solution, reduced to iodide with sodium sulfate and then determined with an ion selective electrode.

Reduction tests with the metal reactor

H_2 as reducing agent

The first reaction to be tested was the O_2-H_2 reaction. Figure 7 shows the complete reduction of O_2 with H_2 as a function of reactor temperature and throughput. The higher the throughput, that means the lower the residence time, the higher the temperatures that are necessary for complete removal of O_2. For the higher H_2 surplus (curves a and c) the reaction temperature can be lower than for the lower surplus (curves b and d). It is interesting to note that for the lower O_2 concentration tested (0,5 %) for the highest throughput of 1000 l/h [STP] higher reaction temperatures were measured (curves c and d).

In the next test series with NO and H_2 the NH_3 formation and the reaction temperature were checked.

Figure 8 shows the results for a feed of 1500 ppm NO. The numbers in the curves give the H_2 concentration in the reactor

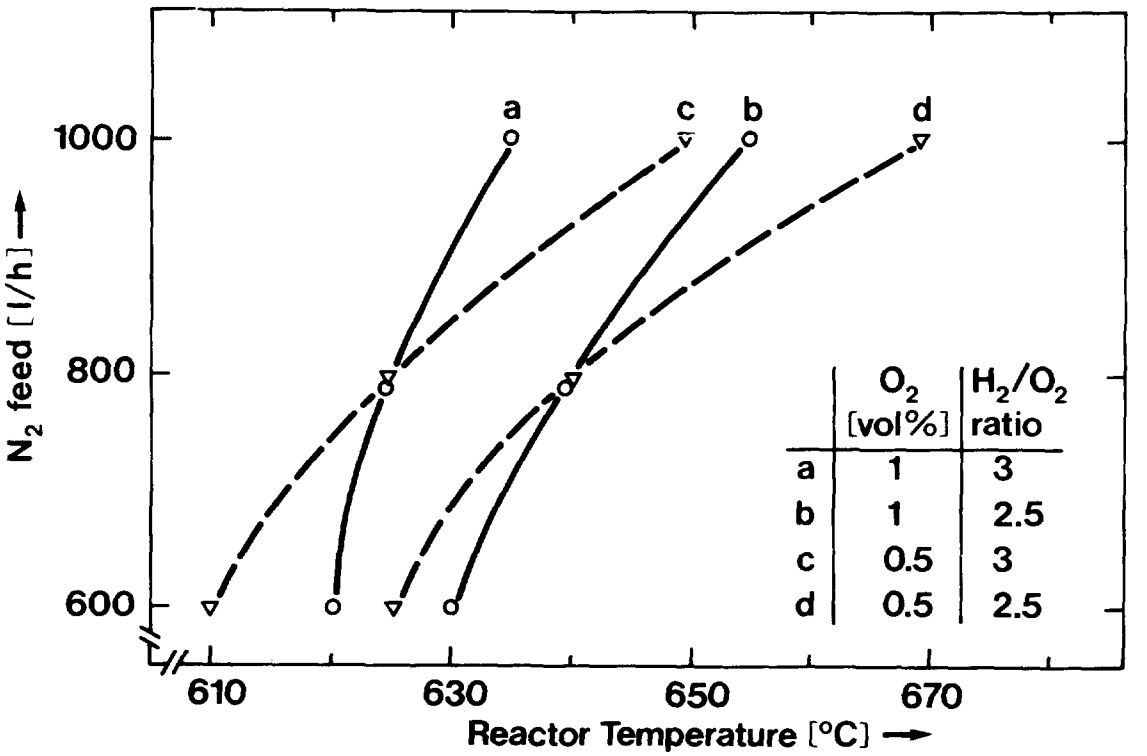

Figure 7: Complete Reduction of O_2 with H_2 as a Function of Reactor Temperature and Throughput

effluent. Below 500°C NO is reduced and NH_3 formed. It can be seen that for higher H_2 surplus NO is reduced at a lower temperature and that the formation of NH_3 depends on the amount of H_2 present. For 1,5 % H_2 in the effluent all NO is reduced to NH_3. The NH_3 dissociates at temperatures above 450°C, and at 630°C the NH_3 concentration is below the detection limit of 50 ppm.

In the diagram no throughput was entered as parameter because the curves are identical for the three tested throughputs of 600, 800 and 1000 l/h [STP]. For a feed of 750 ppm NO the curves are similar in shape and do not render any different results.

From the tests described so far it can be seen that both NO and O_2 can be removed completely by reaction with H_2. The next step was to test the simultaneous reduction of NO and O_2 with H_2. Again the N_2-feed of 600, 800 and 1000 l/h [STP], O_2 feed concentrations of 0.5 % and 1 %, NO feed concentrations of 750 and 1500 ppm, and H_2 concentrations in the effluent of 0.5 %, 1 % and 1.5 % (corresponding to stoichiometric surplusses between 23 % and 140 %) were tested.

Figure 9 shows the results of one of these tests with a feed of 0.5 % O_2, 750 ppm NO, and 2 % H_2 (which corresponds to 93 % stoichiometric surplus).

For the specific gas composition shown in Figure 9 O_2 is removed completely for a N_2 feed of 600 l/h [STP] at 520°C, for a N_2 feed of 800 l/h [STP] at 630°C. For a N_2 feed of 1000 l/h [STP] 3 ppm O_2 remain, even at 740°C. For NO_x the temperature is always

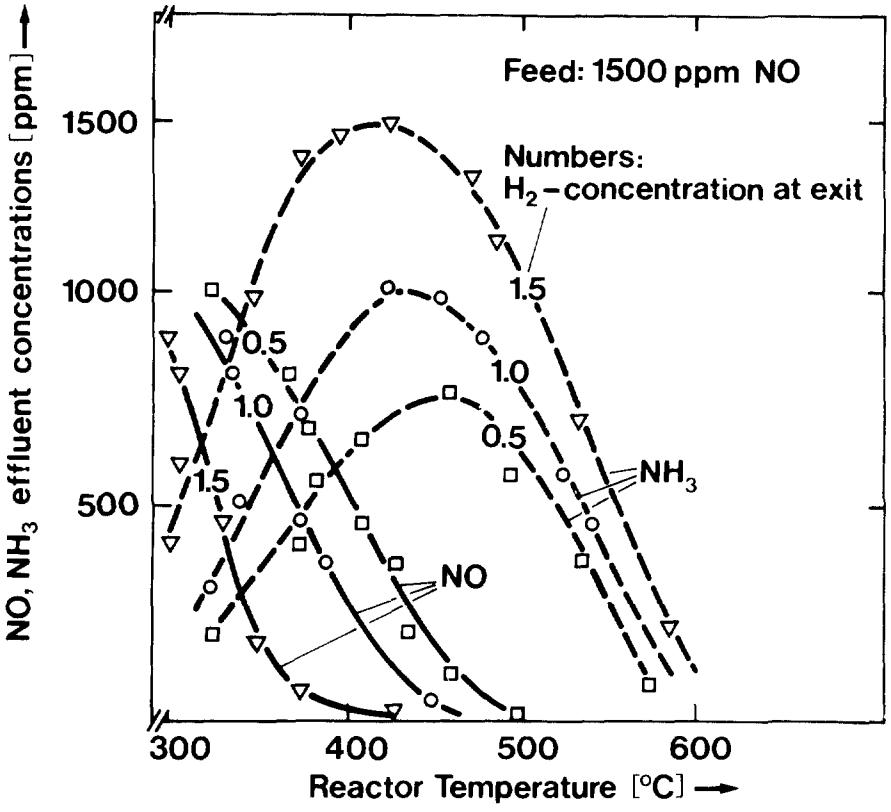

Figure 8: NO and NH_3 Effluent Concentrations vs. Reactor Temperature

lower than for O_2. NH_3 in all cases needs 730°C to 750°C for complete dissociation.

Summing up the different runs with N_2-O_2-NO_x-H_2-gas mixtures it can be said that

- in all tests on the reduction of O_2 and NO_x with H_2 NH_3 was formed. The NH_3 formation depends mainly on the NO_x concentration, the H_2 concentration, and to a lesser degree on the throughput, with the lowest concentration at a N_2 feed of 800 l/h [STP] and the highest at 600 l/h [STP],

- for a N_2 feed of 600 l/h [STP] (corresponding to a residence time of 3,5 s) for all tested O_2 and NO_x concentrations and independent of the H_2 surplus no O_2, NO_x or NH_3 can be detected behind the reactor for a reactor temperature of 730°C ± 20°C,

- for a N_2 feed of 1000 l/h [STP] (corresponding to a residence time of 2,1 s) for all tested mixtures traces of O_2 and NO_x $\leq$ 10 ppm and also traces of NH_3 $\leq$ 160 ppm were found in the effluent.

This means that if a mean reactor temperature of 730°C + 20°C is maintained and the residence time is $\geq$ 3,5 s than for all tested gas mixtures no O_2, NO_x or NH_3 is found in the reactor effluent.

Since the dissolver off-gas is saturated with water vapor, its influence was tested by adding 10.000 ppm water vapor to the gas

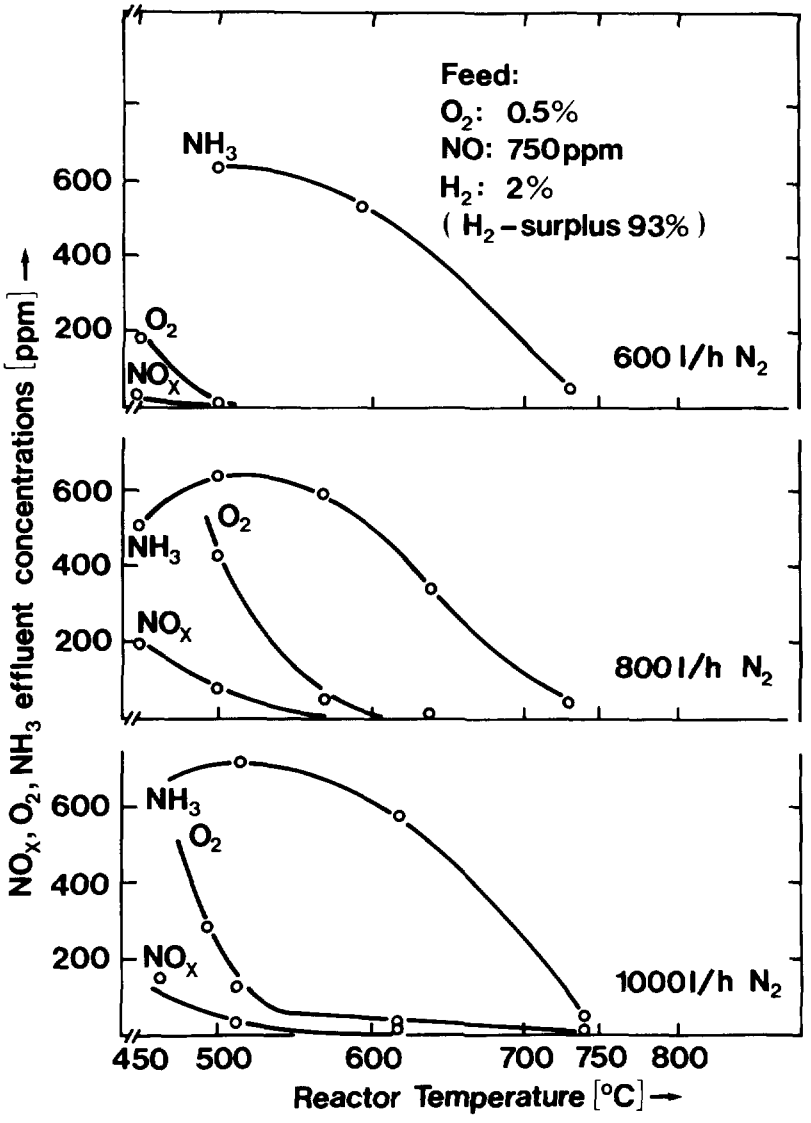

Figure 9: O_2, NO_x, NH_3 Concentrations in Effluent vs. Reactor Temperature and Throughput

mixture. Generally speaking it can be stated that by the presence of water the reaction temperatures for O_2 and NO_x were lowered and the NH_3 formation was enhanced. But at the temperature of 730°C ± 20°C all NH_3 had dissociated so that in the end no difference was noticeable.

NH_3 as reducing agent

In the following test series NH_3 was used as reducing agent. Again a N_2 feed of 600, 800 and 1000 l/h [STP], O_2 concentrations of 0.5 and 1 %, but only one NO concentration of 1500 ppm were tested. NH_3 was varied between - 40 and + 60 % of the stoichiometric amount. Figure 10 shows the results of varying amounts of NH_3 on the O_2 and NO_x concentrations in the effluent. O_2 is reduced to NO for under-stoichiometric NH_3 supply and only at ~ 40 % overstoichiometric supply no NO_x is detectable in the effluent. Furtheron it can be seen that only for the lowest N_2 feed stream of 600 l/h [STP] all O_2 is reduced. For the two higher throughputs even at 40 % over-

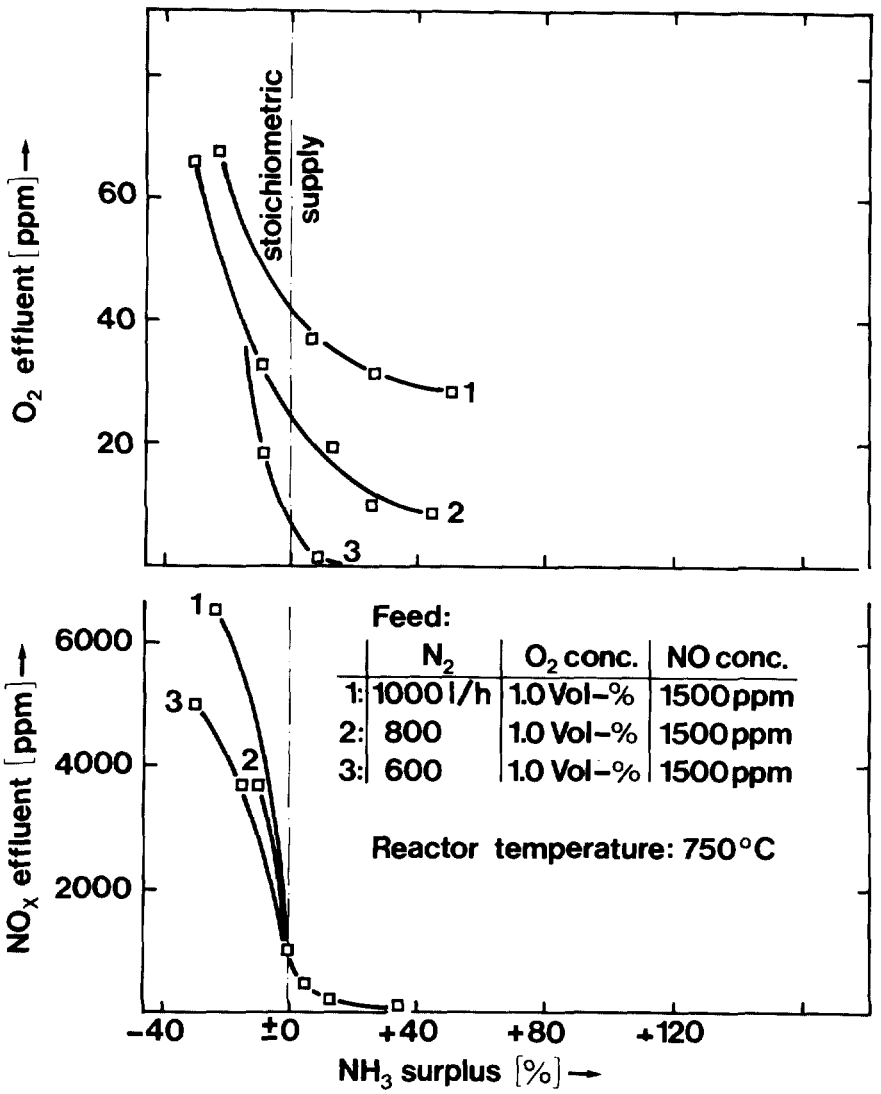

Figure 10: O_2 and NO_x Concentrations in Effluent for NH_3 as Reducing Agent

stoichiometric NH_3 supply 10 to 30 ppm O_2 are detectable in the effluent.

In Figure 11 the O_2, NO_x, and NH_3 concentrations in the reactor effluent versus the feed stream are shown. Only for the N_2 feed of 600 l/h [STP] O_2 and NO_x are removed below 1 ppm. But even for the lowest throughput NH_3 is found in the effluent: NH_3 concentration is 170 ppm and 320 ppm for a feed of 0.5 % O_2 and 1 % O_2 respectively. That means that a longer residence time than the one tested is necessary to remove NH_3 completely.

Introduction of 10.000 ppm H_2O did not influence the results.

Reduction tests with the quartz reactor

To clarify the question whether the reactor material influences the described reactions, part of the tests were repeated in a quartz reactor of the same dimensions as the stainless steel reactor.

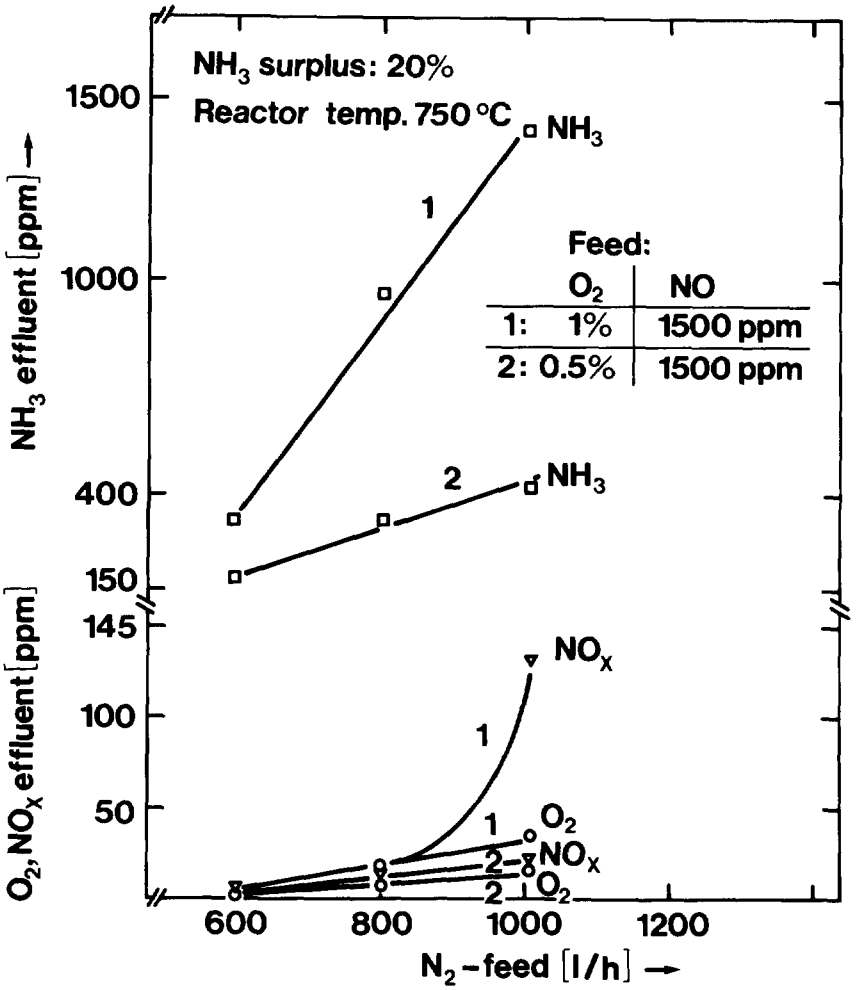

Figure 11: O_2 and NO_x Reduction with NH_3

The tests were made with a N_2 feed of 600 l/h [STP], an O_2 feed concentration of 1 %, a NO feed concentration of 1500 ppm, and a reactor temperature of 750°C.

In the O_2-H_2 reaction O_2 was removed completely at a stoichiometric H_2 surplus of only 1 %. The NO-H_2 reaction did not take place.

The tests were repeated with NH_3 as reducing agent. And again no reaction took place.

When a few pieces of the stainless steel reactor material were put into the quartz reactor all reactions rendered the same results as in the stainless steel reactor. It is obvious that the NO_x-H_2- and the O_2-NO_x-NH_3 reactions are catalyzed by stainless steel. Since the steel Nr. 1.4571 (DIN) which we used is not the right material for a reactor with a prolonged life time, and the recommended material for temperatures around 750°C which is not suceptible to embrittlement by N_2 is Incoloy 800, it would be advisable to check the influence of this material on the reactions.

Influence of iodine on the reactions

The last test series was made to determine the effect of iodine

on the described reactions. The tests were made in the metal reactor at 740°C and a N_2 feed of 600 l/h [STP]. Summing up the data, it can be stated that below 25 ppm I_2 in the gas no influence was noted. More then 25 ppm I_2 led to traces of O_2 and NO_x ($\leq$ 10 ppm) in the effluent. An I_2 excursion of 3000 ppm caused the complete breakdown of all reactions. If the I_2 influx is stopped and the reactor flushed for a few minutes with a N_2-H_2 mixture the reactor recovers and the reactions take place again.

In the quartz reactor only the O_2-H_2 reaction was tested, since other reactions do not take place as mentioned above. At an I_2 concentration of 140 ppm the H_2-O_2 reaction broke down completely.

It is assumed that iodine atoms interrupt the H_2-O_2 chain reaction with the consequence that the reaction rate drops and the gas needs a longer residence time for complete reaction. It is also possible that the catalytic centers of the metal are poisoned by the iodine and the NO_x-H_2 reaction is impaired. To clear this point more experiments would be necessary.

Summary

Summing up the tests with thermal reactors it can be said, that

- O_2 and NO_x can be reduced with H_2 at 730 $\pm$ 20°C. No O_2, NO_x, or NH_3 is detected in the effluent if the residence time is $\geq$ 3.5 s.
- O_2 and NO_x can also be reduced with NH_3, but a longer residence time than for H_2 is needed, because more intermediate reactions are involved.
- The reactions are catalysed by stainless steel.
- Traces of iodine $\geq$ 25 ppm impair the reactions.
- Saturation of the gas with water vapor does not increase the reaction temperature or the residence time.

III. References

(1) H. Barnert-Wiemer, M. Heidendael, H. Kirchner, E. Merz, G. Schröder, H. Vygen:
Burner and Dissolver Off-Gas Treatment in HTR Fuel Reprocessing
Proc. of the 15th DOE Nuclear Air Cleaning Conference, Boston, Massachusetts, 7-10 Aug. 1978

(2) H. Barnert-Wiemer, E. Merz:
Abgasbehandlung bei der Wiederaufarbeitung von Brennelementen des Hochtemperaturreaktors (HTR)
Jahrestreffen der Verfahrensingenieure, Straßburg 1.-3.10.1980

(3) U. Brinkmann, W. Heid, H. Huschka, G. Kaiser, W. Theymann:
Research and Development Work in HTR Fuel Fabrication, Fuel Performance, Spent Fuel Treatment in the FRG
Conf. on Gascooled Reactors Today, Bristol, 20-24 Sept. 1982

(4) J.G. Wilhelm, J. Furrer:
Jodabscheidung in Wiederaufarbeitungsanlagen
Tagungsbericht V/2266/78 der Kommission der Europäischen Gemeinschaft, Luxemburg, Febr. 1978

(5) L. Abraham, P.M. Hirsch:
Consolidated Fuel Reprocessing Program, Interim Development Report: Off-Gas Treatment System
GA-A16292 (June 1981)

(6) W. Kast:
Adsorptive Trocknungsverfahren für Gase
Haus der Technik, Essen, Vortragsveröffentlichungen 404 (1977)

(7) R.H. Perry, C.H. Chilton:
Chemical Engineers' Handbook
Mc Graw Hill, 5th Edition

(8) H. Sawistowski:
Chem. Engng. Science, Vol. 6, pp 138/140 (1957)

(9) R. v. Ammon et al.:
Die katalytische Reduktion von Sauerstoff und Stickoxiden mit Wasserstoff im Abgas von Wiederaufarbeitungsanlagen
Laborversuche zum Katalysatorverhalten
KFK 2437 (1977)

(10) H. Barnert-Wiemer, B. Bendick:
Untersuchungen an Katalysatoren zur Reduktion von Stickoxiden und Sauerstoff mit Wasserstoff
Jül-1677 (1980)

(11) T.R. Thomas, D.H. Munger:
An Evaluation of NO_x Abatement by NH_3 over Hydrogen Mordenite for Nuclear Fuel Reprocessing Plants
ICP-1133 (1978)

(12) P.M. Hirsch:
Off-Gas Treatment System NO_x Converter Component Tests
GA-A 16559 (1982)

(13) B. Bendick:
Verfahren zur Abtrennung von Sauerstoff und Stickoxiden aus dem Auflöserabgas einer Wiederaufarbeitungsanlage für HTR-Brennelemente
Jül-1759 (1982)

SURFACE DEPOSITION OF RADON DECAY PRODUCTS WITH AND WITHOUT ENHANCED AIR MOTION

S.N. Rudnick, E.F. Maher, W.C. Hinds, and M.W. First
Harvard Air Cleaning Laboratory
Boston, MA 02115

Abstract

The effectiveness of fan-induced air motion in reducing airborne activity of short-lived radon decay products was evaluated in a 78-m^3 chamber. Observed reductions were as high as 50% for RaA (^{218}Po), 79% for RaB (^{214}Pb), and 86% for RaC (^{214}Bi). Activity Measurements of these nuclides on chamber and fan surfaces, along with airborne activity, were used to calculate material balances. Greater than about 90% of deposited activity was found on chamber surfaces, although areal activity density was higher on fan surfaces. Deposition velocity and diffusional boundary thickness were also determined. When no fans were used, boundary layer thickness was estimated to be 25 times the recoil distance of a RaB atom and, with fans, about 4 times the recoil distance, suggesting that recoiling RaB atoms probably do not play a significant role in the relationship between surface and airborne activity. The results of this study have relevance for all habitable spaces having excessive radon concentration.

Introduction

Engineering strategies to control short-lived radon decay products in buildings or mines can be divided into three types: 1) prevention of radon entry (e.g., sealants, ventilated crawl spaces, and judicious selection of building materials); 2) dilution with outside air directly or through heat exchangers; 3) removal of radon or its decay products from the indoor airspace by various air treatments. Historically, air dilution has been most effective, although not employed for this specific purpose. Recently, it has become less acceptable because of high energy costs for heating and air conditioning dilution air. Research conducted in the present study was directed to a subdivision of strategy 3, removal of radon decay products due to air motion produced by fans.

Fans remove radon decay products from the airspace by causing surface deposition, which is often termed plateout. The primary mechanism causing plateout by fans is diffusion, and although this mechanism is also active when no fans are in use, fan-induced air motion can enhance its importance greatly. Because partitioning of radon decay products between the airspace and surfaces is fundamental to understanding the health hazards associated with radon, experimental data on plateout, as well as on the fate of all radon decay products, are necessary for formulation and verification of a mathematical model.

Plateout due to fan-induced air motion has been reported previously by several investigators.[1,2,3] Wrenn[1] observed reductions in working level of up to 90% in two uranium mines due to air motion caused by air recirculation rates between 20 and 60/h, far in excess of that which would be used in buildings. Holub[2] reported working level reductions of 41% in an experimental chamber when a mixing fan was used. His tests indicated that this reduction was the result of radon decay product deposition on the fan rather than on chamber surfaces. Abu-Jarad[3] reported a 28% reduction in working level for an experimental chamber when a mixing fan was operating. Using plastic track etch α-detectors, he compared activities on fan blades and chamber surfaces, before and after treatment, and found that fan deposition accounted for about 2% of activity lost from the airspace. He concluded that enhanced deposition on chamber surfaces was responsible for most of the working level

reduction.

Experimental Methods

Experimental studies were designed to simulate closely conditions occurring in a residence or building. Nonetheless, transient effects, such as time-dependent variations in air infiltration rate or radon intrusion rate, were not studied because experimental results would have been too difficult to analyze. Consequently, all measurements were made after steady-state experimental conditions were attained.

Apparatus

Experiments were made in a chamber having a volume of 78-m^3 and surface area of 122 m^2. This chamber was unfurnished and had a linoleum floor, painted metal walls, and five sealed windows. Air infiltration rates were established by exhausting the requisite airflow through a calibrated venturi flowmeter. Although air was forced to infiltrate through cracks and pores in chamber surfaces, pressure in the chamber was less than barometric pressure by at most 3 mm of mercury. Aerosol particles in the chamber entered with air that infiltrated from adjacent air-conditioned laboratory spaces. Aerosol concentration ranged from 12 to 83 $\mu g/m^3$ during the experimental program.[4]

Radon (^{222}Rn) was generated by bubbling 0.2 L/min of humidified air through a 100-μCi ^{226}Ra solution. Gas exiting the bubbler passed through a droplet trap and a filter and, then, flowed to a distribution manifold on the floor of the chamber. This arrangement simulated seepage of radon through the floor.

Sampling ports were located in the exhaust duct and in one wall of the chamber. Both ports accepted 50-mm diameter open-faced filter holders, which minimized aerosol sampling losses. Tests made with carbon monoxide released in the chamber as a tracer gas showed that these locations gave representative samples of concentrations in the chamber and confirmed that the chamber air was well mixed.[4] Air samples for radon were taken from the exhaust duct through a filter into an evacuated 100-cm^3 Lucas flask.[5]

Measurement of Radon Decay Product Concentration

Radon decay product concentrations were determined from a 5-minute air sample collected on a Millipore AA membrane filter, which was counted by alpha scintillation after the filter was placed in direct contact with the Ag-activated ZnS-phosphor-coated side of a disposable mylar film (W.B. Johnson and Associates, Montville, N.J.). The mylar film was touching the window of a photomultiplier tube in a light-tight enclosure during the counting period, which started 2 minutes after the end of the sampling period and continued for 30 minutes. Working level and concentrations of RaA, RaB, and RaC were calculated from the counts in three time intervals using the modified Tsivoglou method.[6]

Measurement of Radon Decay Product Surface Activities

Different equipment and procedures were used to measure surface activities of radon decay products on chamber surfaces and on fan parts.

On Chamber Surfaces. Steady-state radon decay product activities on chamber surfaces were measured in the following manner: 47-mm diameter paper or aluminum-foil disks were affixed to various locations on ceiling, floor, and walls and allowed to remain in the chamber for a sufficient time to establish steady-state activities of RaA, RaB, and RaC. The disks were removed one at a time from the chamber; by comparing activities of

successive samples at the same location, we determined that our entry into the chamber had no effect on plateout measurements. The disks were counted under vacuum by alpha-particle spectrometry using a 12.6-cm^2 silicon surface-barrier detector. Total number of counts under the RaA and the RaC' (^{214}Po) alpha peaks during one time interval and total number of counts under the RaC' alpha peak for a later time interval were determined for 4 or more disks removed from various locations. From these 3 counts, the steady-state activities of RaA, RaB, and RaC on the surfaces were estimated using a computer program written for radon decay product airborne concentration[7] and modified for calculation of surface activity.[4] No significant differences in areal density were observed when using aluminum-foil or paper disks at the same location, although peak resolution was considerably better with foil. This resolution difference results from higher energy loss of an α particle when escaping the rougher paper surface on its way to the detector, an observation reported by previous investigators.[8,9]

On Fan Blades and Housing. Steady-state activities on fan blades and fan housing were measured using 6 identical, 75-cm^2, Ag-activated-ZnS scintillation detectors. Each detector was provided with a protective rigid grill to permit direct contact with surfaces and a 1-mg/cm^2 aluminized mylar film to shield the photomultiplier tube from room light (model 43-1, Ludlum Measurements, Sweetwater, TX).

Activities on front and back fan blade surfaces and fan housing were measured simultaneously with as many detectors as could be positioned within the first 2 minutes after removing the fan from the chamber. The modified Tsivoglou method,[6] adapted for calculation of surface activity,[4] was used to back-calculate steady-state radon decay product activities to the instant when the fans were removed from the chamber.

When measuring deposition on the 51-cm box fan, usually 4 detectors were placed on front and back surfaces of 2 blades out of a total of 14 and another 2 detectors on 2 inside locations of the housing. Three detectors per blade side were used to characterize average activity on 1 of the 4 blades of the 130-cm ceiling fan. Deposition was not uniform with distance along the blade, as shown in Table I.

Table I Relative areal activity density on blade of 130-cm ceiling fan.

	Relative areal activity density					
Air infiltration rate	0.23/h			0.52/h		
Decay product	RaA	RaB	RaC	RaA	RaB	RaC
Position on blade						
Inner third	1.00	1.00	1.00	1.00	1.00	1.00
Middle third	1.30	1.85	1.78	1.20	1.65	1.60
Outer third	1.74	2.30	2.53	1.20	2.00	2.48

Surfaces near the blade tip were found to have up to 2.5 times the areal activity density as those near the inner part of the blades. Similar trends were noted for top and bottom blade surfaces, but as expected, no differences in areal density with position were found when the fan blades were still. The higher activity areal density at the tips of the fan blades was probably due to the thinner boundary layer thickness and to the larger air volume per blade area swept out by the faster moving surface.

Results

The importance of radon decay product plateout was quantified from activity measurements in the air, on chamber surfaces, and on fan parts. These measurements were also used to calculate individual material balances and estimate plateout rates, deposition

velocities, and diffusion boundary layer thicknesses for RaA, RaB, and RaC.

Plateout

Plateout of radon decay products will always occur to some extent. Its importance can be greatly enhanced through air mixing caused by fans.

Without Fans. Measurements of working level (WL) and airborne concentrations of RaA, RaB, and RaC at various air infiltration rates are given in Figure 1. Theoretical curves, shown also in Figure 1 and based on the assumptions of no plateout, spatially uniform steady-state concentrations, and infiltration air free of radon and its decay products, were plotted from Equations 1, 2, 3, and 4[4]:

$$WL = \frac{S\lambda_r}{(\lambda_r+I)(\lambda_a+I)}\left[k_1 + \frac{k_2\lambda_a}{\lambda_b+I}\left(1 + \frac{\lambda_b}{\lambda_c+I}\right)\right] \quad (1)$$

$$C_a = \frac{S\lambda_r\lambda_a}{133.2(\lambda_r+I)(\lambda_a+I)} \quad (2)$$

$$C_b = \frac{C_a\lambda_b}{\lambda_b+I} \quad (3)$$

$$C_c = \frac{C_b\lambda_c}{\lambda_c+I} \quad (4)$$

where

WL = working level (i.e., any combination of RaA, RaB, RaC, and RaC' atoms in one liter of air that will, on decay to Pb-210, release 130,000 MeV of alpha-particle energy), WL

C = radon decay product concentration, pCi/L

S = radon intrusion rate per chamber volume, atoms/(h·L)

I = air infiltration rate (i.e., volumetric flow rate of infiltrating air divided by chamber volume), 1/h

λ = radioactive decay constant (λ_r = 0.00758, λ_a = 13.7, λ_b = 1.55, and λ_c = 2.11), 1/h

k = dimensional conversion factor (k_1 = 1.052 x 10^{-4} and k_2 = 5.908 x 10^{-5}), WL·L/atom

r, a, b, and c are subscripts indicating radon, RaA, RaB, and RaC, respectively.

In all cases, the measured concentrations were less than the theoretical curves, a result of plateout on chamber surfaces. Differences, which varied from 8.4 to 26% for WL, 11 to 26% for RaA, 9.1 to 25% for RaB, and 7.4 to 26% for RaC, were larger at lower air infiltration rates, suggesting that longer residence times at lower infiltration rates had a greater effect on plateout than the diffusional boundary layer thickness, which would be expected to be thicker at lower infiltration rates.

With Fans. Reduction in radon decay product concentration resulting from increasing plateout by air mixing was studied using a ceiling fan and a portable box fan. Manufacturer's specifications for these fans are given in Table II.

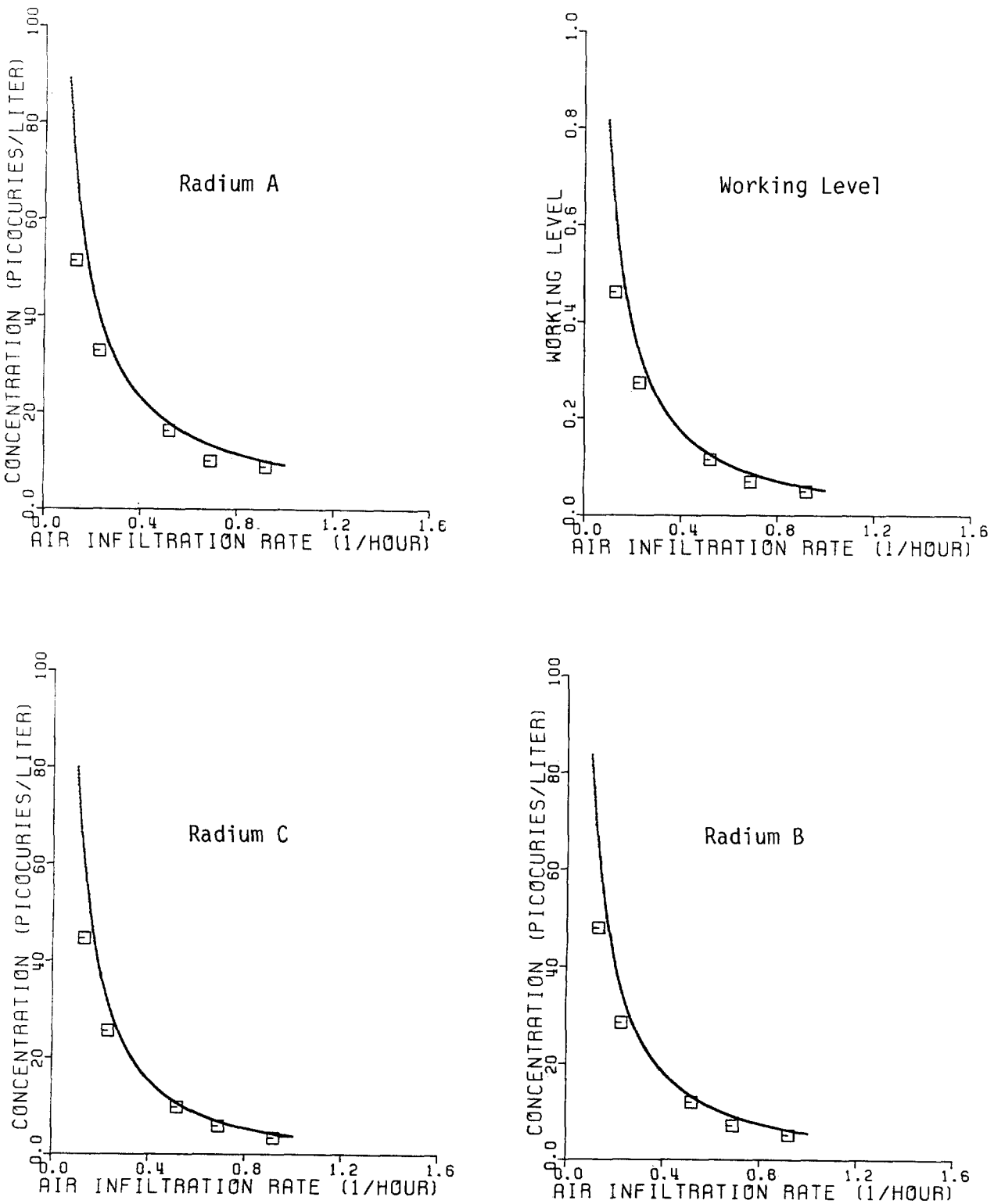

Figure 1 Effect of air infiltration rate on radon decay product concentration with no fans in use. (Square symbols denote experimental data; solid lines denote theoretical curves based on the assumptions of no plateout, spatially uniform steady-state concentrations resulting from decay of 100-μCi Ra-226 into 78-m^3 chamber, and radon- and radon-decay-product-free infiltrating air.)

Table II Manufacturer's fan specifications.

Fan type	51–cm box fan			130–cm ceiling fan	
Model number	11077*			22306–7J*	
Setting	High	Medium	Low	High	Low
Airflow rate, m^3/min**	156	147	136	198	113
Fan speed, rev/min	1000	930	750	200	115
Power consumption, W	185	150	100	155	80

*Hunter Comfort Conditioning Division, Robbins & Myers, Inc., Memphis, TN 38114.
**NEMA method

Figure 2 shows the ratio of radon decay product concentration with a fan to the concentration without a fan versus air infiltration rate. Use of box fans reduced WL by 43 to 76% and concentrations of RaA by 32 to 50%, RaB by 45 to 79%, and RaC by 43 to 86%.

Material Balance Calculations

Steady-state material balance equations for radon, RaA, RaB, and RaC in terms of atoms per unit time are given by Equations 5 through 8. The left side of these equations accounts for entry of radon and its decay products into the chamber, including its airspace and surfaces, and the right side for their exit in the exhausted air and elimination by decay.

For radon,

$$SV + n_r^i VI = n_r VI + N_r \lambda_r \tag{5}$$

where

V = chamber volume (i.e., its airspace volume), L

n_r^i = radon concentration in infiltrating air, atoms/L

N_r = number of airborne radon atoms in the chamber

n_r = radon concentration in exiting air, atoms/L

We assumed that radon adsorption on chamber surfaces was negligible.

Similarly, for RaA, RaB, and RaC,

$$N_r \lambda_r + n_a^i VI = n_a VI + N_a \lambda_a + W_a \lambda_a \tag{6}$$

$$N_a \lambda_a + W_a \lambda_a + n_b^i VI = n_b VI + N_b \lambda_b + W_b \lambda_b \tag{7}$$

$$N_b \lambda_b + W_b \lambda_b + n_c^i VI = n_c VI + N_c \lambda_c + W_c \lambda_c \tag{8}$$

where

n^i = radon decay product concentration in infiltrating air, atoms/L

n = radon decay product concentration in exiting air, atoms/L

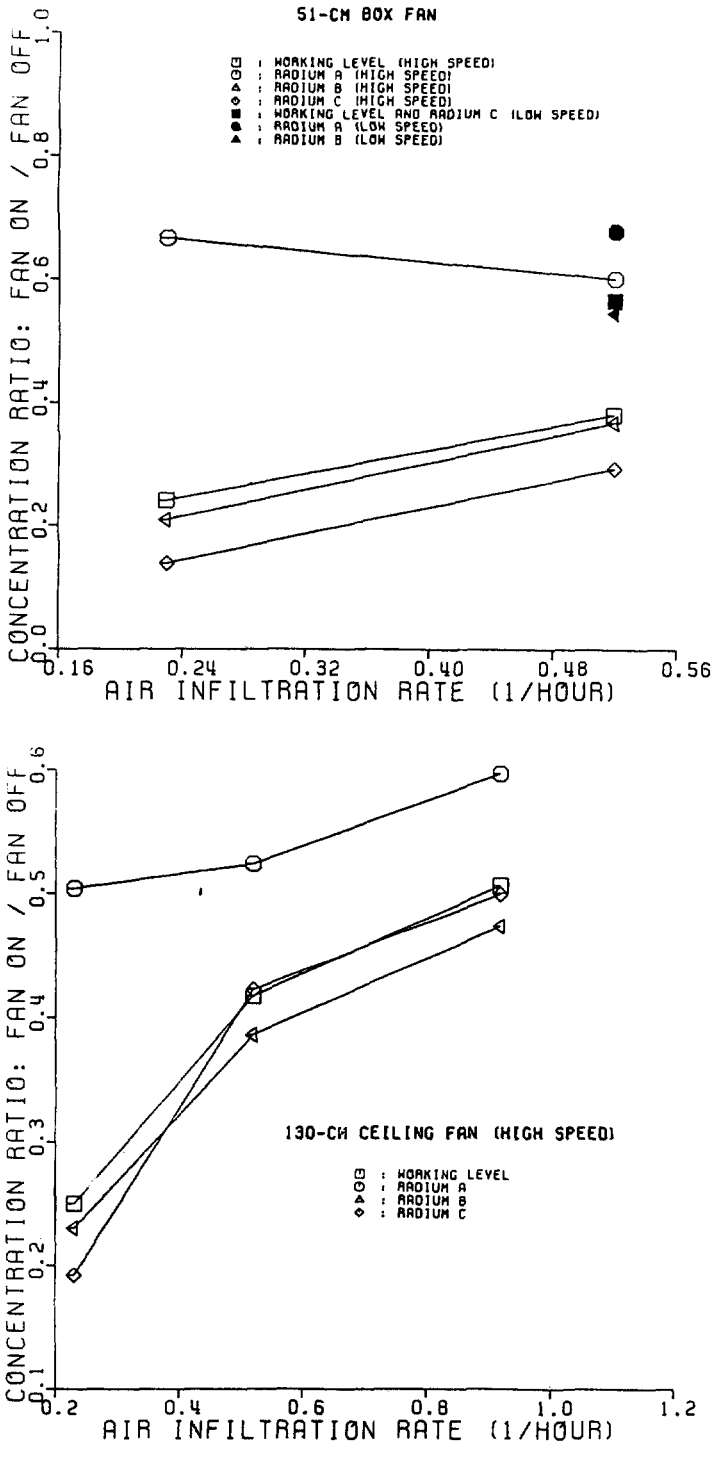

Figure 2 Effect of mixing fans on radon decay product concentration.

N = number of airborne radon decay product atoms in the chamber

W = number of radon decay product atoms on chamber surfaces

Measurements indicated that infiltration air was free of radon and its decay products (i.e., $n_r^i \approx n_a^i \approx n_b^i \approx n_c^i \approx 0$) and that point-to-point concentrations were fairly uniform and not much different from exhaust concentrations[4] (i.e., $n \approx N/V$ for radon and its decay products).

Applying these approximations to Equations 5 through 8 and rearranging gives surface activities (i.e., disintegrations per unit time) of each decay product:

$$W_a \lambda_a = SV\lambda_r/(I+\lambda_r) - n_a V(I+\lambda_a) \tag{9}$$

$$W_b \lambda_b = SV\lambda_r/(I+\lambda_r) - n_b V(I+\lambda_b) - n_a VI \tag{10}$$

$$W_c \lambda_c = SV\lambda_r/(I+\lambda_r) - n_c V(I+\lambda_c) - (n_a+n_b)VI \tag{11}$$

The amount of radon decay products on chamber surfaces can also be expressed in terms of potential alpha energy in MeV ($\overline{PAE}$); i.e.,

$$\overline{PAE} = E_a W_a + E_{c'}(W_a + W_b + W_c) \tag{12}$$

where

E_a = energy of alpha particle from RaA = 6.00 MeV

$E_{c'}$ = energy of alpha particle from RaC' = 7.68 MeV

Inserting Equations 9 through 11 into Equation 12 and rearranging yields

$$\overline{PAE} = [E_a\lambda_a^{-1} + E_{c'}(\lambda_a^{-1} + \lambda_b^{-1} + \lambda_c^{-1})]SV\lambda_r/(I + \lambda_r)$$

$$-[n_a + n_b + n_c + n_a I(\lambda_a^{-1} + \lambda_b^{-1} + \lambda_c^{-1})$$

$$+ n_b I(\lambda_b^{-1} + \lambda_c^{-1}) + n_c I/\lambda_c]VE_{c'} - (1 + I/\lambda_a)n_a VE_a \tag{13}$$

The right side of Equations 9, 10, 11, and 13 can be used to calculate activities of radon decay products and potential alpha energy on chamber surfaces. The measured parameters required are air infiltration rates, airspace volume, airborne concentrations of RaA, RaB, and RaC, and radon intrusion rate. If these calculated values are in agreement with measured values of RaA, RaB, and RaC activities and potential alpha energy on chamber surfaces, and the fate of all radon decay products has been confirmed.

Material balance results for 5 tests in which surface measurements were made are shown in Table III for radon decay products and Table IV for potential alpha energy. The amount of radon decay products on chamber surfaces and fan parts are given in Table V. As shown in Table III, measured activity of RaA on all surfaces ranged from 46% to 86% of calculated activities based on Equation 9. The range was 46% to 114% for RaB and 56% to 250% for RaC based on Equations 10 and 11, respectively. Measured potential alpha energy on surfaces, shown in Table IV, ranged form 52% to 116% of calculated amounts based on Equation 13. If the test with two box fans are ignored, this range would narrow to 94% to 116%.

Table III Material balance based on radon decay product activities.

Air Treatment	Air Infiltration Rate, h^{-1}	Radon Decay Product	Radon Decay Product Activities, μC_i (Coef. var.*)		Total Measured / Calculated	p-value
			Total Measured	Calculated from Eq. 9-11		
None	0.23	RaA	0.459 (10.7%)	0.536 (36.9%)	0.855	0.704
		RaB	0.746 (14.7%)	0.700 (9.73%)	1.064	0.726
		RaC	0.826 (8.30%)	0.855 (8.56%)	0.965	0.772
None	0.52	RaA	0.132 (30.5%)	0.287 (46.9%)	0.459	0.271
		RaB	0.119 (73.7%)	0.172 (31.1%)	0.689	0.630
		RaC	0.267 (19.3%)	0.106 (52.1%)	2.500	0.035
130-cm ceiling fan (high speed)	0.23	RaA	1.35 (7.60%)	1.81 (5.75%)	0.742	<0.003
		RaB	2.40 (9.30%)	2.54 (1.40%)	0.943	0.529
		RaC	2.57 (6.20%)	2.63 (1.42%)	0.976	0.704
130-cm ceiling fan (high speed)	0.52	RaA	0.528 (12.0%)	0.716 (12.8%)	0.736	0.093
		RaB	1.03 (14.7%)	0.900 (3.98%)	1.143	0.407
		RaC	1.09 (8.60%)	0.857 (4.35%)	1.270	0.021
Two 51-cm box fans (high speed)	0.52	RaA	0.494 (15.3%)	0.693 (13.1%)	0.712	0.093
		RaB	0.466 (28.3%)	1.01 (3.63%)	0.458	<0.003
		RaC	0.570 (13.5%)	1.01 (3.61%)	0.561	<0.003

* Coefficient of variation for counting error in percent is given parenthetically.

Table IV Material balance based on potential alpha energy.

Air Treatment	Air Infiltration Rate, h^{-1}	Potential Alpha Energy MeV (Coef. var.*)		Total Measured / Calculated	p-value
		Total Measured	Calculated from Eq. 13		
None	0.23	9.53×10^{8} (8.37%)	9.49×10^{8} (6.65%)	1.005	0.960
None	0.52	2.25×10^{8} (28.0%)	2.03×10^{8} (23.6%)	1.105	0.787
130-cm ceiling fan (high speed)	0.23	3.00×10^{9} (5.54%)	3.19×10^{9} (1.02%)	0.941	0.271
130-cm ceiling fan (high speed)	0.52	1.27×10^{9} (8.61%)	1.10×10^{9} (2.90%)	1.156	0.134
Two 51-cm box fans (high speed)	0.52	6.49×10^{8} (14.6%)	1.25×10^{9} (2.59%)	0.517	<0.001

* Coefficient of variation for counting error in percent is given parenthetically.

Table V Distribution of radon decay products between chamber surfaces and fan.

Air Treatment	Air Infiltration Rate, h^{-1}	Radon Decay Product	Deposition on Chamber Surfaces μCi (% of total)[a]	Deposition on Fan Blades μCi (% of total)[a]	Deposition on Fan Box Housing μCi (% of total)[a]	Total Deposition μCi
None	0.23	RaA	0.453 (98.7%)	0.00575 (1.3%)[b]	-	0.459
		RaB	0.739 (99.0%)	0.00723 (1.0%)[b]	-	0.746
		RaC	0.820 (99.2%)	0.00624 (0.8%)[b]	-	0.826
None	0.52	RaA	0.131 (99.4%)	0.000786 (0.6%)[b]	-	0.132
		RaB	0.118 (99.5%)	0.000531 (0.5%)[b]	-	0.119
		RaC	0.226 (99.6%)	0.00116 (0.4%)[b]	-	0.267
130-cm Ceiling Fan (high speed)	0.23	RaA	1.30 (96.6%)	0.0459 (3.4%)	-	1.35
		RaB	2.32 (96.7%)	0.0802 (3.3%)	-	2.40
		RaC	2.48 (96.5%)	0.0902 (3.5%)	-	2.57
130-cm Ceiling Fan (high speed)	0.52	RaA	0.515 (97.6%)	0.0128 (2.4%)	-	0.528
		RaB	0.100 (97.2%)	0.0290 (2.8%)	-	1.03
		RaC	0.105 (96.5%)	0.0380 (3.5%)	-	1.09
Two 51-cm Box Fans (high speed)	0.52	RaA	0.442 (89.4%)	0.0228 (4.6%)	0.0294 (6.0%)	0.494
		RaB	0.414 (88.8%)	0.0296 (6.4%)	0.0224 (4.8%)	0.466
		RaC	0.513 (90.0%)	0.0383 (6.7%)	0.0182 (3.2%)	0.570

a Percentage of total deposition is given parenthetically

b Deposited on stationary blades of 130-cm ceiling fan

Measured and calculated values of activities and potential alpha energy on surfaces had an error attributable to counting. Counting error associated with calculated activities and potential alpha energy was traceable to measurements of airborne radon decay product concentrations used in Equations 9, 10, 11, and 13. We assumed that the number of counts measured followed a Poisson distribution and that counting error could be estimated using the standard error propagation equation.

To determine whether differences between measured and calculated values could be explained solely by counting errors, we tested the null hypothesis that the difference is zero. We assumed that the difference was distributed normally with a variance equal to the sum of the counting-related variances of measured and calculated values. Counting-related variances are given in Tables III and IV in terms of the coefficient of variation. Entries in the last column of these tables are p-values, the probability of erroneously rejecting the null hypothesis. Values of p less than 0.05 indicate significance at the 95% confidence level; i.e., the difference between measured and calculated values of activity or potential alpha energy cannot be explained solely by counting errors. Alternative explanations for material balance discrepancies (i.e., $p < 0.05$), other than counting error, are uncertainties in radon source activity, air infiltration rate, sampling rate, and detector efficiency, as well as nonuniform airborne concentrations in the chamber (i.e., deviations from a well-mixed model) and nonuniform radon decay product deposition on chamber surfaces. Because activity measurements were made on only a small fraction of the surface area of the chamber, nonuniform deposition is probably the primary cause for material balance discrepancies.

For 15 material balances shown in Table III, counting error can account solely for the differences between measured and calculated values in 10 cases. For 5 material balances shown in Table IV, 4 of the differences can be explained by counting error.

Plateout Parameters for Radon Decay Products

Various parameters, such as plateout rate, deposition velocity, and boundary layer thickness, can be used to quantify plateout of radon decay products. These parameters are useful for mathematical modeling and for comparison purposes.

Plateout Rates. The plateout rate of RaA, P_a, is defined as the number of equivalent chamber volumes of RaA that are completely deposited on chamber surfaces per unit time. An equivalent chamber volume of RaA is equal to N_a, the number of RaA atoms airborne in the chamber, whether attached to particles or not. Thus, the number of atoms of RaA plating out per unit time is equal to $P_a N_a$. At steady state, $P_a N_a$ is also equal to the number of atoms of RaA on chamber surfaces that decay per unit time (i.e., surface activity of RaA). Thus,

$$P_a = W_a \lambda_a / N_a \tag{14}$$

As shown schematically in Figure 3, evaluation of the plateout rate for RaB is more complicated than for RaA because of two reasons: (1) when atoms of RaA on chamber surfaces decay, they become RaB atoms; and (2) they also recoil when the alpha particle is emitted and may therefore become resuspended. The steady-state material balance for RaB on chamber surfaces is given by Equation 15:

$$P_b N_b + W_a \lambda_a = W_b \lambda_b + W_a \lambda_a R \tag{15}$$

where R is the fraction of RaA atoms on chamber surfaces that, upon decay to RaB, become resuspended into the chamber airspace, which is assumed to be well mixed. Evaluation of R requires experiments that we did not conduct, and as far as we know, R has never been measured for conditions resembling a building or a mine. To overcome this deficiency, we defined P_b' as a net plateout rate of RaB; i.e.,

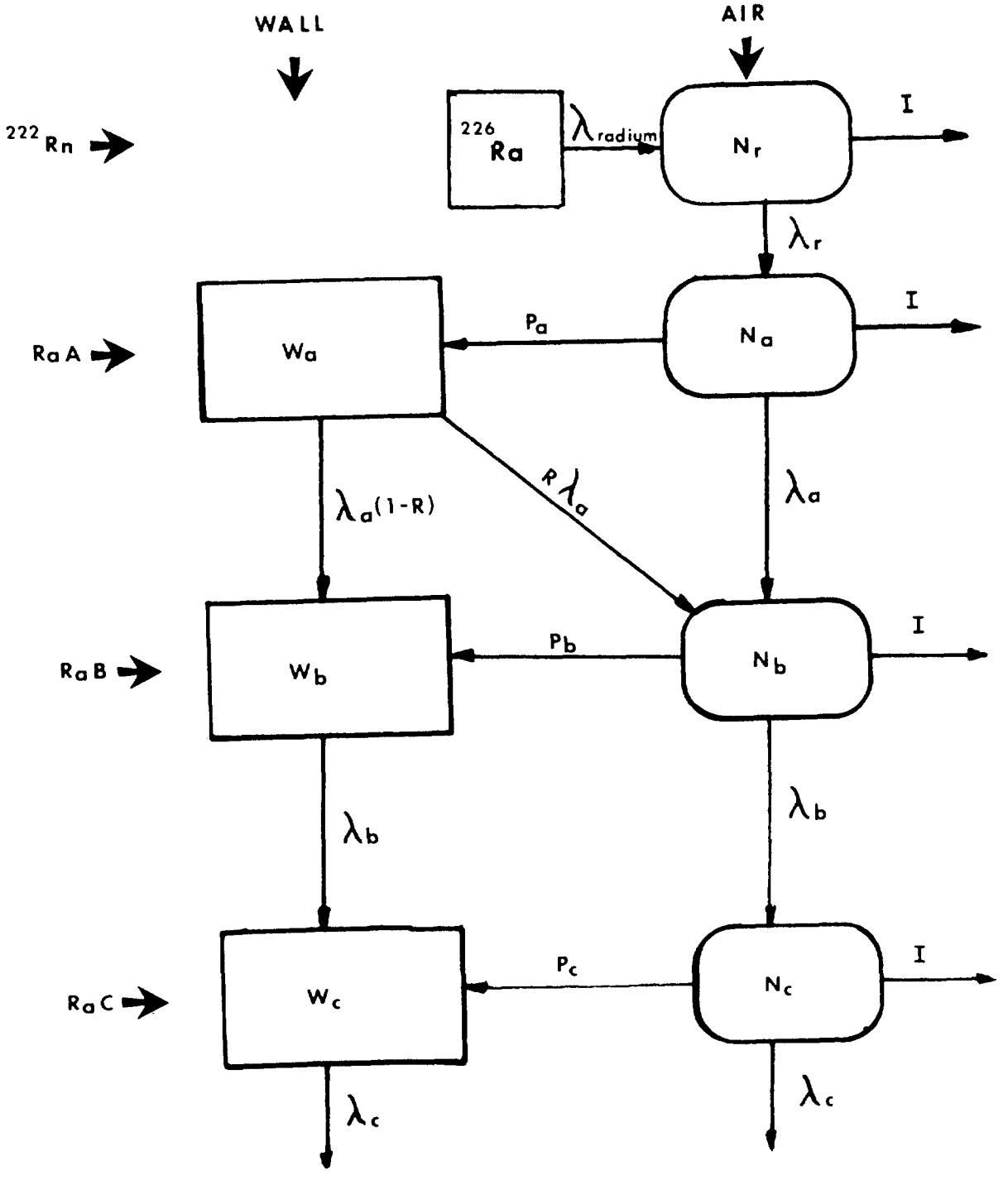

Figure 3 Schematic chart showing model for fate of radon decay products.

$$P_b' = (P_b N_b - W_a \lambda_a R)/ N_b \tag{16}$$

Thus,

$$P_b' = (W_b \lambda_b - W_a \lambda_a)/ N_b \tag{17}$$

One expects R to take on values between 0 and 0.5 because half the atoms recoil into the surface. When $R = 0$, $P_b' = P_b$ and when $R = 0.5$, $P_b' = P_b - 0.5 W_a \lambda_a / N_a$. The plateout rate for RaC can also be obtained from a material balance:

$$P_c = (W_c \lambda_c - W_b \lambda_b)/ N_c \tag{18}$$

Beta recoil from decay of RaB to RaC and RaC to RaC' was assumed to be unlikely.[15]

Using Equations 14 through 18, we calculated plateout rates, which are summarized in Table VI. For W_a, W_b, and W_c, we used the average of measured and calculated values given in Table III; although this is somewhat arbitrary, the average should be a good estimate of true surface activities because material balances must be satisfied. The plateout rate of RaB (P_b) was calculated assuming $R = 0$ or $R = 0.5$; the correct value for P_b should lie somewhere between these two calculated values. Coefficients of variation due to counting errors are also given in Table VI. Coefficients of variations for RaB and RaC tend to be much larger than for RaA, reflecting the statistical penalty incurred when two large numbers are subtracted and the difference is small. For this reason, measured plateout rates for RaA are probably more accurate than for RaB and RaC. P_a can be more accurately determined also because it is larger than P_b or P_c inasmuch as more RaA is unattached to particles than RaB or RaC and most of the plateout is attributable to unattached species. By the same reasoning, P_b should be greater than P_c. With the exception of the no-air-treatment test at an infiltration rate of 0.52/h, $P_a > P_b > P_c$, as expected.

Deposition Velocities. Deposition velocity is defined as the flux of atoms to the chamber surfaces, i.e., atoms per unit time per unit area, divided by the concentration in the chamber airspace, which is assumed to be well mixed. Inasmuch as deposition velocity is a measure of how rapidly these atoms move from the well-mixed airspace to chamber surfaces, different deposition velocities would be obtained for atoms attached and unattached to particles. Because unattached atoms have a deposition velocity that is about 500 greater than attached atoms[10], we assumed that only the former play a significant role in plateout. Thus,

$$v_a = P_a V / A f_a \tag{19}$$

where

v_a = deposition velocity of unattached RaA atoms, m/s

A = area of chamber surfaces

f_a = unattached RaA atoms/total RaA atoms

Measurements using a diffusion battery indicated that $f_a \approx 1/3$ in our experimental chamber.[4] Approximate deposition velocities for unattached RaA atoms were calculated from Equation 19 and are given in Table VII.

Boundary Layer Thickness. In a very simplistic model for the distribution of radon decay products in a chamber, concentrations are assumed to be spatially uniform except in a very thin boundary layer in which they decrease linearly to zero at the surface. If plateout of unattached RaA atoms is a molecular diffusion process, then in the boundary layer

Table VI Calculation of plateout rate.

AIR TREATMENT	AIR INFILTRATION RATE, h^{-1}	PLATEOUT RATE, h^{-1} (Coef. Var.[a])			
		RaA	RaB		RaC
			R=0.5[b]	R=0[b]	
NONE	0.23	2.57(21.8%)	0.346(17.5%)	0.166(53.4%)	0.141(70.1%)
NONE	0.52	2.61(35.6%)	0.0680(15.3%)	-0.109(135%)	0.130(155%)
130-cm ceiling fan (high speed)	0.23	16.1(8.9%)	4.91(9.2%)	2.61(16.2%)	0.690(107%)
130-cm ceiling fan (high speed)	0.52	12.4(15.6%)	2.69(14.5%)	1.40(28.6%)	0.000401(1321%)
Two 51-cm box fans (high speed)	0.52	11.4(15.8%)	2.38(19.3%)	0.780(63.1%)	0.00351(158%)

[a]Coefficient of variation for counting error is given parenthetically
[b]Resuspension fraction R is unknown, but is between 0.0 and 0.5

Table VII Deposition velocity and boundary layer thickness for RaA.

Air Treatment	Air Infiltration rate, h^{-1}	Deposition Velocity (cm/s)	Diffusion Boundary Layer Thickness (mm)
None	0.23	0.14	3.6
None	0.52	0.14	3.6
130-cm Ceiling Fan (High Speed)	0.23	0.86	0.58
130-cm Ceiling Fan (High Speed)	0.52	0.66	0.75
Two 51-cm Box Fans (High Speed)	0.52	0.61	0.82

Fick's first law will be obeyed, i.e.,

$$J = -D_a \frac{\partial C_a}{\partial l} \tag{20}$$

where

J = flux of unattached RaA atoms to chamber surfaces, atoms/(s·m^2)

D_a = diffusion coefficient for unattached RaA atoms, m^2/s

C_a = concentration of unattached RaA atoms, atoms/m^3

l = distance from the surface, m

Combining Equations 19 and 20 and incorporating the assumptions yields

$$L_a = D_a / V_a \tag{21}$$

where L_a is the diffusion boundary layer thickness for unattached RaA atoms.

Boundary layer thicknesses for RaA, based on D_a = 0.05 cm^2/s,[11] are summarized in Table VII. Boundary layer thicknesses for RaB and RaC were not calculated because their measured plateout rates are not believed to be accurate. Deposition velocity and diffusion boundary layer thickness for unattached RaB and RaC, however, would be expected to be approximately equal to those for RaA.

Conclusions and Summary

In a 78-m^3 chamber, observed reductions in airborne activity caused by air motion induced by a 130-cm ceiling fan were as high as 50% for RaA, 77% for RaB, 81% for RaC, and 75% for *WL*; with a 51-cm box fan, reductions were 40% for RaA, 79% for RaB, 86% for RaC, and 76% for *WL*. Although these reductions are roughly comparable, the ceiling fan has significant advantages: it consumes less energy than the box fan, is considerably quieter, is probably better designed to operate continuously for many years, and produces less noticeable air motion. The manufacturer claimed that the ceiling fan can be used profitably all year round; i.e., by altering the direction of rotation or pitch of the blades, it can be used to "reduce air conditioning cost during the cooling season and reduce wasteful heat stratification during the heating season."[12] Use of ceiling fans in the winter, however, tends to make a residence feel colder except possibly for buildings using local heat sources or having very high ceilings.[13]

To determine the fate of radon decay products, a material balance was calculated based on measurements of decay product activities on chamber surfaces, on the fan, in the airspace, and in exiting air. Less than 7% of the surface deposition of radon decay products took place on fan blades or fan housing, as shown in Table V. Holub et al.[2] found deposition on a fan, but none on walls, when conducting similar experiments. The reason for these contradictory results can be explained as follows: the surface area of a fan is significantly less than that of walls, and, therefore, areal activity density on a fan could be many times higher. Thus, the relative external activity on the fan measured by the beta-gamma detection system of Holub et al. may have been in a measurable range with their equipment, whereas the wall activity was not. Holub[14] found no activity on the fan when he replaced his nichrome-wire condensation nuclei generator with a different type of generator. He suggested that the activity he measured on the fan in his original experiments was due to the charged state of the condensation nuclei.[14]

Deposition velocities for unattached radon decay products were found to be 0.14 cm/s when no fans were used and between 0.61 and 0.86 cm/s with fans; boundary layer thicknesses for unattached decay products were 3.6 mm without fans and between 0.58 and 0.82 mm with fans. The likelihood of recoil-caused resuspension of a radon decay product atom into the well-mixed airspace can be estimated by comparing the boundary layer thickness and the stopping distance of a recoiling RaB atom. When the boundary layer thickness is much larger than the stopping distance, recoil can be neglected, whereas if the opposite is true, resuspension must be taken into account. When they are about the same, the importance of recoil is less clear. The stopping distance in air of a recoiling RaB atom has been reported to be equal to about 0.1 mm.[8,15] This is about one quarter the boundary layer thickness calculated for those tests in which fans were used and about one twenty-fifth the boundary layer thickness when no fans were in operation. Thus, recoil probably did not play a significant role in the interaction of airborne and surface activity of RaB under the conditions of our experiments, although special tests are necessary to validate this speculation.

Acknowledgement

This work was supported in part by the United States Environmental Protection Agency Contract No. 68-01-6250, Ronald Bruno, project officer.

References

1. Wrenn M.E., Eisenbud M. and Costa-Ribeiro C., "Reduction of radon daughter concentrations in mines by rapid mixing without makeup air," *Health Phys.* 17:405 (1969).

2. Holub R.F., Droullard R.F., Ho W., Hopke P.K., Parsley R. and Stukel J.J., "The reduction of airborne radon daughter concentration by plateout on an air mixing fan," *Health Phys.* 36:497 (1979).

3. Abu-Jarad F. and Fremlin J.H., "The effect of a fan in reducing the concentration of the radon daughters inside a room by plate-out to the surface of the wall using plastic α-detectors," *Health Phys.* 42:82 (1982).

4. Rudnick S.N., Hinds W.C., Maher E.F., Price J.M., Fujimoto K., Gu F. and First M.W., "Effect of indoor air circulation systems on radon decay product concentration," Final Report for U.S.E.P.A. Contract No. 68-01-6050, Harvard University School of Public Health, Boston, MA (25 February 1982).

5. Lucas H.F., "Improved low-level alpha-scintillation counter for radon," *Rev. Sci. Instrum.* 28:680 (1957).

6. Thomas J.W., "Measurement of radon daughters in air," *Health Phys.* 23:783 (1972).

7. Kerr G.D., "Measurement of radon progeny concentrations in air by alpha-particle spectrometry," Oak Ridge ORNL-TM-4924 (1975).

8. Busigin A., van der Vooren A.W. and Philips C.R., "Collection of radon daughters on filter media," *Envir. Sci. Technol.* 14:533 (1980).

9. Shreve J.D., Jr. and Cleveland J.E., "Effects of depressing attachment ration of radon daughters in uranium mine atmosphere," *Amer. Ind. Hyg. Assoc. J.* 33:304 (1972).

10. Porstendorfer J., Wicke A. and Schraub A., "The influence of exhalation, ventilation and deposition processes upon the concentration of radon (^{222}Rn), Thoron (^{220}Th) and their decay products in room air," *Health Phys.* 34:465 (1978).

11. Raabe O.G., "Concerning the interactions that occur between radon decay products and aerosols," *Health Phys.* 17:177 (1969).

12. Robbins & Myers, Inc., Hunter Division, Manufacturer's literature provided to retailers, Memphis, TN (1981).

13. Consumer's Union, "Summer cooling," *Consumer Reports*, 47:350 (July 1982).

14. Holub R.F., private communication to S. Rudnick at EPA International Meeting on Radon and Radon Progeny Measurement, Montgomery, AL (27-28 August 1981).

15. Jonassen N. and McLaughlin J.P., "The effect of RaB recoil losses on radon daughter measurements," *Health Phys.* 80:234 (1976).

DISCUSSION

YOUNG: Has the use of aerosol additions with subsequent filtration with high efficiency filters been used to selectively remove radon and daughter products from process streams or ventilation systems:

FIRST: We also included that aspect in our studies. I did not report on that today because it is going to be published in Health Physics in an issue devoted exclusively to radon and decay products. We did find, of course, that decay products seek any surface. Once you put in aerosols, or allow aerosols to come in, you get a large fraction attached to particles. We performed studies using diffusion batteries whereby we could remove the unattached radon decay products and get the attached out the other end in pretty pure form. We related the results to particle size and to particle numbers and ended up by having a rather serious disagreement among ourselves as to whether it was better to have more particles or whether it was worse from the standpoint of health. We looked at where the radon decay products would deposit if they were unattached. Some think they may go deep into the lungs. My impression from the diffusion constants that we worked with is that they probably would not get very far down before they would deposit by diffusiophoresis, whereas small particles would go down deep into the alveola spaces. Which is worse from the standpoint of lung cancer is a matter of some debate in the literature. I think it is still up in the air.

YOUNG: I wasn't thinking primarily in terms of stripping decay products from the air in homes or business buildings. I was thinking more about process systems,or where you want to remove radon selectively. It seems like the utilization of aerosols or downstream filters might be one technique of doing it.

FIRST: We also did filter studies. A HEPA filter strips unattached radon daughter products out of the air at 100% efficiency with one passage but you end up with the remaining radon in the air.

ROUYER: According to your study, what do you recommend as the most effective means to decrease working level in insulated buildings? Is it to put fans and increase plateout, or is it to increase the ventilation rate?

FIRST: The easiest and simplest thing to do is to increase the ventilation rate. Almost everywhere, it was never a problem in buildings and residences until we started conserving energy and tightened up the buildings so that there was little natural or mechanical air exchange. Proposals have been made to use heat exchangers so that one can continue to ventilate buildings, but recover some of the heat (or some of the air conditioning) in the exhausted air. That is a very inefficient way of recovering heat because the temperature differential will be very small and one does not get much heat recovery for the large amount of equipment that must be purchased and installed. In addition, you have to expend energy for blowers, motors, and so on. We were looking for simple ways that wouldn't cost anything, wouldn't take up any space, and wouldn't require any

maintanence. One of the ways you can do that, for example, is to greatly increase the surface area in a room, but this is very awkward. However, if you have a hot air heating system, you can fill the ducts with egg crate separators and this will impose almost no added resistance, but will give a many-fold surface area increase and you can strip out decay products by diffusion very nicely. That was another of the things we looked at but did not report on in this paper.

FORMATION AND CHARACTERIZATION OF FISSION-PRODUCT AEROSOLS UNDER POSTULATED HTGR ACCIDENT CONDITIONS

I. N. Tang and H. R. Munkelwitz
Brookhaven National Laboratory
Upton, N. Y. 11973

Abstract

The paper presents the results of an experimental investigation on the formation mechanism and physical characterization of simulated nuclear aerosols that could likely be released during an HTGR core heat-up accident. Experiments were carried out in a high-temperature flow system consisting essentially of an inductively heated release source, a vapor deposition tube, and a filter assembly for collecting particulate matter. Simulated fission products Sr and Ba as oxides are separately impregnated in H451 graphite wafers and released at elevated temperatures into a dry helium flow. In the presence of graphite, the oxides are quantitatively reduced to metals, which subsequently vaporize at temperatures much lower than required for the oxides alone to vaporize in the absence of graphite. A substantial fraction of the released material is associated with particulate matter, which is collected on filters located downstream at ambient temperature. The release and transport of simulated fission product Ag as metal are also investigated. Electron microscopic examinations of the collected Sr and Ag aerosols show large agglomerates composed of primary particles roughly 0.1 μm in diameter.

I. Introduction

The potential evolution of substantial amounts of radioactive aerosols as a consequence of high-temperature vaporization of nuclear materials during a reactor accident is a major consideration in reactor safety analysis. In an earlier study [1], the rate and extent of aerosol formation were reported for HTGR core graphite heated up to 1600°C in either a dry or moist helium. It was shown that particles in the Aitken nuclei size range were formed with initial concentrations as high as 10^7 particles per cm^3. Since airborne particles at high concentrations readily serve as condensation or adsorption sites for gaseous species, it would be expected that, under appropriate conditions, the presence of aerosol particles could greatly facilitate the gas-phase transport of vaporized fission products.

In the present paper, we report the results of an investigation concerning the release and transport of simulated fission products Ag, Sr and Ba as particulate matter. Although extensive research efforts have been expended during the past fifteen years or so, both in the United States and abroad, on the formation and characterization of radioactive aerosols pertaining to LWR and LMFBR safety [2,3], only meager consideration has been given to the potential aerosol problems in HTGR safety [4]. The results of the present study show that fission product transport via aerosols is an important safety problem to be seriously considered in HTGR accident analyses.

II. Experimental Procedure

A high-temperature flow apparatus, shown schematically in Figure 1, was constructed. Basically, it consisted of a quartz tube inside which a graphite sample was heated inductively in flowing dry helium. A filter assembly was located some distance downstream from the heated release source. The quartz tube had an enlarged section (8 cm dia. x 40 cm length) immediately above the heated sample region for effective deposition of condensible vapor species on the walls. Fission products

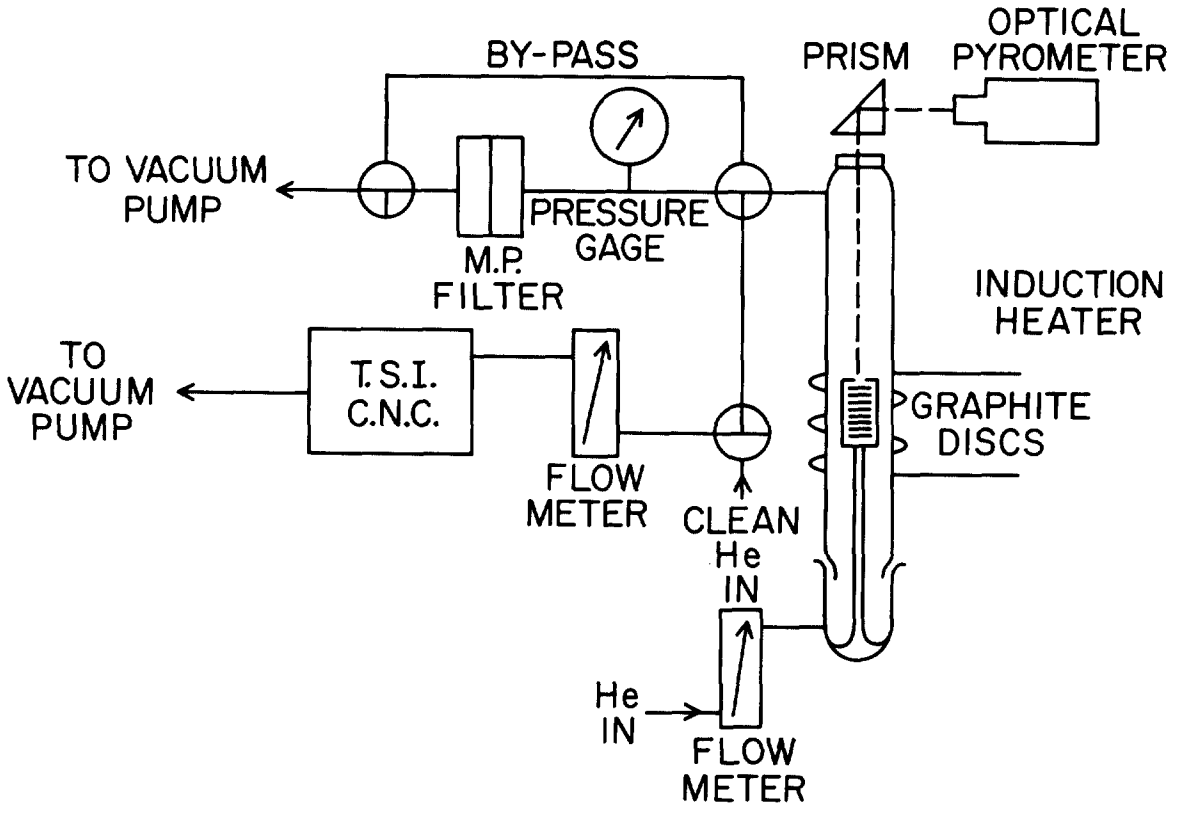

Figure 1. Schematic Diagram of Fission Product Transport Apparatus

associated with particles passed through the vapor deposition section and were subsequently collected on a 0.2 μm filter (Fluoropore or Nucleopore) placed in the filter assembly. The quantity of the collected material was analyzed by atomic absorption.

The simulated fission products Sr and Ba were initially in the form of nitrate, whereas metallic Ag, except otherwise indicated, was used in the experiments. A typical experiment with Sr was conducted in the following manner. Thin wafers (2 mm thickness x 2 cm diameter) of H451 graphite were first dried at 150°C in a vacuum oven to a constant weight. The preweighed wafers were then placed in a glass vessel, which was evacuated and back-filled with an aqueous $Sr(NO_3)_2$ solution of predetermined concentration. After an overnight soak, the wafers were removed from the vessel and dried in the vacuum oven to a constant weight. The final weights were noted. The amount of $Sr(NO_3)_2$ salt absorbed in the pore structure of the graphite was then calculated from the weights before and after impregnation for each wafer.

The $Sr(NO_3)_2$ impregnated wafers were then enclosed in an H451 graphite crucible having a 3 mm-diameter sight hole on its cover for temperature monitoring. The optical path (sight glass and prism) and pyrometer were calibrated together for temperature measurement using foils of gold, silver, palladium, nickel and platinum, whose melting points are accurately known. In later experiments, however, the wafers were simply stacked together and mounted on a graphite pedestal.

The assembled source was then heated inductively in flowing helium, with the filter assembly bypassed, to a temperature of about 1100°C at which $Sr(NO_3)_2$ is converted to SrO according to the following reaction:

$$2\ Sr(NO_3)_2 \xrightarrow{\Delta} 2SrO + 4NO_2 + O_2 \qquad (1)$$

After allowing a sufficient time for conversion (usually 30 min.), the filter was valved back to the gas stream. The sample temperature was then increased to a predetermined level and held constant during a sampling period. At the conclusion of the sampling period, the exposed filter was removed and immediately replaced with a new filter before the temperature was raised again. Occasionally, the filter assembly was left in the gas stream during the initial heating period to ascertain whether or not Sr was released during the conversion process. In no instance was a significant amount of Sr found. When desired, a small flow (100 cc/min.) could be diverted into a continuous-flow condensation nuclei counter for monitoring the particle concentrations of the gas stream.

III. Results and Discussion

Vaporization Mechanism for Ag, Sr and Ba

Both $Sr(NO_3)_2$ and $Ba(NO_3)_2$ decompose at ~ 1100°C to form respective oxides, which are stable refractory material having a high melting point and low vapor pressures at moderate temperatures. Electron probe microanalysis [5] has shown that fission product Sr and Ba form ceramic oxides in irradiated oxide fuel kernels. Fission product Ag, on the other hand, is present in the fuel kernels as metal since it is not stable in its oxide form at temperatures as low as 300°C. Some of the relevant physical properties are given in Table I for Ag, SrO, and BaO, along with the approximate release temperatures observed for each species in the presence of graphite.

Table I

Selected Physical Properties

F.P.	m.p., °C	b.p., °C	Observed* Release Temp., °C	Vapor Pressure at Release Temp, torr
Ag	961	2212	~1100	~0.04
SrO	2430	~3000	~1250	~1.3×10^{-7}
BaO	1923	~2000	~1500	~ 1×10^{-3}

* In presence of graphite

The release temperatures given in Table I for Ag, SrO and BaO were derived from a series of experiments in which the simulated fission products were each released from a heated H451 graphite source into dry helium flowing at 2.5 ℓ/min. The material collected on filter at each temperature was analyzed and the amount was converted into percent of the initial fission product loading as element. A summary of the results is shown in Figure 2, where cumulative percentage of the material collected as particulate matter in each experiment was plotted vs. release temperatures. The steepest portion of the release curve was taken as a rough estimation of the release temperature for the fission product under investigation.

The vapor pressures of the two oxides at the release temperatures, as shown in the last column of Table I, are rather low for vaporization to take place significantly. Thermodynamic considerations, however, indicate that chemical reactions of the oxides with graphite could proceed to reduce the oxides to the metallic state, which would then vaporize at relatively low temperatures. In the case of SrO, for example, the overall reaction could be as follows:

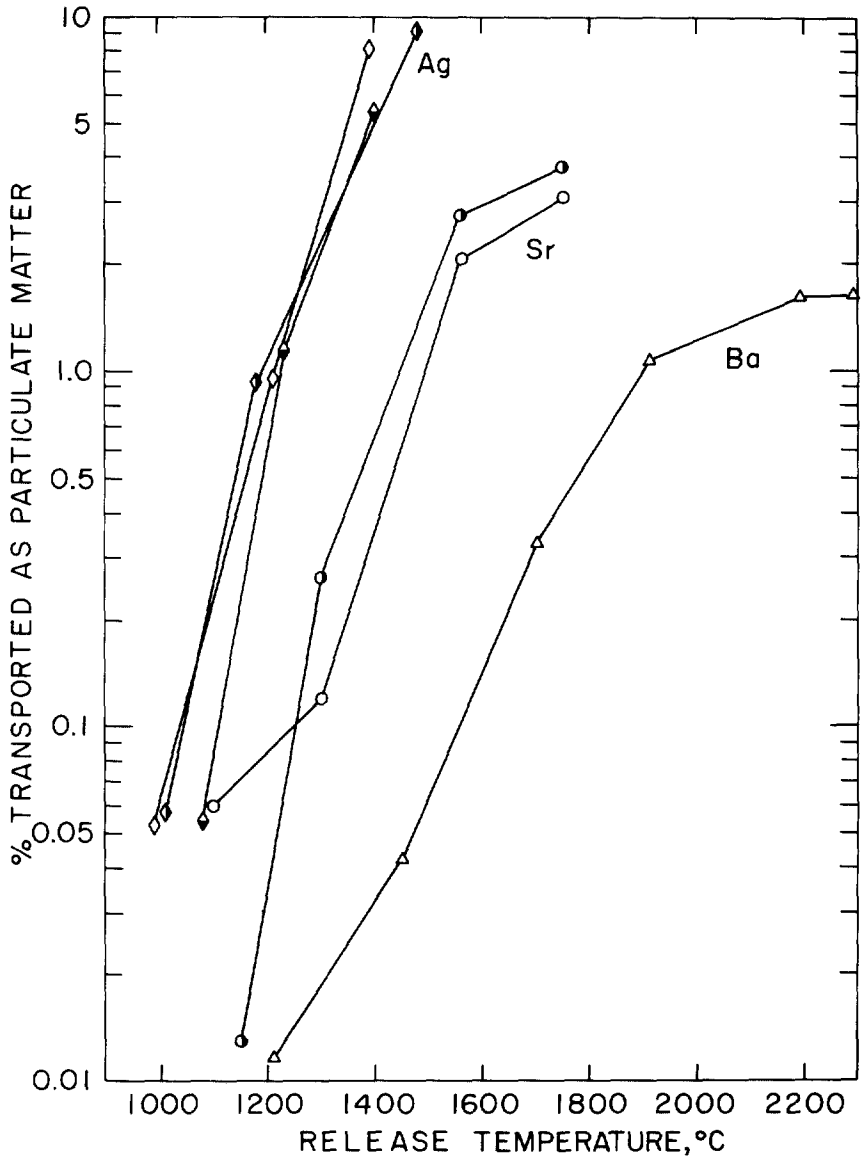

Figure 2. Particulate Transport as a Function of Source Temperature

$$SrO\ (s) + C\ (s) = Sr\ (g) + CO\ (g) \qquad (2)$$

where the letter in the parenthesis indicates the state of substance being either solid or gas. The thermodynamic equilibrium of Reaction (2) may be represented by

$$P_{CO} \cdot P_{Sr} = K_p = e^{-\Delta G^\circ/RT} \qquad (3)$$

where the activity of a solid substance is taken as unity, K_p is the equilibrium constant, ΔG° is the Gibb's free energy of reaction, and R is the gas-law constant. A computation of the equilibrium partial pressure for metallic Sr at T = 1500°K yields a value of 0.14 torr for P_{Sr}, as compared to the vapor pressure of the oxide, $P^\circ_{SrO} \simeq 1.2 \times 10^{-7}$ torr at the same temperature. The above calculation clearly indicates that, in the presence of graphite, fission product strontium would vaporize as metal rather than as oxide. In order to further confirm this hypothesis, another experiment was carried out, in which SrO was placed in a

tungsten crucible and heated in the absence of graphite. The results from this experiment were compared with those of an earlier experiment performed in the presence of graphite. As shown in Figure 3, SrO was not vaporized appreciately in the absence of graphite, even at temperatures as high as 1760°C.

Physical Characterization of Sr and Ag Aerosols

The color of the freshly collected Sr aerosol on Fluoropore filters usually varied from light brown to black, depending upon the thickness of the deposit. Upon exposure to room air, the deposit always lost its color, indicating the conversion of elemental Sr to the oxide, and eventually to the hydroxide form.

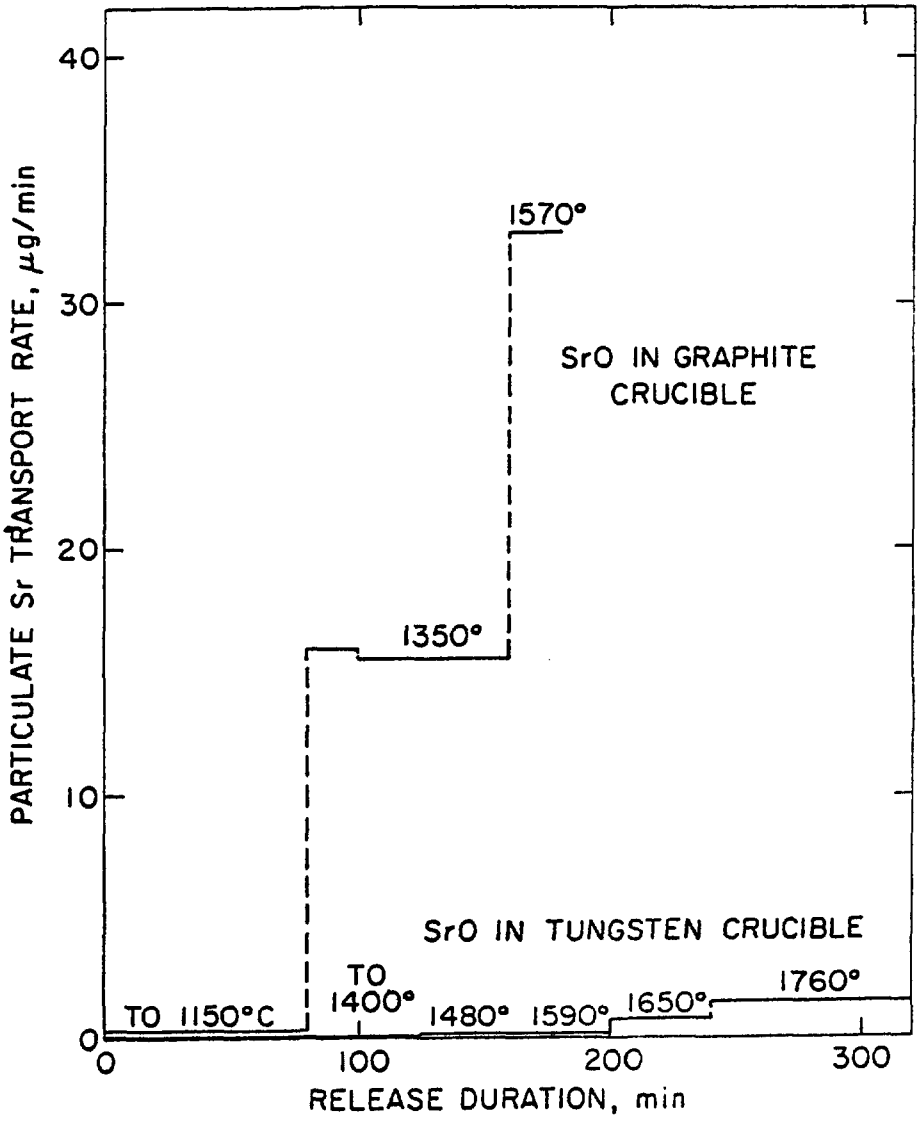

Figure 3. Effect of Graphite on SrO Vaporization

In an effort to study the particle size and morphology of the Sr deposit, electron microscope samples were prepared in experiments where the filters were exposed only briefly to the aerosol stream. At 1 liter/min flow rate, filter samples with aerosol collection times of 120, 60, 30 and 10 sec were obtained. These samples were kept under inert atmosphere before electron microscopic examinations. It turned out that with even the shortest collection time the aerosol deposit on filter was very heavy. A picture at 42000X magnification is shown in the upper insert of Figure 4, together with the Sr elemental analysis result (lower insert) by the x-ray fluorescence microprobe method. Although the electron micrograph is not in very sharp focus the picture shows essentially agglomerates with primary particles roughly 0.1 μm in diameter, which were most likely formed by vapor-phase nucleation.

Figure 5 shows a composite of electron micrographic pictures of Ag aerosols at four different magnifications. These Ag aerosols, produced from a $AgNO_3$ impregnated graphite source in the same manner as Sr and Ba aerosols, were collected on Nucleopore filters for better examination. Unlike Sr and Ba aerosols which are chemically reactive in ambient air, Ag aerosols are stable in air and, therefore, they provide a good means for studying the morphology of fission product aerosols. Such information is needed to understand the aerosol formation mechanism. In this particular case, agglomerates composed of primary particles almost uniform in size (d_g=0.098 μm, σ_g = 1.20) are clearly revealed, indicating the condensational nature of the particles, as opposed to fission product adsorption on existing particles.

Sr Transport vs. Initial Loading in Graphite

The experiments reported in the present study were all made with simulated fission products impregnated in the graphite matrix with concentrations between approximately 1 mg to 10 mg of Sr, for example, per g of graphite. A legitimate question then arises as to whether or not the extent of aerosol formation depends on the initial loading of fission products in the graphite matrix. To answer this question, we present in Figure 6 the results from six experiments made under identical conditions. Here, the % Sr collected on filter is plotted vs. initial Sr loading in the graphite samples. In addition, the concentration corresponding to one monolayer coverage on graphite was calculated for Sr on the basis of an estimated graphite surface area of 1 m^2/g. As shown in Figure 6, the extent of aerosol formation in terms of percentage collected on filter as particulate matter is independent of the initial loading for concentrations down to approximately one monolayer coverage of Sr in H451 graphite. Work is in progress to reduce the initial Sr concentration further down to below one monolayer coverage.

IV. Conclusion

The experimental results of our investigation to date have clearly demonstrated that the formation of nuclear aerosols under certain HTGR accident conditions could be an important mechanism by which vaporized fission products such as Ag, Sr and Ba are transported in the gas phase. Electron microscopic examinations of the collected Sr and Ag aerosols have revealed large agglomerates composed of primary particles roughly 0.1 μm in diameter. These primary particles are most likely formed by vapor phase nucleation. The percentage of aerosol formation is independent of the initial loading in the graphite matrix for concentrations down to one monolayer coverage, as demonstrated for the case of Sr.

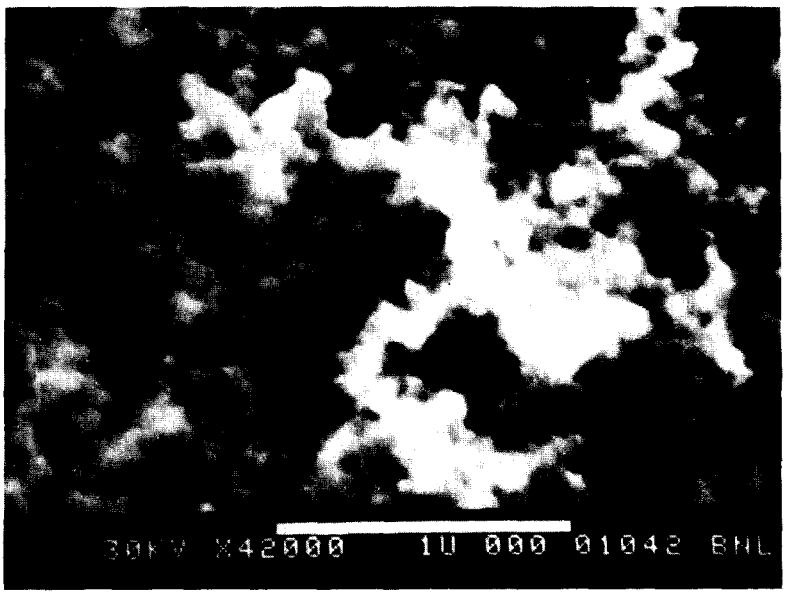

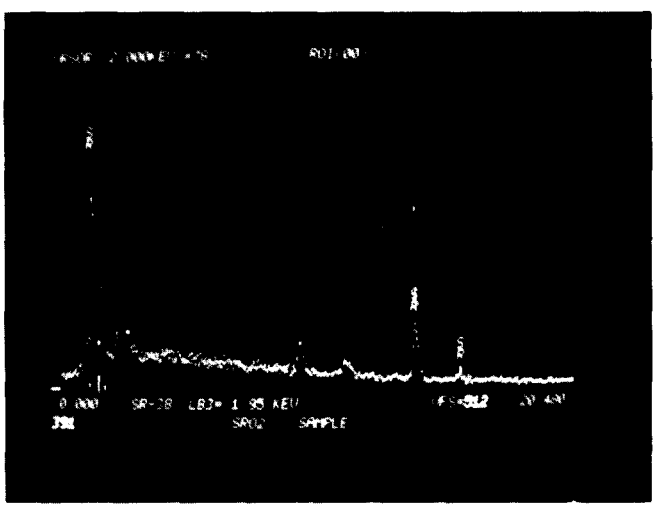

Figure 4. Sr Aerosol Deposit on Fluoropore Filter

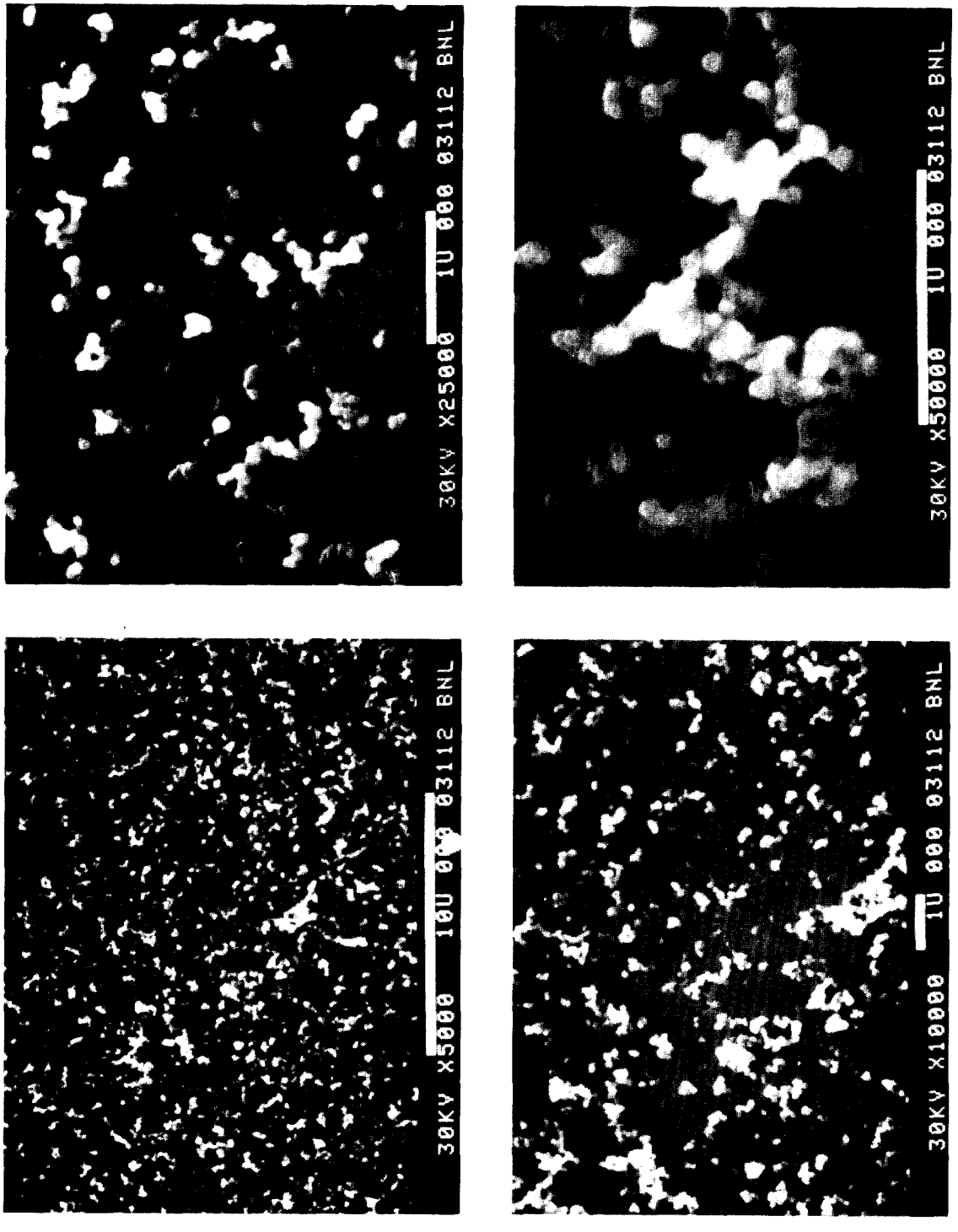

Figure 5. Ag Aerosol Deposit on Nucleopore Filter

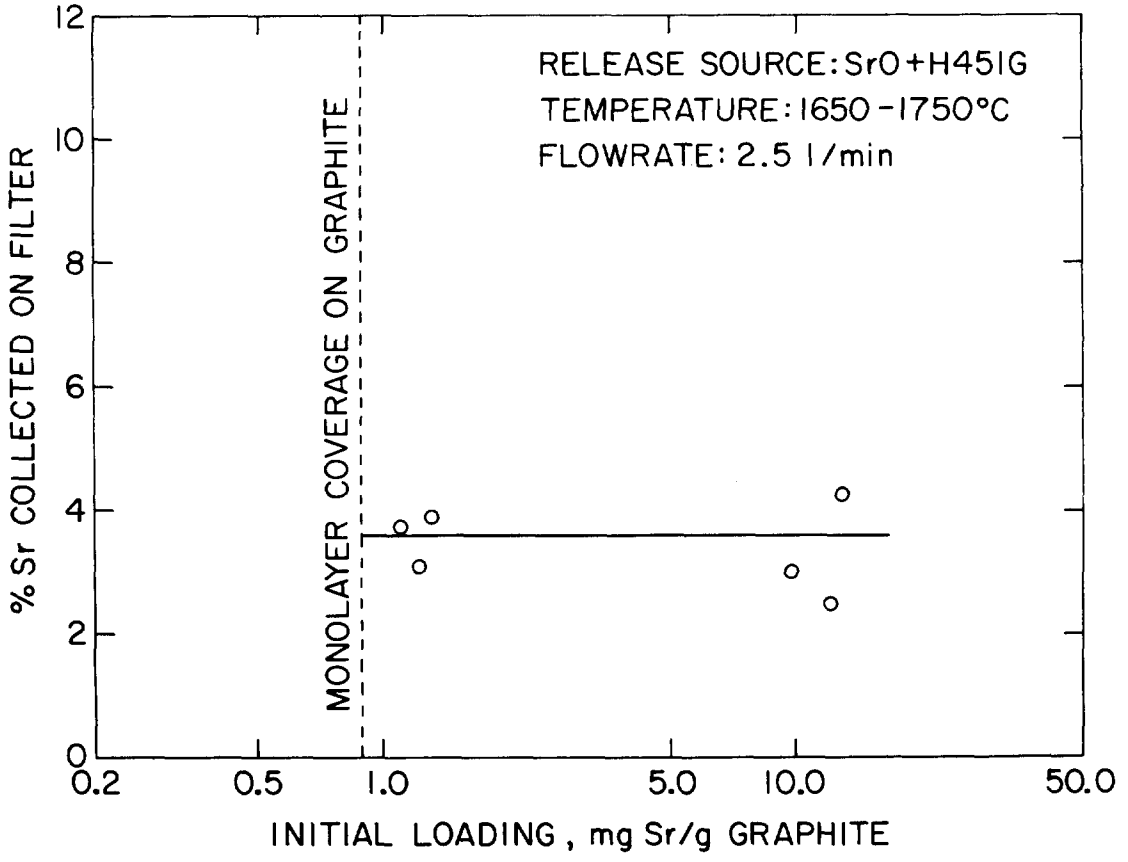

Figure 6. Effect of Initial Sr Loading on Particulate Transport

V. Acknowledgement

This work was performed under the auspices of the U. S. Nuclear Regulatory Commission.

The authors would like to thank George S. Smith and Judson G. Davis for assistance in performing the experiments, Robert Wilson for filter sample analyses, and John B. Warren for the electron microscopic work. The guidance of C. A. Sastre and D. G. Schweitzer of the HTGR Safety Division at BNL is greatly appreciated.

VI. References

1. I. N. Tang, H. R. Munkelwitz and S. L. Nicolosi, ''Aerosol formation from core graphite heated in dry and moist helium.'' Brookhaven National Laboratory, BNL-NUREG-25330, 1980.

2. Nuclear Aerosols in Reactor Safety , CSNLI/SOAR No. 1, Nuclear Energy Agency, June 1979.

3. J. A. Gieseke, R. C. Behn, A. C. Chace and L. D. Reed, ''Analytical studies of aerosol behavior predictions for fast reactor safety,'' BMLI-1932, Battelle Columbus Laboratory, Columbus, Ohio, 1975.

4. See, for example, General Atomic Standard Safety Analysis Report (GASSAR).

5. H. Kleykamp, ''Mikrosondenuntersuchungen zum verhalten der spalt produkte in hoch abgebrannten HTR-brennstoffen,'' KFK 2213, Karlsruke, 1975.

CONCLUDING REMARKS OF SESSION CHAIRMAN:

Summarizing, most of the papers on fuel reprocessing were from overseas. We hope that this ratio will change in the future. We have had both experimental data and modeling papers presented and I think the conclusion is that we still need additional experimental data to confirm the design of off-gas cleanup systems, to evaluate potential failures of these cleanup systems, and to assure that we have safe fuel reprocessing facilities. We certainly appreciate the contribution by our foreign visitors to this technology and we hope that this will fill in some of the gaps that we in the U.S. have not had a chance to work on the past few years. I want to thank all the authors for their work and for their presentations. I would also like to apologize for some of the equipment failures we had. When we had two simultaneous failures in our audiovisual system just in one session, I am wondering if we are justified in looking at single failures even in nuclear applications. The number of components here is much smaller than in a nuclear power plant, if we tried to apply statistics. I think we had better look at multiple failures and make sure we can protect our systems from them.